

**SPRING AND SUMMER PHYTOPLANKTON COMMUNITY DYNAMICS AND
COMPARISON OF FRRF- AND ¹³C-DERIVED MEASUREMENTS OF PRIMARY
PRODUCTIVITY IN RIVERS INLET, BRITISH COLUMBIA**

by

VICTORIA JADE SHILLER

B.Sc., University of British Columbia, 2006

A THESIS SUBMITTED IN PARTIAL FULFILLMENT OF
THE REQUIREMENTS FOR THE DEGREE OF

MASTER OF SCIENCE

in

The Faculty of Graduate Studies

(Oceanography)

THE UNIVERSITY OF BRITISH COLUMBIA

(Vancouver)

November 2012

Abstract

Spring and summer phytoplankton community dynamics were monitored in the temperate coastal fjord, Rivers Inlet, British Columbia, to understand their impact on the growth of juvenile sockeye salmon. Spatial patterns in timing and magnitude of the diatom-dominated spring bloom appeared to be controlled by differences in mixing and stratification. At the sheltered head of the inlet, riverine input stratified the water column, the phytoplankton bloom appeared earlier and more intense. At the well-mixed mouth, where currents diluted the phytoplankton seed population, the bloom appeared delayed and reduced in intensity. The spring bloom was terminated by nitrate depletion except where salinity was low and phosphate became limiting due to oligotrophic freshwater input. While the spring community was diatom-dominated, the summer community was more diverse, with increased abundance of flagellates and ciliates.

Primary productivity measurements using fast repetition rate fluorometry (FRRF) correlated well ($\sim 1:1$) with estimates derived from 2-hour ^{13}C -uptake incubations when phytoplankton were healthy in the lab. In contrast, under high light or low nutrient conditions, FRRF underestimates primary productivity. Community composition may also influence FRRF estimates of primary productivity. We calculated annual FRRF-derived primary productivity of $550 - 1100 \text{ g C} \cdot \text{m}^{-2} \cdot \text{yr}^{-1}$. Potential sockeye production was estimated using primary productivity estimates derived from our ^{13}C data. These calculations suggest that the sockeye carrying capacity of the fjord and lake are well matched and that current levels of primary production could support the ~ 10 -fold higher historical sockeye returns. This implies that contemporary and historical levels of primary production are similar and are not the cause of the sockeye decline. More likely, a timing mismatch between trophic levels is negatively impacting sockeye smolts. Our results suggest that future sockeye production in Rivers Inlet may be negatively impacted by increased freshwater input and stratification, both of which may be influenced by climate warming. This physical forcing may precipitate a shift to a flagellate-dominated phytoplankton community, a longer food chain, and reduced energy transfer to smolts. Continued monitoring of phytoplankton dynamics is critical for refining predictions of ecosystem change and facilitating improvements in sockeye stock management policies.

Preface

The fieldwork described in Chapter 2 is part of a large field program conducted in the Rivers Inlet. Dr. Brian Hunt, Dr. Evgeny Pakhomov, Lora Pakhomova, Chris Payne, Asha Ajmani, Mike Hodal, and Désirée Tommasi accompanied and trained me during bio-oceanographic surveys in 2009 and 2010. All fieldwork was conducted collaboratively. Upon our return to The University of British Columbia, Chris Payne analyzed nutrient samples, Dr. Hunt and others analyzed chlorophyll *a* samples, and Dr. David Cassis trained me to identify and isolate phytoplankton. Beyond these extremely generous contributions, I have been responsible for the analysis and interpretation of data for this chapter. Chapter 2 will be revised into a manuscript co-authored with Dr. Maldonado, Dr. Hunt, Dr. Pakhomov, and Dr. Tortell. As the first author, I was responsible for literature review, data analysis, and preparation of the manuscript with guidance from Dr. Maldonado.

Table of Contents

Abstract	ii
Preface	iii
Table of Contents	iv
List of Tables	vi
List of Figures	ix
Acknowledgements	xi
Chapter 1: General introduction	1
1.1 Introduction to the Rivers Inlet ecosystem.....	1
1.2 Background on primary productivity measurements	5
1.3 Photosynthesis and fluorometry background	6
1.4 Research objectives	15
Chapter 2: Spring and summer phytoplankton community dynamics and comparison of FRRF- and ¹³C-derived measurements of primary productivity in Rivers Inlet, British Columbia	16
2.1 Introduction	16
2.2 Materials and methods.....	19
2.2.1 Study area and sampling scheme	19
2.2.2 Photosynthetically active radiation	21
2.2.3 Chlorophyll <i>a</i>	22
2.2.4 Nutrients.....	23
2.2.5 Surface stratified layer	23
2.2.6 Phytoplankton community composition	23
2.2.7 Strain isolation	24
2.2.8 Culturing techniques	24
2.2.9 Fast Repetition Rate Fluorometry (FRRF) method during 2009 sampling season at surface irradiance.....	25
2.2.10 Simultaneous Fast Repetition Rate Fluorometry (FRRF) and ¹³ C method during 2010 sampling season at <i>in situ</i> light levels	26
2.2.11 Calculation of primary productivity from FRRF measurements	29
2.2.12 Calculation of primary productivity from ¹³ C bottle incubations	31
2.3 Results	33
2.3.1 Chemical and physical properties	33
2.3.1.1 Macronutrient seasonal cycle	33
2.3.1.2 Nutrient drawdown	38
2.3.1.3 Surface stratified layer depth.....	39
2.3.1.4 Euphotic zone	39
2.3.2 Phytoplankton	41
2.3.2.1 Seasonal chlorophyll <i>a</i> cycle	41
2.3.2.2 Phytoplankton community composition.....	41
2.3.3 Correlations between nutrients and phytoplankton.....	43
2.3.4 FRRF- ¹³ C primary productivity calibration	45
2.3.5 FRRF-derived primary productivity	47
2.3.6 Correlations between macronutrients, chlorophyll <i>a</i> concentrations, and FRRF-derived measurements of primary productivity.....	48

2.4	Discussion	51
2.4.1	Characterizing the spring phytoplankton bloom in Rivers Inlet: nutrients, chlorophyll, and phytoplankton community dynamics	51
2.4.2	Comparison of FRRF and $^{13/14}\text{C}$ calculations of primary productivity	54
2.4.3	Primary productivity in Rivers Inlet	60
2.4.4	Outlook	62
Chapter 3: Conclusion		65
3.1	General conclusions	65
3.2	Future work	66
Bibliography		70
Appendix A: Sampling scheme and dates.....		82
Appendix B: Measuring photosynthetic unit size (n_{PSII}^{-1}) in representative Rivers Inlet phytoplankton using an oxygen electrode		84
1.1	Introduction and rationale	84
1.2	Methods	86
1.2.1	Phytoplankton isolation and culturing techniques	86
1.2.1.1	Comparison to Suggett et al. (2009b)	86
1.2.2	Representative Rivers Inlet phytoplankton	87
1.2.3	Experimental design.....	88
1.2.4	Oxygen flash yields.....	90
1.2.5	Chlorophyll <i>a</i> determination	90
1.2.6	Data processing and calculation.....	91
1.3	Results	94
1.3.1	Comparison to n_{PSII}^{-1} from Suggett et al. (2009b).....	94
1.3.2	n_{PSII}^{-1} of representative Rivers Inlet phytoplankton	94
1.4	Discussion and conclusions.....	95
Appendix C: All phytoplankton data observed using light microscopy		98

List of Tables

Table 1. FRRF acquisition parameter settings. ST, single turnover. MT, multiple turnover. Only ST data were used to calculate primary productivity. Inc: percent increase in flashlet intensity. Block time: length of block of flashlets.	26
Table 2. List of fast repetition rate fluorometer (FRRF) and ¹³ C fixation parameters used to calculate primary productivity.	32
Table 3. Example primary productivity calculation based on fluorescence measurements collected using an FRRF. Sample data from the centre of the inlet April 16, 2009. Where z is depth (m); E _z is photosynthetically active radiation (PAR; μE · m ⁻² · s ⁻¹); σ _{PSII} is the functional absorption cross section of photosystem II (PSII; Å ² · quanta ⁻¹); ϕ _p is the quantum yield of photosynthesis (dimensionless); ϕ _e is the actual quantum yield of electron transport (0-1, dimensionless); F _v /F _m is photochemical efficiency in dark-adapted samples (dimensionless); f is the fraction of potentially open functional PSII reaction centres (RCII; dimensionless); [chl _a] is the concentration of chl _a (μg · L ⁻¹); P _f ^e is the steady-state photosynthesis normalized to RCII (e ⁻ · (RCII · s) ⁻¹); P _f ^B is the photosynthetic electron flow calculated from fluorescence yields (mg C · (mg chl _a · h) ⁻¹); and FRRF-PP is primary productivity derived from FRRF measurements (mg C · m ⁻³ · h ⁻¹). †When (E _z × σ _{PSII} × q _p) ≤ τ _p ⁻¹ , ϕ _e = 1 (low light) and when (E × σ _{PSII} × q _p) > τ _p ⁻¹ , ϕ _e = (E _z × σ _{PSII} × q _p × τ _p) ⁻¹ (high light). Where q _p is photochemical quenching (dimensionless) and τ _p is the minimum time required to transfer an electron from water to the terminal electron acceptor in steady-state light saturation (4.3 ms).	33
Table 4. Surface stratified layer depth (SLD, m), secchi depth (m), and euphotic zone characteristics (surface irradiance, I ₀ , μE · m ⁻² · s ⁻¹ ; euphotic zone depth, m; average PAR in the euphotic zone, μE · m ⁻² · s ⁻¹ ; and average PAR in the mixed layer, μE · m ⁻² · s ⁻¹) in 2009 and 2010. Where more than one measurement was collected at a station during a single cruise, the values were averaged. Euphotic zone depth was calculated from 1% I ₀ . When euphotic zone depth exceeded sampling depth, euphotic zone is reported as > sampling depth and average PAR in the euphotic zone is reported as average PAR from surface to deepest depth sampled. Average PAR in the euphotic zone was calculated from I ₀ × (k × D) ⁻¹ × (1 - e ^{-(k × D)}), where k is the extinction coefficient (1.7) and D is the depth of the euphotic zone. Average PAR in the SLD is calculated in the same manner, using SLD instead of euphotic zone depth.	40
Table 5. Maximum spring nutrient concentrations (PO ₄ , Si, and NO ₃ ; μM) at the head, centre, and mouth of the inlet were divided by the Redfield ratio (1 P : 15 Si : 16 N). Lowest values (<i>italics</i>) are the nutrient that will run out first. 30m data excluded because no drawdown was observed at that depth.	45
Table 6. FRRF-derived measurements of primary productivity [FRRF-PP; μg C · (L · h) ⁻¹] collected during 2009 and 2010 bio-oceanographic surveys.	48
Table 7. Primary productivity [PP, μg C · (L · h) ⁻¹] calculated from chl _a data using C:chl _a molar ratios of 65 and 45 (when an increase in chl _a was observed) and from nutrient concentrations using the Redfield ratio (when nutrient drawdown was observed). PP measured using a fast	

repetition rate fluorometer [FRRF-PP, $\mu\text{g C} \cdot (\text{L} \cdot \text{h})^{-1}$] are reported here as a range of values that occurred at the same time as *chl a* increase and nutrient drawdown. 51

Table 8. Spring phytoplankton bloom dates predicted by Wolfe (2010). Model data is not available for 2010, though the bloom was already underway in early March (data not shown).. 54

Table 9. FRRF-PP:¹³C-PP slopes for experiments run in the laboratory and in Rivers Inlet. (*) denotes significant correlation. 55

Table 10. Ratios are reported as ETR:^{13/14}C-PP, calculated in units $\text{mol e}^- \cdot (\text{g chl a} \cdot \text{h})^{-1} : \text{mol CO}_2 \cdot (\text{g chl a} \cdot \text{h})^{-1}$ or $\text{mol e}^- \cdot (\text{L} \cdot \text{h})^{-1} : \text{mol CO}_2 \cdot (\text{L} \cdot \text{h})^{-1}$. The final ratio is in units of $\text{mol e}^- \cdot (\text{mol CO}_2)^{-1}$. ETR: electron transfer rate of photosystem II. SIS: simulated *in situ*. PE: photosynthesis light response. Inc: incubation. Modified from Suggett et al. (2009a, 2010). (*) denotes ratios that were reported in the literature as FRRF-PP:^{13/14}C-PP. These were calculated using a conversion factor of 4:1 ETR:FRRF-PP based on the minimum 4 e⁻ (derived from 2 H₂O) required to evolve 1 O₂. 56

Table 11. Ranges of annual primary productivity in temperate estuaries. Table modified from Hodal (2011) and Riche (2011). 63

Table 12. Summary of cruise dates and samples collected. X denotes sample collected. 0, 5, and 30 refer to depths at which samples were collected (m). 82

Table 13. List of photosynthetic unit size [n_{PSII}^{-1} ; $\text{mol chl a} \cdot (\text{mol e}^-)^{-1}$] values reported in the literature. Growth conditions are reported as number of light (E) or nutrient treatments. Values are listed highest to lowest because n_{PSII}^{-1} tends to decrease with increasing light levels or nutrient concentrations. (*) indicates increasing n_{PSII}^{-1} with increasing light, likely due to photoinhibition. Modified from Suggett et al. (2010). 85

Table 14. Example calculation of photosynthetic unit size (n_{PSII}^{-1}) from oxygen flash yields using *Skeletonema costatum* grown under medium light (ML) conditions. Gain: electrical setting on the O₂-electrode control box; in this case, gain was not changed during the experiment. Raw O₂ evolution: data output from linear regression of O₂ measurements by labjackoxy.exe. Gross O₂ evolution: calculated by multiplying raw O₂ evolution and the oxygen saturation constant (in this case, 543.77 $\mu\text{mol} \cdot \text{L}^{-1}$ for salinity 35 and temperature 12°C) then dividing by gain. Slope: the slope of the linear portion of the graph (Figure 17), in this case, 0-20 Hz (*italicized*). Flash yield: *chl a* concentration of the concentrated sample divided by slope. n_{PSII}^{-1} : assumes a 4:1 ratio of O₂:e⁻. 93

Table 15. Comparison of photosynthetic unit size (n_{PSII}^{-1}) values against those in the literature. PFD: photon flux density. μ : growth rate. SE: standard error. Replicates are measurements of independent cultures. Grey columns contain data from Suggett et al. (2009b). 94

Table 16. Photosynthetic unit size (n_{PSII}^{-1}) of species representative of the spring phytoplankton community in Rivers Inlet, BC. PFD: photon flux density. SE: standard error. Replicates are measurements of independent cultures. n_{PSII}^{-1} from F_v/F_m is calculated as a function of F_v/F_m measured by FRRF (Kolber and Falkowski 1993; Section 2.2.11). 95

Table 17. Relative abundances of phytoplankton observed in preserved samples from the head of the inlet in 2009.	98
Table 18. Relative abundances of phytoplankton observed in preserved samples from the centre of the inlet in 2009.	99
Table 19. Relative abundances of phytoplankton observed in preserved samples from the mouth of the inlet in 2009.	100
Table 20. Relative abundances of phytoplankton observed in preserved samples from the head of the inlet in 2010.	101
Table 21. Relative abundances of phytoplankton observed in preserved samples from the centre of the inlet in 2010.	102
Table 22. Relative abundances of phytoplankton observed in preserved samples from the mouth of the inlet in 2010.	103

List of Figures

- Figure 1. Bathymetric map of Rivers Inlet, British Columbia, Canada. Modified from Hodal (2011). 2
- Figure 2. Schematic diagram of electron transport in photosystems (PS) II and I in ambient (a) dark and (b) light conditions. (c) The Z-scheme of electron transport illustrates the change in free energy from solar excitation of electrons. See text for abbreviations. Modified from Falkowski and Raven (2007). 8
- Figure 3. Fluorescence in open and closed photosystem II and I reaction centres (RCII and RCI, respectively). Open RCs have low fluorescence because excitation energy (E) can be quenched by photochemistry (excited electrons are passed to the electron transfer system beginning with Q_A or A_1). Both $P680^+$ and $P700^+$ are equally capable of quenching excitation energy, but the lifetime of $P680^+$ is several orders of magnitude shorter than the lifetime of the closed RCII. $P680^+$ is re-reduced to $P680$ before Q_A^- is re-oxidized to Q_A . Any energy absorbed by $P680$ before Q_A^- is re-oxidized must be dissipated. As a result, the fluorescence yield (F) is high in PSII. Rate-limiting step is circled for each RC. Modified from Oxborough (2007). 10
- Figure 4. Fluorescence kinetics during a FRRF acquisition. Minimum fluorescence, F_o , is determined using only the weak measuring light (dark arrow). Next, a saturating pulse of light is turned on (grey arrow up) to induce maximum fluorescence, F_m . An actinic light is then turned on (white arrow up) to drive photosynthesis, while fluorescence is induced using a series of short, bright flashlets, allowing measurement of light-adapted maximum fluorescence, F_m' . Immediately after the actinic light is turned off (white arrow down), light-adapted minimum fluorescence, F_o' , can be measured. Because this is technically challenging, F_o' is calculated from other fluorescence parameters rather than being measured directly (See Methods). Modified from Büchel and Wilhelm (1993). 11
- Figure 5. The time required to reopen closed photosystem II reaction centres (RCII) is dependent on the redox state of the plastoquinone pool. Lower panels show the effect of single (ST) and multiple (MT) turnover methods on the plastoquinone (PQ) pool. OEC: oxygen evolving complex. Modified from Oxborough (2007). 13
- Figure 6. Schematic representation of fluorescence yields from single (ST) and multiple (MT) turnover FRRF sequences. The duration of each block of flashlets is indicated in bold below the saturation (increase) and relaxation (decrease) phases of each sequence. Numbers in parentheses indicate the number of flashlets during that time block and the frequency with which they are delivered. Note that in the relaxation phase of the MT sequence, flash frequency is measured in Hz, whereas other frequencies are measured in kHz. Modified from Oxborough (2007). 15
- Figure 7. Map of Rivers Inlet, British Columbia including primary sampling stations DFO5 at the head of the inlet, DFO2 at the centre of the inlet, and UBC7 at the mouth of the inlet, Dawson's Landing, and the Laska weather station. In the text, DFO5, DFO2, and UBC7 are referred to as head, centre, and mouth, respectively. 20

Figure 8. Phosphate, silicic acid, and nitrate concentrations (μM) at 0, 5, and 30m at the head of the inlet (station DFO5) from late February to mid-August 2009 (A-C) and mid-March to mid-July 2010 (D-F).....	35
Figure 9. Phosphate, silicic acid, and nitrate concentrations (μM) at 0, 5, and 30m at the centre of the inlet (station DFO2) from late February to mid-August 2009 (A-C) and mid-March to mid-July 2010 (D-F).....	36
Figure 10. Phosphate, silicic acid, and nitrate concentrations (μM) at 0, 5, and 30m at the mouth of the inlet (station UBC7) from late February to mid-August 2009 (A-C) and mid-March to mid-July 2010 (D-F).....	37
Figure 11. Chlorophyll <i>a</i> concentrations ($\mu\text{g} \cdot \text{L}^{-1}$) in 2009 at the (A) head, (B) centre, (C) mouth of the inlet, and in 2010 at the (D) head, (E) centre, and (F) mouth of the inlet.	42
Figure 12 Bloom and high abundance occurrences of phytoplankton taxa in 2009 and 2010 (rankings of 4 and 3, respectively; see text). Solid symbols are blooms, hollow symbols are high-abundance events. Diamonds are diatoms, circles are dinoflagellates. Grey area: no samples analyzed. Ch: <i>Chaetoceros</i> spp. Psn: <i>Pseudo-nitzschia</i> spp. Sk: <i>Skeletonema costatum</i> . Th: <i>Thalassiosira</i> spp. Cyl: <i>Cylindrotheca closterum</i> . Het: <i>Heterocapsa triquetra</i> . Lep: <i>Leptocylindrus minimus</i> . Pro: <i>Prorocentrum minimum</i> . Thn: <i>Thalassionema nitzschioides</i> ; Rhi: <i>Rhizosolenia styliformes</i>	44
Figure 13. Comparison of primary productivity measurements ($\mu\text{g C} \cdot \text{L}^{-1} \cdot \text{h}^{-1}$) calculated from FRRF measurements and from ^{13}C bottle incubations (A) in the laboratory using cultures of <i>Skeletonema costatum</i> and <i>Chaetoceros</i> sp. isolated from Rivers Inlet and field data from (B) 5m, (C) 0m, and (D) 30m depth. Vertical and horizontal scales of A, B, and D are equal in each panel. Note that in C, vertical and horizontal scales are not equal.	46
Figure 14. Comparison of NO_3 (μM), chl <i>a</i> ($\mu\text{g} \cdot \text{L}^{-1}$), and FRRF-derived primary productivity measurements [FRRF-PP, $\mu\text{g C} \cdot (\text{L} \cdot \text{h})^{-1}$] from 5m depth in 2009 at the (A) head, (B) centre, (C) mouth, and (D) in 2010 at the centre of the inlet. FRRF-PP is on the primary axis. NO_3 and chl <i>a</i> are on the secondary axis.	49
Figure 15. Detail of (a) oxygen electrode and (b) electrode chamber used to measure oxygen flash yields.	89
Figure 16. Oxygen evolution trace from <i>Skeletonema costatum</i> grown under medium light (ML) conditions. Vertical lines indicate different sections of the experiment. Sat.: O_2 -saturated synthetic ocean water (SOW). Zero: N_2 -bubbled, O_2 -minimum SOW. All other sections measure O_2 evolution on the concentrated phytoplankton culture. Large shifts between sections are an artifact of the experiment. Because slope is measured, these shifts do not affect results. 92	
Figure 17. Example plot of oxygen flash yield results from <i>Skeletonema costatum</i> grown under medium light (ML) conditions. The initial linear slope of this graph, in this case 0 – 20 Hz, is used to calculate photosynthetic unit size (n_{PSII}^{-1}). See text and Table 13.....	93

Acknowledgements

I would like to thank Dr. Maite Maldonado for her invaluable guidance, insight, patience, and support throughout my degree, without which this would not have been possible. Her keen editor's eye has made this thesis much stronger than it would otherwise have been. Thank you to Dr. Evgeny Pakhomov, who shared his knowledge of the Rivers Inlet ecosystem and allowed me to see how my project fit into the bigger picture. Thank you to Dr. Brian Hunt, who was unfailingly patient in the face of my many requests and questions. And thanks to Dr. Philippe Tortell for his assistance with isotopic calculations of primary productivity and for his feedback on this thesis.

Thank you to all of those involved in the Rivers Inlet field program: Dr. Hunt, Dr. Pakhomov, Lora Pakhomova, Chris Payne, Désirée Tommasi, Asha Ajmani, Mike Hodal, Kang Wang, and Jessica Nephin from UBC; Dr. Rick Routledge, Nicole Gerbrandt, and Jennifer Parkhouse from SFU; the Bachen family, the Wuikinuxv First Nation, and the crew of the MV *Western Bounty* from Rivers Inlet. I would also like to thank the Tula Foundation, which has generously funded the Rivers Inlet Ecosystem Study.

Thank you to all of those in the Tornado and Pakhomov lab groups for their support and encouragement. Thanks especially to Constance Couture and Dr. David Cassis for their help in the lab. Special thanks to Rebecca Taylor and James Boak, for cheerleading and for showing me by their example that I, too, could do this. Finally, I could not have completed this journey without the steady support of my friends and my families (both my San Diego family and my Vancouver family).

Chapter 1: General introduction

1.1 Introduction to the Rivers Inlet ecosystem

Rivers Inlet is a large (40 km x 3 km) fjord on the central coast of British Columbia, Canada (51.43°N, 127.63°W). The inlet is 200 – 300m deep throughout (Figure 1). Like many temperate fjords, Rivers Inlet is characterized by a strong diatom-dominated spring phytoplankton bloom followed by a copepod-dominated zooplankton bloom (e.g., Harrison et al. 1983). Also typical of temperate fjords, water movement in Rivers Inlet is controlled by estuarine circulation, in which a shallow surface layer of freshwater moves out of the inlet into Queen Charlotte Sound and nutrient-rich deep seawater enters the inlet over a shallow (~100m) sill near the inlet's mouth. Surrounded by steep terrain and temperate rainforests, the fjord drains a catchment area of over 6000 km². Freshwater input to the fjord is primarily from Owikeno Lake via the short Wannock River. The lake is as large as the inlet (Figure 1), glacially fed, and oligotrophic (average chl_a < 1.5 μg · L⁻¹; Shortreed and Morton 2003). In spite of its low nutrient concentrations, Owikeno Lake acts as the main nursery for the Rivers Inlet sockeye population.

In late summer, adult sockeye migrate from the ocean through Rivers Inlet to spawn in freshwater streams and rivers. Females lay their eggs in gravel beds at the stream bottom. Eggs hatch by early spring and the fry swim into the lake in early summer. Unlike many other sockeye populations in the Pacific Northwest (Pauley et al. 1989), Rivers Inlet sockeye fry generally spend only one winter in their freshwater habitat (Gilbert 1915, Foskett 1958, McKinnell et al. 1998, 2001). The juvenile sockeye transition to a marine habitat by migrating out through the fjord in the spring. When they enter the marine environment, Rivers Inlet sockeye smolts are smaller than other British Columbia sockeye smolts (average weight of 2 g

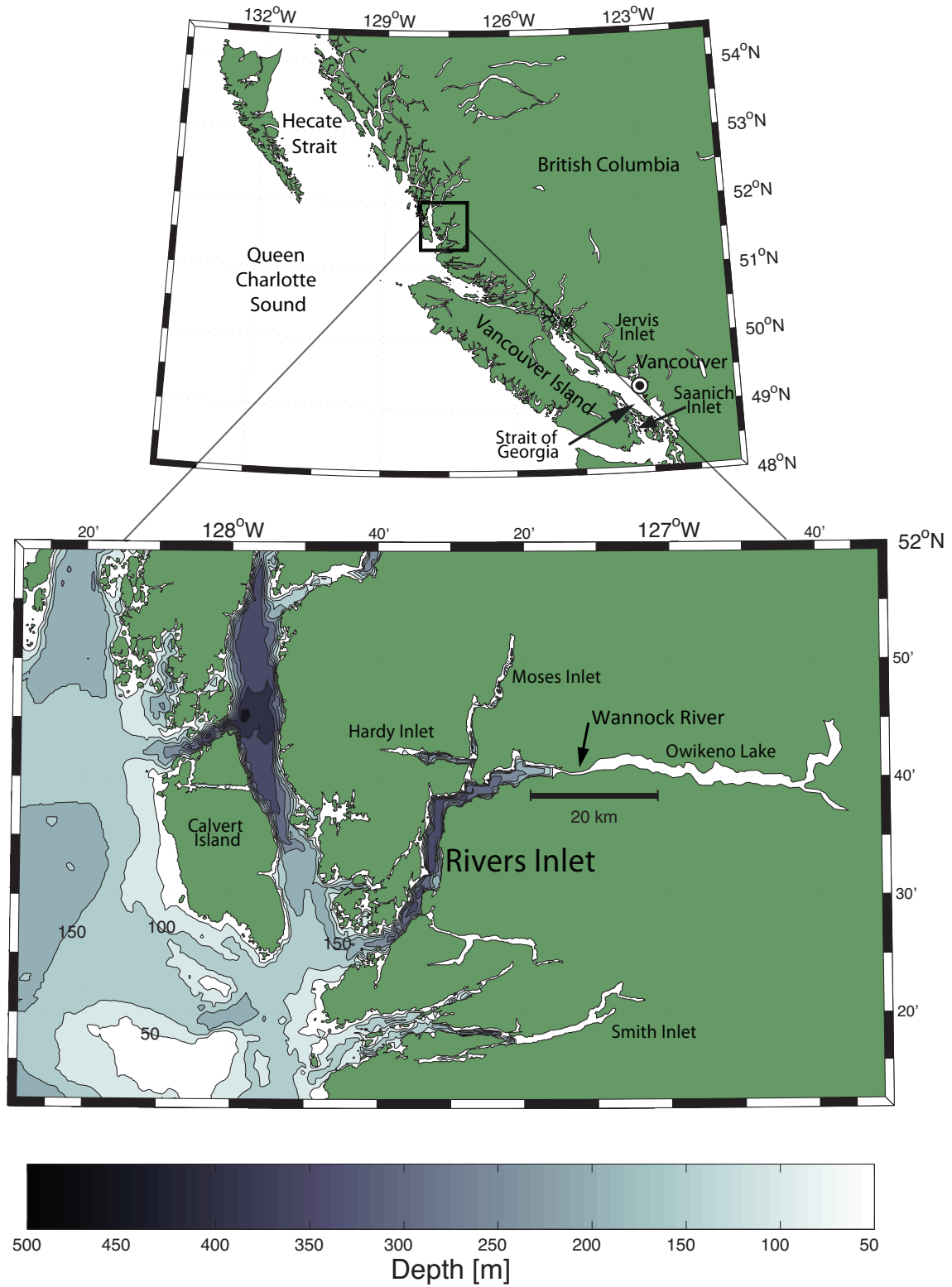


Figure 1. Bathymetric map of Rivers Inlet, British Columbia, Canada. Modified from Hodal (2011).

versus 4-8 g; Foskett 1958). As these small Rivers Inlet smolts migrate to the open ocean, feeding and growth in the fjord are crucial, as larger smolts are more likely to survive to adulthood and return to the inlet to breed (Beamish et al. 1998). The timing of the sockeye smolt out-migration varies little between years, with the smolts entering the inlet in mid-May, peaking at the first new moon in June, and continuing into July (Buchanan 2006). These sockeye typically spend two years at sea, after which they return as adults to their natal streams to spawn and die.

Historically, the sockeye salmon (*Oncorhynchus nerka*) of Rivers Inlet were abundant, with annual returns regularly exceeding a million adults. The stock supported the third-largest sockeye fishery in Canada. In addition to their large economic significance, sockeye are also important to First Nations people and to the Rivers Inlet ecosystem as a whole. The Wuikinuxv First Nation community utilizes sockeye for sustenance, as a central part of their local economy, and it is of great cultural importance. Ecologically, salmon are a keystone species that is critical to the health of the ecosystem. Salmon runs help feed top predators such as seals and orcas. When adult salmon return to their freshwater spawning habitats, they bring nutrients and resources from the open ocean. For example, spawning salmon feed bears and their carcasses fertilize trees (e.g., Helfield and Naiman 2001). Large shifts in salmon populations thus affect the entire ecosystem and the people who rely on them.

In the late 1970s, the Rivers Inlet sockeye stock became unstable and ultimately crashed in the early 1990s. The commercial fishery closed in 1996, but the stock has yet to recover (McKinnell et al. 2001, W. Levesque pers. comm.). Preliminary results indicate that the decline is related to early marine survival (McKinnell et al. 2001, Levy 2006). Previous studies in Rivers Inlet found that higher abundances of the smolts' zooplankton prey during this crucial

period are positively correlated with larger, more robust smolts (Buchanan 2006, Ajmani 2011). A reduced zooplankton bloom or a timing mismatch (Cushing 1990) of zooplankton bloom and smolt out-migration may thus have negatively affected the marine survival of smolts (Buchanan 2006).

An analysis of sockeye smolt gut contents showed a high abundance of copepods, cladocerans, and bivalves (Ajmani 2011). Relative to abundance in the water column, smolts appear to prefer amphipods, cirripeds, decapods, and fish (Ajmani 2011). Prey types consumed by the smolts changed interannually, reflecting between-year changes in zooplankton community composition (Ajmani 2011). Tommasi (2008) and Tommasi et al. (2012a, b) observed that a late spring phytoplankton bloom corresponded to a delayed and reduced zooplankton bloom with zooplankton community composition shifting to smaller copepod species. For example, while copepods were abundant in all years, there were fewer large calanoids and more acartiids and ectinosomatids associated with a late spring phytoplankton bloom (Tommasi et al. 2012a). There was also a reduction in the biomass of carnivorous zooplankton (chaetognaths, polychaetes, amphipods, ostracods), pteropods, appendicularians, and euphausiids in late bloom years. In contrast, small fast-growing omnivorous zooplankton (bryozoan larvae and the copepods *Oithona* spp. and *Acartia longiremis*) were able to maintain comparable biomass between years despite shifts in the timing of the phytoplankton bloom (Tommasi et al. 2012b). Controls of zooplankton community composition and succession are not fully understood and may be controlled by species-specific effects of physical (temperature and advection) and/or biological factors (e.g., food availability as a result of the phytoplankton bloom; (Tommasi et al. 2012b). As a result of these physical and biological controls, the timing, magnitude, and

composition of the zooplankton bloom is highly variable between years (Tommasi 2008, Ajmani 2011, Tommasi et al. 2012a, b).

Like the zooplankton bloom, there is also variability in the timing of the spring phytoplankton bloom. In general, phytoplankton bloom timing is dependent on light and nutrient availability (Reynolds 2006). In Rivers Inlet, bloom initiation is also strongly influenced by freshwater discharge from the Owikeno River and outflow wind events (Wolfe 2010). High freshwater discharge causes strong stratification in the surface layer. This decreases nutrient availability but also increases light availability (Wolfe 2010). Outflow wind events increase estuarine circulation and upwelling of nutrients, but also push the surface layer rapidly out to sea, flushing large portions of the phytoplankton population out of the inlet (Wolfe 2010). As a result of these influences, initiation of the spring bloom varies widely between years (mid-March to late April in 2006-2010; Tommasi 2008, Wolfe 2010). Ware and Thomson (2005) found strong bottom-up trophic links between phytoplankton biomass, zooplankton biomass, and fish yields in southern British Columbia. Thus, variability in the timing and magnitude of the spring phytoplankton bloom affects the zooplankton population that relies on phytoplankton for food and this, in turn, affects the sockeye smolts that eat the zooplankton. As such, it is critical to measure the timing and magnitude of the spring phytoplankton bloom, the rate at which phytoplankton biomass turns over (i.e., primary productivity), and how primary productivity changes throughout the season in order to understand phytoplankton community dynamics.

1.2 Background on primary productivity measurements

Classical primary productivity (PP) measurements are made using either carbon-uptake (Steemann Nielsen 1952) or oxygen-evolution (e.g., Bryan 1976, Williams and Jenkinson 1982,

Bender et al. 1987) methods. These methods are time-consuming, involving lengthy (hours to a day) bottle incubations and measurements after the incubations are over. Because considerable time and effort are required, these methods generate data at low spatial and temporal resolution. In addition, incubating discrete water samples in bottles creates small-scale artificial ecosystems where tracer molecules can be exchanged through various possible pathways (Falkowski and Raven 2007). Furthermore, once a sample is isolated in a bottle, it is difficult to mimic the natural light variability that the cells would have experienced *in situ* due to turbulent mixing (e.g., Marra 1980, MacIntyre et al. 2000). Working with radioisotopes is also both expensive and hazardous. As a result of these constraints, researchers are increasingly favouring fluorometric techniques to study PP. Chlorophyll *a*-specific fluorometers such as the fast repetition rate fluorometer (FRRF; Kolber et al. 1998) allow for rapid, minimally invasive, highly spatially and temporally resolved sampling that is not possible with bottle incubations. The instruments themselves are commercially available, compact, and can be deployed into the water, making them very versatile.

1.3 Photosynthesis and fluorometry background

While classical primary productivity measurements use the ‘currencies’ (Suggett et al. 2009a) of carbon and oxygen, fluorescence techniques use the currency of electrons, specifically the electron turnover rate of photosystem II (ETR). In order to understand what is measured by these different currencies, the biophysical theory underlying fluorescence-based measurements of primary productivity is discussed below. Further information can be obtained from many texts (e.g., Kolber and Falkowski 1993, Kromkamp and Forster 2003, Falkowski et al. 2004, Falkowski and Raven 2007).

Photosynthesis is the process by which solar energy is used by autotrophic organisms to convert inorganic carbon into organic molecules. In eukaryotic cells, this process occurs in the chloroplasts, specialized organelles that contain stacks of thylakoids, membrane-bound sacks. Inside the thylakoids is the lumen and surrounding the thylakoids is the stroma. Both spaces are filled with an aqueous matrix. Unlike in eukaryotes, in prokaryotes, the thylakoids are loose in the cytoplasm. Embedded in the thylakoid membranes of both prokaryotes and eukaryotes are the proteins and pigments responsible for photosynthesis.

Photosystems (PS) II and I are protein complexes situated in the thylakoid membranes of the chloroplast. Each PSII and PSI is composed of an antenna pigment complex coupled to a reaction centre (RCII and RCI, respectively). In the antennae are light-harvesting complexes of pigments and proteins that funnel light to the reaction centre. Phytoplankton taxa each have a distinct combination of light-capturing pigments. Light is passed from the antenna to a chlorophyll *a*-protein complex within the reaction centre (P680 in RCII and P700 in RCI). P680 and P700 absorb light at wavelengths 680 and 700 nm, respectively.

The incoming light energy builds up in the reaction centre until an electron (e^-) is sufficiently excited to escape its orbital. In PSII, the excited electron is captured by the electron transfer system (1st ETS) and transported following the z-scheme from the quinone Q_A to Q_B to plastoquinone (PQ) to cytochrome b_6/f to plastocyanin (PC), which links to PSI (Figure 2). P680 replaces the lost electron by taking one from H_2O via a water-splitting manganese-protein complex. In PSI, the excited electron is passed through several electron carriers to ferredoxin (2nd ETS) where an enzyme reduces $NADP^+$ to NADPH. P700 replaces the lost electron by

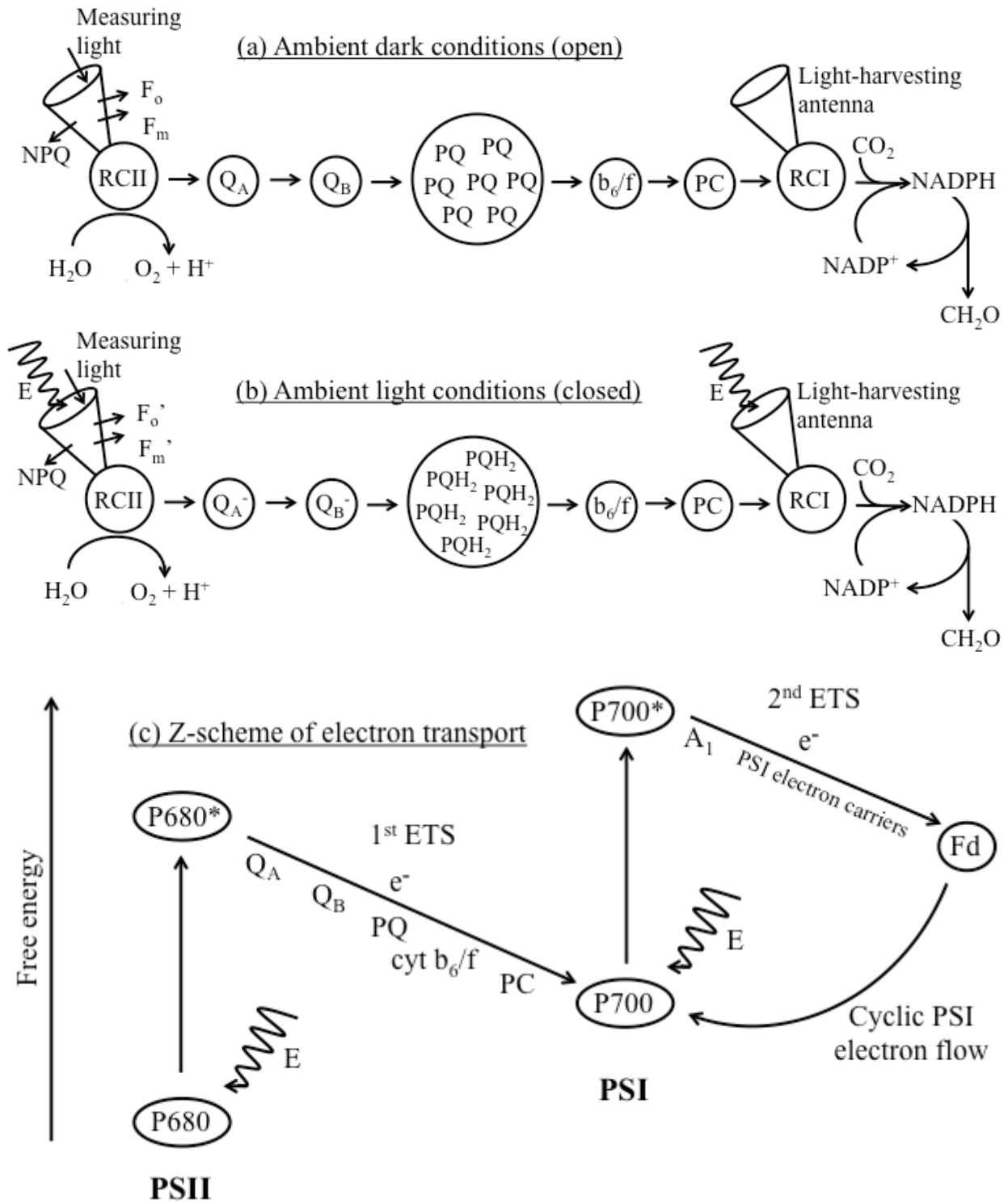
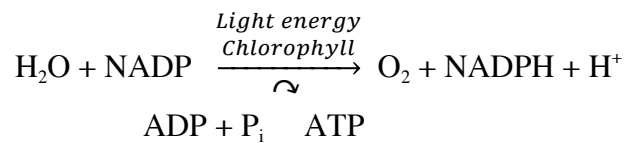
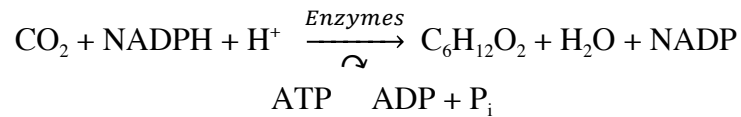


Figure 2. Schematic diagram of electron transport in photosystems (PS) II and I in ambient (a) dark and (b) light conditions. (c) The Z-scheme of electron transport illustrates the change in free energy from solar excitation of electrons. See text for abbreviations. Modified from Falkowski and Raven (2007).

taking one from PC, the final electron carrier in the 1st ETS. This chain of electron transfers causes protons to be pumped from the thylakoid stroma into the lumen, establishing an electrochemical gradient that is used to drive ATP synthesis in the stroma. The above series of events comprise the light reactions of photosynthesis, which can be summarized as:



The light reactions provide the energy to drive the dark reactions of photosynthesis, where CO₂ is integrated into organic matter in the stroma:



The light and dark reactions together describe gross primary production by phytoplankton. However, not all light energy absorbed by phytoplankton is used to drive photosynthesis (photochemistry). Indeed, the absorbed excess energy can be dissipated as non-radiative decay (non-photochemical quenching), such as heat, or can be reemitted as light (fluorescence). These quenching pathways serve to protect the cells by dissipating excess energy that could otherwise cause damage. It is the fluorescence of light by the pigment chlorophyll *a* (chl*a*) that is measured by fluorometers such as the FRRF.

In order to understand the fluorescence measured by the FRRF, we revisit the photosynthetic electron transfer chain (Figure 2). When an electron within PSII is excited, it is donated from P680 to the first stable electron acceptor, Q_A. Q_A becomes reduced to Q_A⁻ and the reaction centre is said to be closed. Any additional light energy received while the reaction center is closed must be dissipated. When Q_A is oxidized, the reaction centre is said to be open and the energy can be passed through the electron transfer system and used for photochemistry. Thus, the proportion of light energy used for photochemistry vs. reemitted as fluorescence

(closed RCII) reflects the relative number of open reaction centres (Q_A oxidized and able to accept electrons from P680). Studies of chl*a* fluorescence focus on PSII because the majority of fluorescence is emitted by PSII (>90%; Barber et al. 1989; Figure 3). In PSII, the rate-limiting step is the reoxidation of Q_A^- to Q_A . As a result, $P680^+$ is unable to pass an electron to Q_A^- and dissipates the energy as fluorescence. The reduction of $P680^+$ to P680 is rapid, meaning that P680 is capable of being re-excited and fluorescing again almost immediately even as the reaction centre remains closed. In PSI, the rate-limiting step is the reduction of $P700^+$ back to P700. $P700^+$ cannot donate another electron or fluoresce until it is re-reduced and must dissipate excess energy through non-photochemical quenching. Because of this, a closed RCI ($P700^+$) is at

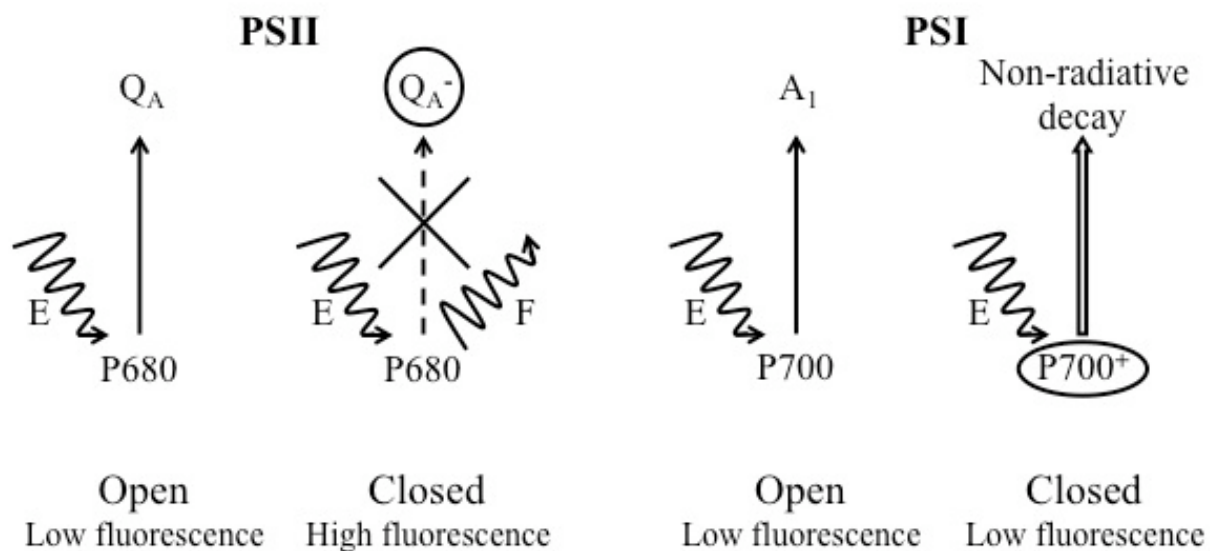


Figure 3. Fluorescence in open and closed photosystem II and I reaction centres (RCII and RCI, respectively). Open RCs have low fluorescence because excitation energy (E) can be quenched by photochemistry (excited electrons are passed to the electron transfer system beginning with Q_A or A_1). Both $P680^+$ and $P700^+$ are equally capable of quenching excitation energy, but the lifetime of $P680^+$ is several orders of magnitude shorter than the lifetime of the closed RCII. $P680^+$ is re-reduced to P680 before Q_A^- is re-oxidized to Q_A . Any energy absorbed by P680 before Q_A^- is re-oxidized must be dissipated. As a result, the fluorescence yield (F) is high in PSII. Rate-limiting step is circled for each RC. Modified from Oxborough (2007).

a low fluorescence state for most of its lifetime, while a closed RCII (P680) is in a high fluorescence state for most of its lifetime (Figure 3).

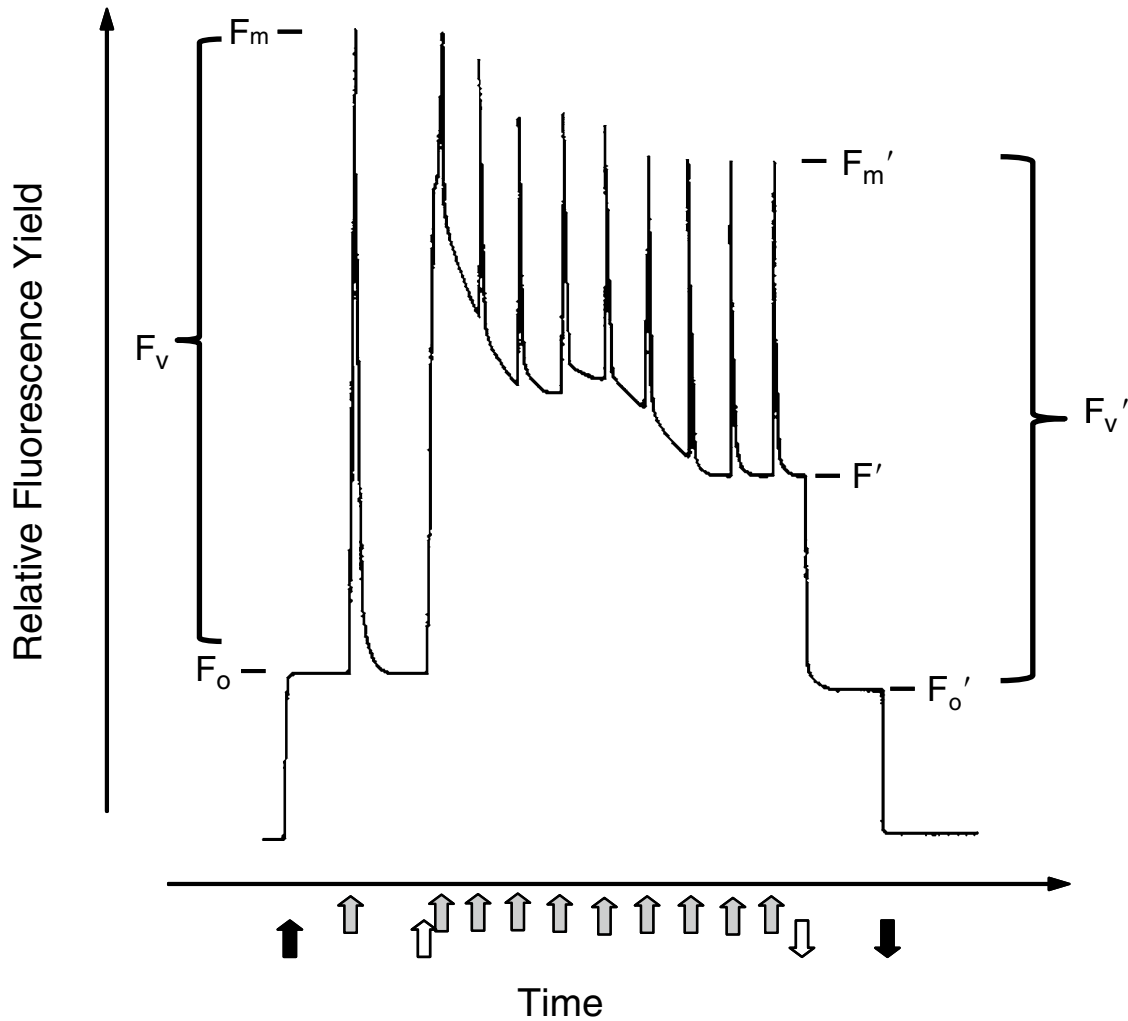


Figure 4. Fluorescence kinetics during a FRRF acquisition. Minimum fluorescence, F_0 , is determined using only the weak measuring light (dark arrow). Next, a saturating pulse of light is turned on (grey arrow up) to induce maximum fluorescence, F_m . An actinic light is then turned on (white arrow up) to drive photosynthesis, while fluorescence is induced using a series of short, bright flashlets, allowing measurement of light-adapted maximum fluorescence, F_m' . Immediately after the actinic light is turned off (white arrow down), light-adapted minimum fluorescence, F_0' , can be measured. Because this is technically challenging, F_0' is calculated from other fluorescence parameters rather than being measured directly (See Methods). Modified from Büchel and Wilhelm (1993).

The use of variable *chl a* fluorescence to measure photosynthetic electron transport is based on examining changes in fluorescence yield changes in relation to the proportion of open reaction centres. Minimum fluorescence (F_o , dimensionless) occurs when approximately all reaction centres are open and capable of using light energy for photochemistry (Figure 4). Maximum fluorescence (F_m , dimensionless) occurs when approximately all reaction centres are closed, none of the incident light energy can be used for photosynthesis, and the energy must be dissipated through fluorescence or other pathways. These parameters can be measured in dark-adapted (F_o , F_m) and light-adapted (F_o' , F_m') cells. F_o' is difficult to measure and is more often calculated from other fluorescence parameters (Oxborough and Baker 1997; see Section 2.2.11). The FRRF has a weak measuring light that allows measurement of F_o without closing any additional reaction centres. FRRFs measure F_m and F_m' with a series of rapid, short, bright flashes (flashlets). Each flashlet is sub-saturating for electron transport, but cumulatively, a block of flashlets in rapid succession saturates the reaction centres (Falkowski and Kolber 1995). The single turnover (ST) method induces a single electron transfer in each PSII by using a relatively short saturating pulse of light (60 – 200 μs) compared to the time required to reopen a closed RCII (300 – 600 μs). Because of the short duration of the saturating pulse, there is minimal change to the redox state of the plastoquinone pool (Figure 5). That is, the ratio of oxidized to reduced down-stream electron acceptors (PQ:PQH₂) is minimally affected and the reactions centres can reopen quickly. In contrast, the multiple turnover (MT) method uses a longer saturating pulse to drive the PQ:PQH₂ ratio very low. As a result, the time required for RCII to reopen (relaxation time) is longer in MT than in ST. F_m measured using the MT method is higher than F_m using ST (Figure 6). As a result, the two are not comparable and caution must

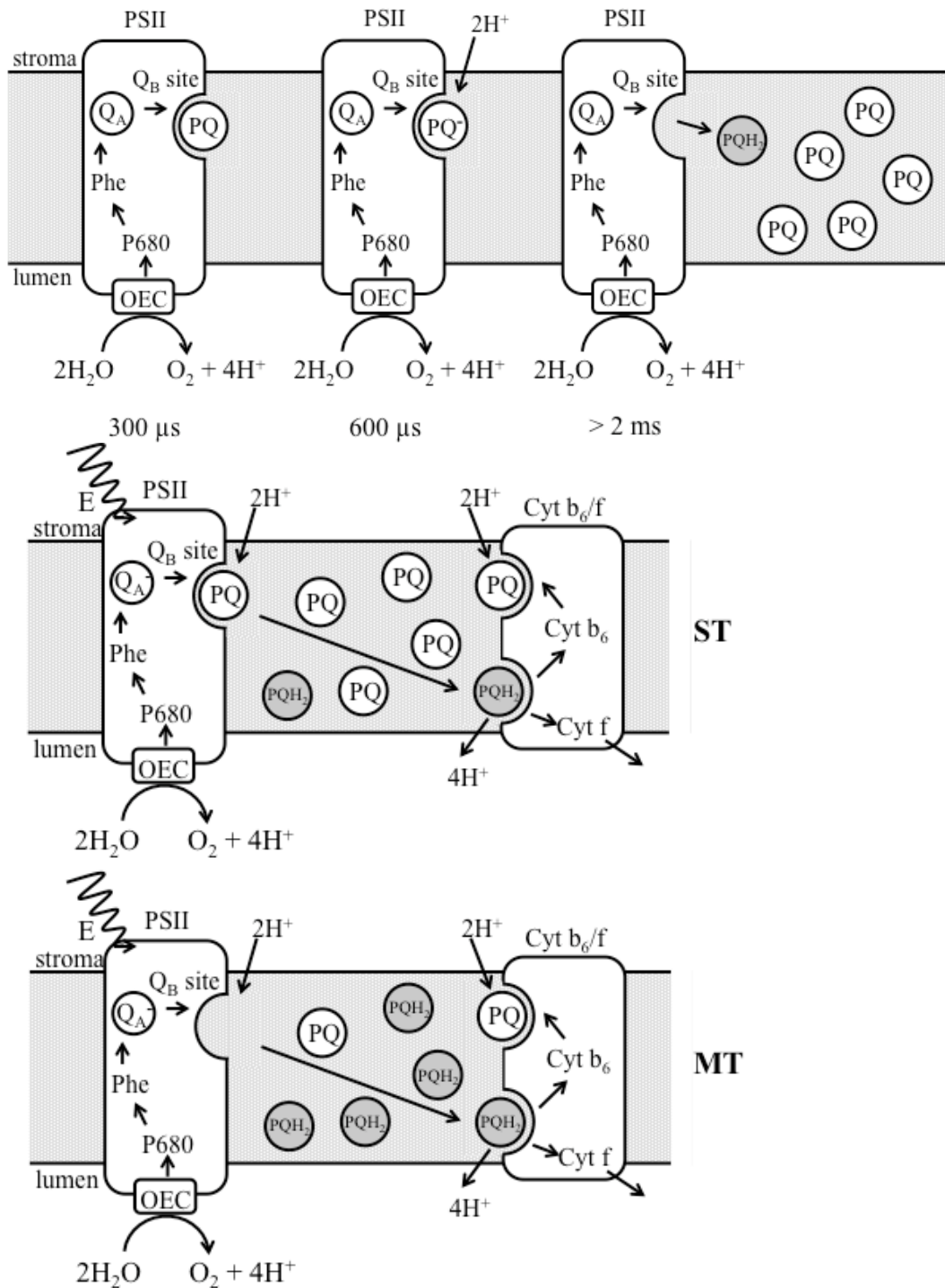


Figure 5. The time required to reopen closed photosystem II reaction centres (RCII) is dependent on the redox state of the plastoquinone pool. Lower panels show the effect of single (ST) and multiple (MT) turnover methods on the plastoquinone (PQ) pool. OEC: oxygen evolving complex. Modified from Oxborough (2007).

be used when interpreting results from early fluorescence studies, where the distinction is often not clear (Maxwell and Johnson 2000).

In this study, we focus our analyses on ST measurements because of weaknesses inherent to the MT method both in data analysis and acquisition. MT measurements are relatively slow, typically requiring several hundred ms for a single sequence. During such a sequence, a fluorometer moving quickly underwater or in a fast current would measure multiple parcels of water, rather than a single relatively constant patch. As a result, F_m would not be reached and the photochemical efficiency of PSII (F_v/F_m , see below) would likely be significantly underestimated. Furthermore, MT sequences cannot measure the functional absorption cross-section (σ_{PSII} , see below), which is needed to calculate primary productivity. We include MT sequences in our protocol because the low flash frequency during the relaxation phase decreases the time needed to reoxidize Q_A (Oxborough 2007).

Using the simple fluorescence parameters described above, we can calculate the photochemical efficiency of PSII, F_v/F_m (dimensionless). Where F_v is the variable fluorescence yield ($F_m - F_o$). Fluorescence yield curves (Figure 6) also give the rate at which RCII's are closed. This initial slope of the saturation phase is termed the functional absorption cross-section of PSII, σ_{PSII} (also referred to as the effective absorption cross-section; $\text{\AA}^2 \cdot \text{quanta}^{-1}$). Using these parameters and independent measures of light (PAR, $\mu\text{E} \cdot \text{m}^{-2} \cdot \text{s}^{-1}$) and chl*a* concentration ($\mu\text{g} \cdot \text{L}^{-1}$), electron turnover rate (ETR) and primary productivity can be calculated (Section 2.2.11).

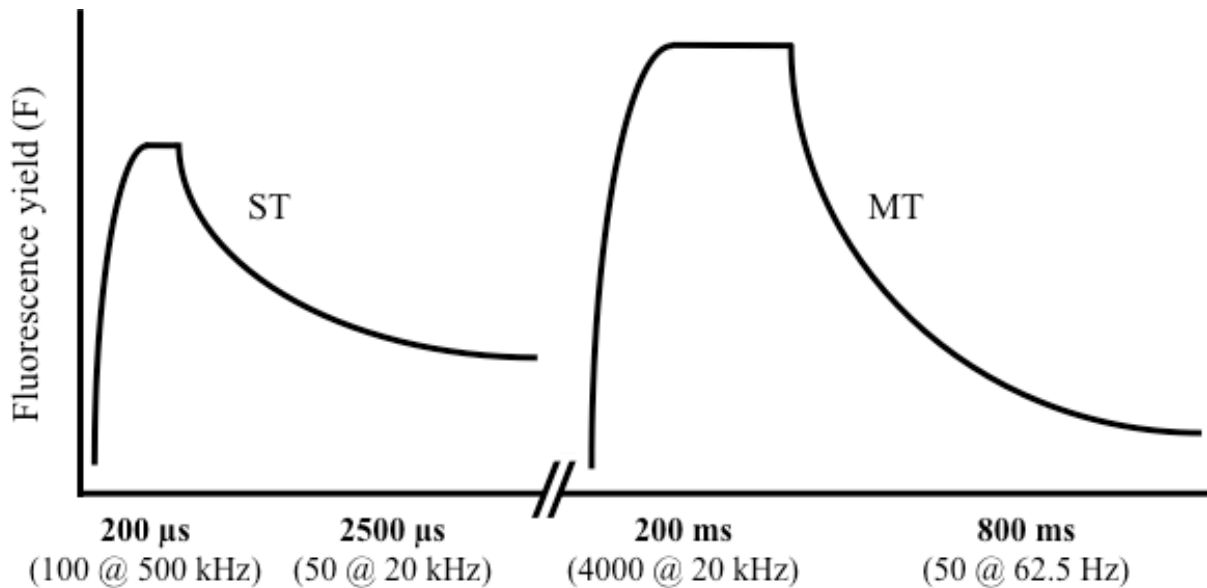


Figure 6. Schematic representation of fluorescence yields from single (ST) and multiple (MT) turnover FRRF sequences. The duration of each block of flashlets is indicated in bold below the saturation (increase) and relaxation (decrease) phases of each sequence. Numbers in parentheses indicate the number of flashlets during that time block and the frequency with which they are delivered. Note that in the relaxation phase of the MT sequence, flash frequency is measured in Hz, whereas other frequencies are measured in kHz. Modified from Oxborough (2007).

1.4 Research objectives

The primary objective of the Rivers Inlet Ecosystem Study (RIES), of which this thesis is a part, is to investigate the factors influencing the early life history of the Rivers Inlet sockeye salmon (*Oncorhynchus nerka*). This thesis focuses on the spring phytoplankton bloom that, through strong bottom-up trophic controls (Ware and Thomson 2005), influences the early marine survival of the Rivers Inlet sockeye salmon. This study aims to (a) describe spring phytoplankton community dynamics in Rivers Inlet to be used as a baseline for future studies and (b) assess the accuracy and precision of fast repetition rate fluorometer (FRRF) measurements of primary productivity in the field. Ultimately, this research will assess the feasibility of using FRRF to measure primary productivity in Rivers Inlet in the future and shed light on the trophic interactions between phytoplankton and salmon.

Chapter 2: Spring and summer phytoplankton community dynamics and comparison of FRRF- and ^{13}C -derived measurements of primary productivity in Rivers Inlet, British Columbia

2.1 Introduction

For the majority of the 20th century, the sockeye salmon (*Oncorhynchus nerka*) of Rivers Inlet, British Columbia, were abundant and supported the third-largest sockeye fishery in Canada. The stock became unstable in the late 1970s and crashed in the early 1990s. Despite the closure of the commercial fishery in 1996, the stock has yet to recover (McKinnell et al. 2001, W. Levesque pers. comm.). It appears that the collapse is related to reduced smolt survival during the early marine phase of their life cycle (McKinnell et al. 2001, Levy 2006). Smolts are present in the fjord in spring as they migrate from the brood lake to the ocean. Sockeye typically spend two years at sea before returning as adults to spawn in their natal streams.

Strong bottom-up trophic linkages have been found between phytoplankton biomass, zooplankton biomass, and fish yields in southern British Columbia (Ware and Thomson 2005). Temperate coastal estuaries typically have intense, highly productive, diatom-dominated spring phytoplankton blooms and a more diverse summer community (e.g., Harrison et al. 1983). Phytoplankton community composition determines the molecular composition of the zooplankton and thus influences the quality of food smolts eat (El-Sabaawi et al. 2009). The timing of the spring bloom is controlled by light and nutrient availability (Reynolds 2006). Modeling studies have demonstrated that advective loss due to freshwater input and outflow wind events also influence bloom timing in Rivers Inlet (Wolfe 2010). Therefore, the timing of the spring bloom varies widely between years (mid-March to late April in 2006-2010; Tommasi

2008, Wolfe 2010). Variability in the timing, magnitude, and composition of the bloom influence the zooplankton that feed on the phytoplankton, and the sockeye smolts that feed on the copepod-dominated zooplankton community (Tommasi 2008). In order to understand factors that influence the current sockeye salmon population and its recovery, it is critical to study phytoplankton dynamics including the rate of biomass turnover (primary productivity) and its seasonality.

Because classical techniques for measuring primary productivity (PP) are time-consuming, expensive, and have difficulty mimicking *in situ* conditions, scientists have increasingly come to rely on newer fluorescence-based measurements of PP over older carbon-uptake (Steemann Nielsen 1952) and oxygen-evolution (e.g., Bryan 1976, Williams and Jenkinson 1982, Bender et al. 1987) techniques. These methods inherently measure different processes. Assuming short incubation lengths, the $^{13/14}\text{C}$ -uptake method measures the incorporation of $^{13/14}\text{CO}_2$ into organic carbon by the light and dark reactions of photosynthesis, while the O_2 -evolution method measures the evolution of oxygen from water by the light reactions of photosynthesis. In contrast, fluorescence-based methods measure the electron turnover rate of photosystem II (ETR) and mainly reflect activity of the light reactions of photosynthesis. The exchange rates between these different “currencies” of photosynthesis are highly variable, highlighting the need to better understand how the processes underlying these methods are coupled (Suggett et al. 2009a).

Over the past two decades, comparative studies between fluorescence and C-uptake measurements of PP have become common (e.g., Kolber and Falkowski 1993, Suggett et al. 2001, 2003, Tripathy et al. 2010). Genty et al. (1989) presented the first evidence that ETR and CO_2 uptake are linearly related in maize. However, linearity does not hold under all

environmental conditions (see Baker and Oxborough 2004). In theory, the ratio between the electron transfer rate of photosystem II (PSII) and CO₂ uptake (ETR:CO₂) should be 4, because 4 PSII electrons (derived from 2 water molecules) are required to produce 1 O₂ molecule. The reported ratios, however, range from 2.5 to 12 mol e⁻ · (mol CO₂)⁻¹ for phytoplankton (Suggett et al. 2009a). The mechanisms underlying ratios < 4 are not clear. Ratios > 4 are indicative of various cell processes that decouple ETR and CO₂ uptake and may include: (a) alternate physiological electron sinks (Lewitus and Kana 1995, Badger et al. 2000, Beardall et al. 2003) such as the Mehler reaction (Behrenfeld et al. 2008, Suggett et al. 2009a); (b) cyclic electron transfer around PSII (Prášil et al. 1996); and/or (c) electron slippage back to the water-oxidizing complex (Quigg et al. 2006). The wide range of reported ratios point to inherent differences in FRRF and C-uptake methodologies (Suggett et al. 2009a). FRRF measures activity in the light reactions of photosynthesis, while C-uptake (CO₂ incorporation into organic carbon) measures processes in both the light and dark reactions of photosynthesis. In addition, FRRF measurements are collected on a timescale of microseconds, though multiple individual measurements are often averaged (e.g., Corno et al. 2005, Suggett et al. 2006), giving a timescale of seconds to minutes. As a result, FRRF measurements yield a snapshot, which may not represent the average conditions experienced by the phytoplankton population (Suggett et al. 2009a). In contrast, bottle incubations to measure carbon assimilation are hours to a day in length and consequently incorporate longer-scale physiological processes such as photoinhibition, photoacclimation, pigment turnover, and protein synthesis (MacIntyre et al. 2000). Furthermore, the method of incubation (*in situ*, simulated *in situ*, using a photosynthetron) may also affect C-uptake measurements (Suggett et al. 2009a).

It is also assumed that there is a constant relationship between oxygen evolution (and thus

electron transport) and carbon fixation (photosynthetic quotient, PQ; Section 2.2.11). Species composition of natural phytoplankton assemblages and their nutrient status (e.g., nutrient replete, nutrient starved, acclimated to nutrient limitation) complicate analysis of FRRF data. Interpretation of FRRF PP data and comparison with other PP methods is further complicated by the fact that no single method of calculation is currently universally accepted (Suggett et al. 2010). In spite of these challenges, researchers have had good success comparing FRRF PP measurements with those made by C-uptake incubations in a wide range of environments. Few studies (e.g., Raateoja et al. 2004, Estevez-Blanco et al. 2006, Melrose et al. 2006, Tripathy et al. 2010), however, have been made in coastal waters where suspended solids and other terrigenous materials influence the optical properties of the water. As such, this study aims to characterize the phytoplankton dynamics in a coastal fjord in British Columbia, Canada. Specifically, we will describe how nutrient levels and stratification control primary productivity and how phytoplankton abundance and community composition change throughout the growing season. We also compare primary productivity measurements collected using a fast repetition rate fluorometer (FRRF) and 2-hour ^{13}C -uptake incubations to assess the accuracy of the FRRF in measuring primary productivity in natural phytoplankton assemblages. With this information, we consider how future changes to phytoplankton community dynamics will impact the sockeye salmon stock in Rivers Inlet.

2.2 Materials and methods

2.2.1 Study area and sampling scheme

Rivers Inlet is a large coastal fjord (40km long and 3km wide) located on the central coast of British Columbia, Canada. The inlet is approximately 200 – 300m deep, with a shallow

sill (~100m) near the mouth. It receives much of its fresh water input from the glacially fed Owikeno Lake via the Wannock River (Figure 7). Owikeno Lake is approximately the same size as the inlet and is surrounded by temperate rainforest. Due to steep terrain and the remote location of the watershed, minimal development surrounds the inlet, though some logging has occurred on the watershed.

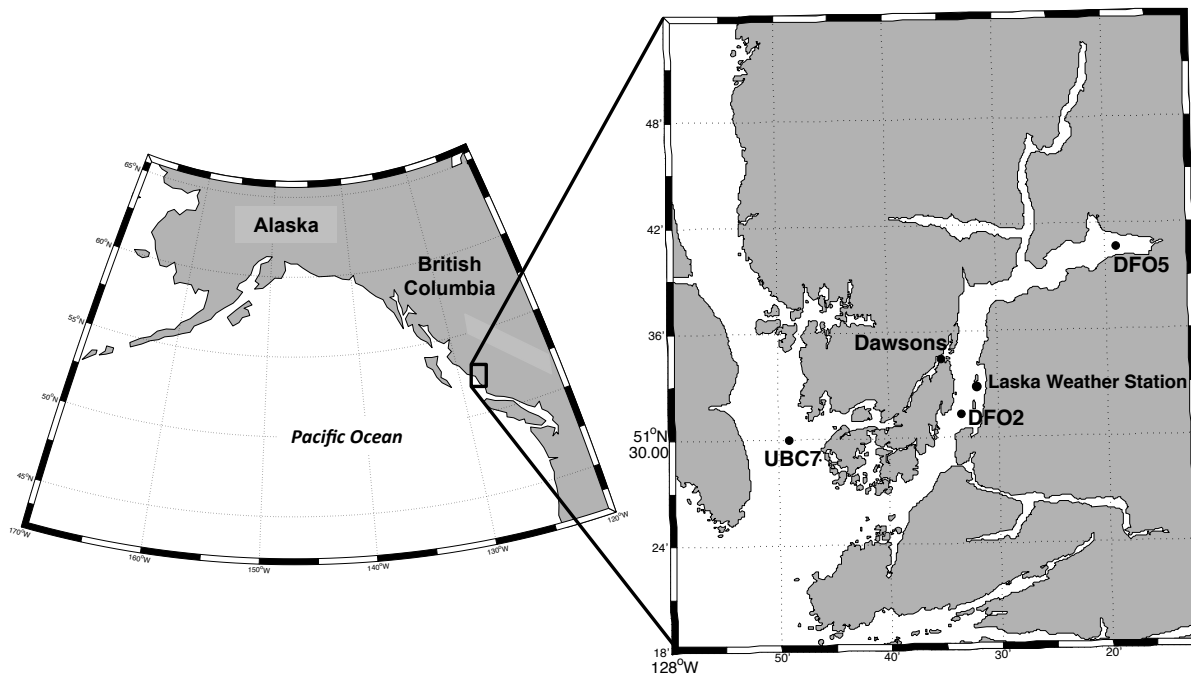


Figure 7. Map of Rivers Inlet, British Columbia including primary sampling stations DFO5 at the head of the inlet, DFO2 at the centre of the inlet, and UBC7 at the mouth of the inlet, Dawson's Landing, and the Laska weather station. In the text, DFO5, DFO2, and UBC7 are referred to as head, centre, and mouth, respectively.

In 2009, we conducted 11 fortnightly oceanographic surveys aboard the MV *Western Bounty* from late February to mid-August. Three primary stations were surveyed: DFO5 (51.677°N, 127.317°W) located at the head of the inlet, DFO2 (51.522°N, 127.557°W) located in the centre of the inlet, and UBC7 (51.500°N, 127.817°W) located outside the mouth (henceforth head, centre, and mouth, respectively; Figure 7). The mouth station is influenced more by mixing processes and currents in the strait than processes occurring in the fjord. CTD data

(temperature, salinity, and depth; SBE 25, Seabird Electronics, Inc., Bellevue, WA, USA), photosynthetically active radiation (PAR), and measurements of photophysiology using a fast repetition rate fluorometer (FRRF) were acquired on site. Samples were collected for subsequent laboratory-based analysis of chlorophyll *a* (chl*a*), nutrients (PO₄, NO₃+NO₂, and Si), and microscopic identification of phytoplankton community composition.

In 2010, sampling was carried out monthly from mid-March to mid-July, following the same protocol as 2009. In addition to these monthly cruises, primary productivity experiments comparing FRRF estimates of primary productivity and ¹³C bottle incubations were conducted at the centre of the inlet and at nearby Dawson's Landing (51.574°N, 127.5862°W; Figure 7). A summary of cruise dates and samples collected can be found in Appendix A; protocols outlining the collection of these samples are detailed below.

2.2.2 Photosynthetically active radiation

At each station, a sensor measuring photosynthetically active radiation (PAR; LI-COR LI-193 Spherical Quantum Sensor, Lincoln, Nebraska, USA; RBR Ltd., Kanata, ON, Canada) was lowered to 30m depth in order to measure water column profiles of PAR. These data were used to determine the depth of the euphotic zone (1% of surface irradiance) and average euphotic zone PAR levels. The PAR data were also used in conjunction with chl*a* (Section 2.2.3) and FRRF data (Sections 2.2.9 – 2.2.11) to estimate primary productivity.

When PAR data were not available, PAR was estimated from secchi depth and incoming surface short wave radiation ($W \cdot m^{-2}$) was measured at the nearby Laska weather station (51.5486°N, 127.5316°W; Figure 7). For these measurements, we used an estimate of albedo (18%) from Wolfe (2010) and an extinction coefficient (*k*) of $k = 1.7 \times d_s$, where 1.7 is

commonly used to calculate k in turbid coastal waters and d_s is secchi depth (m; Poole and Atkins 1929).

2.2.3 Chlorophyll *a*

Niskin bottles were used to collect water at 0, 5, and 30m depths. Chl*a* samples were filtered immediately following the collection of water. A known volume of water (either 125mL or 150mL) was filtered through a 47mm Whatman GFF filter. The filters were then frozen and stored at -20°C until they could be analyzed. Once in the lab, each filter was soaked in 10mL 90% acetone and left in a dark, -20°C freezer for 24 hours to extract the chlorophyll. The following day, samples were warmed to room temperature (~20°C) and the concentration of chl*a* was determined with a Water Properties Turner 10 AU fluorometer (Sunnyvale, CA, USA). Sample fluorescence was recorded both before and after acidification with 30μL of 10% HCl (Strickland and Parsons 1968). Fluorescence was converted to $\mu\text{g chl}a \cdot \text{L}^{-1}$ using the following calibration equation:

$$[\text{chl}a] = 2.68 \times (F_b - F_a) \times (v \times V^{-1})$$

where $[\text{chl}a]$ is the concentration of chl*a* in $\mu\text{g} \cdot \text{L}^{-1}$; 2.68 is a fluorometer-specific correction factor ($\mu\text{g chl}a \cdot \text{L}^{-1}$); F_b is the fluorescence reading before acidification (dimensionless); F_a is the fluorescence reading after acidification (dimensionless); v is the volume of acetone (L); and V is the volume of seawater sample filtered (L).

2.2.4 Nutrients

Nutrient samples were collected at 0, 5, and 30m depths. Approximately 50mL of water was filtered through a 25mm Whatman GFF filter and immediately frozen and stored at -20°C. Samples were later analyzed in the lab for phosphate, nitrate, and silicic acid content [PO_4 , NO_3+NO_2 (hereafter NO_3), and Si, respectively] on an AutoAnalyzer 3 (Bran & Luebbe GmbH, Norderstedt, Germany) using air-segmented continuous flow.

2.2.5 Surface stratified layer

The depth of the surface stratified layer (SLD) was calculated using the density criterion described by Levitus (1982). Briefly, the bottom of the SL was defined as the depth at which the density (sigma-t from CTD) was $0.125 \text{ kg} \cdot \text{m}^{-3}$ greater than surface density. This is the same criterion used to calculate mixed layer depth (MLD; Levitus 1982); though in Rivers Inlet and other estuaries this is not a true mixed layer (Lucas et al. 1998, Noh and Lee 2008). The classical MLD calculation does not account for losses of phytoplankton from the surface layer (due to turbulent diffusion and sinking) that are observed in relatively shallow, tidally influenced systems (Lucas et al. 1998).

2.2.6 Phytoplankton community composition

Whole water samples were collected in 250mL amber bottles from the head, centre, and mouth of the inlet at 0, 5, and 30m and preserved with unbuffered Lugol's iodine solution. In the lab, samples were analyzed using light microscopy. Samples were settled in 5mL, 10mL, or 25mL tubular plankton settling chambers (Hydro-Bios, Kiel, Germany) depending on chl*a* concentration ($[\text{chl}a] > 3 \mu\text{g} \cdot \text{L}^{-1}$, $1-3 \mu\text{g} \cdot \text{L}^{-1}$, and $< 1 \mu\text{g} \cdot \text{L}^{-1}$, respectively). Phytoplankton

cells were identified to species whenever possible and were ranked based on species presence using the following qualitative scale: a ranking of 0 meant a species was not present in a given sample, a ranking of 1 meant a species was present in very low abundance, 2 was low abundance, 3 was high abundance, and 4 denoted a bloom. This system was used to determine the dominant species and semi-quantitatively describe the phytoplankton community.

2.2.7 Strain isolation

To determine the photosynthetic unit size (n_{PSII}^{-1}) of dominant phytoplankton species from Rivers Inlet, three abundant genera contributing to the phytoplankton spring bloom were identified from preserved samples: *Skeletonema costatum*, *Chaetoceros* spp., and *Thalassiosira pacifica/aestivales/nordenskioldii* (an electron microscope is required to distinguish these species). Representative species from the first two genera were successfully isolated from live seawater samples collected in July 2009 at Dawson's Landing in Rivers Inlet, BC (Figure 7) using a micropipette (described in Andersen and Kawachi 2005) and grown in Harrison's enriched natural seawater (HENSX; Harrison et al. 1980). Cultures were checked daily, then weekly, to ensure that only the desired species was growing. If necessary, cells were re-isolated to remove contaminants. Both *Skeletonema costatum* and a small *Chaetoceros* species were isolated and grown successfully for laboratory trials measuring photosynthetic unit size (Appendix B) and primary productivity using FRRF and ^{13}C (Section 2.2.10).

2.2.8 Culturing techniques

Three strains representing the main genera of the spring phytoplankton bloom in Rivers Inlet were cultured under laboratory growth conditions. Two were Rivers Inlet isolates

(*Skeletonema costatum* and a small *Chaetoceros* species) and the third was *Thalassiosira aestivalis* (CCMP 975; Provasoli-Guillard National Center for Marine Algae and Microbiota, East Boothbay, ME, USA). Phytoplankton strains were cultured in 28mL polycarbonate tubes and maintained in exponential growth phase using sterile, semi-continuous batch culturing techniques. To simulate natural growth conditions in Rivers Inlet, cells were grown in Harrison's enriched natural seawater (HENSX; Harrison et al. 1980) at 12°C and under continuous illumination by cool-white fluorescent lights ($110 \mu\text{mol quanta} \cdot \text{m}^{-2} \cdot \text{s}^{-1}$; Sylvania, Mississauga, Canada). Cultures were considered acclimated to these conditions when growth rates varied by less than 10% between consecutive transfers (Brand et al. 1981). As a proxy for biomass, *in vivo* chlorophyll *a* (chl*a*) fluorescence was measured daily using a Water Properties Turner 10 AU fluorometer (Sunnyvale, CA, USA). Absolute growth rates (d^{-1}) were determined using simple linear regressions of the natural log (ln) of *in vivo* chl*a* fluorescence versus time (days).

2.2.9 Fast Repetition Rate Fluorometry (FRRF) method during 2009 sampling season at surface irradiance

A Mk II Fast_{tracka} fast repetition rate fluorometer (FRRF; Chelsea Technologies Group Ltd., Surrey, UK) was used to collect chl*a* fluorescence data on all Rivers Inlet 2009 (RI09) research cruises, with the exception of RI09-08 and RI09-09 when the fluorometer was not working (Appendix A). FRRF measurements were performed at surface irradiance levels in discrete samples (2L polycarbonate bottles) collected from three water column depths (0, 5, and 30m) using a 5L Niskin bottle. Samples were collected at the centre of the inlet during every cruise, as well as at the mouth and head when time permitted (Appendix A). Each 2L bottle was

placed in front of the FRRF acquisition window on the boat deck and the protocol described in Table 1 was initiated. The protocol included both single turnover (ST) and multiple turnover (MT) acquisitions, but only data from ST acquisitions were analyzed. The program was allowed to run for at least 20 ST acquisitions, with the aim that at least 10 fully saturated, minimally scattered ST acquisitions were recorded. After completing this light-adapted data collection for a given depth, the bottle was placed in a dark container where it was dark-adapted for 15 to 30 minutes at surface water temperatures. Dark-adapted samples were run in the same manner as the light-adapted samples, taking care not to expose the bottles to the light during handling and FRRF acquisitions. Primary productivity calculations are described in Section 2.2.11 below.

Table 2. FRRF acquisition parameter settings. ST, single turnover. MT, multiple turnover. Only ST data were used to calculate primary productivity. Inc: percent increase in flashlet intensity. Block time: length of block of flashlets.

Protocol 1 – ST	Block	Flashlets	On (μs)	Off (μs)	Inc (%)	Block time
Acquisition time: 0.5s	1	100	1.000	1.000	0	200μs
Acquisition pitch: 2s	2	50	1.000	49.000	0	2.5μs
Sequence per acquisition: 10						
Sequence interval: 50ms						
<hr/>						
Protocol 2 – MT						
Acquisition time: 0.12s	1	3200	1.000	49.000	0	160ms
Acquisition pitch: 2s	2	50	1.000	600.000	12	1.4s
Sequence per acquisition: 1						
Sequence interval: 120m						
<hr/>						
Minimum series time: 4s						
<hr/>						

2.2.10 Simultaneous Fast Repetition Rate Fluorometry (FRRF) and ¹³C method during 2010 sampling season at *in situ* light levels

In 2010, the protocol for collecting primary productivity data was modified to focus on comparing primary productivity measurements derived from FRRF fluorescence and ¹³C fixation. Due to the logistical constraints of bottle incubations, all experiments were performed

from the dock at Dawson's Landing. Samples were collected either at the centre of the inlet or from the Dawson's Landing dock itself. The PAR sensor was attached to a sampling line directly above the FRRF, which was orientated horizontally in the water column, and after activation the combined instruments were lowered to a depth of 25m. A Niskin or van Dorn bottle (used at centre and Dawson's Landing, respectively) was subsequently lowered to 25m to collect a water sample adjacent to the FRRF, after which the sample was transferred to a 2L polycarbonate bottle. The bottle was then placed in a dark cooler, where it dark-adapted for at least 15 minutes. This water was used for the dark-adapted FRRF measurements (following the same protocol described in Section 2.2.9), as well as for *chl a* samples and ^{13}C incubations. Once water was collected and sufficient high-quality *in situ* FRRF data had been recorded (see Section 2.2.9), the FRRF and PAR sensor were raised from 25m to 5m and the procedure was repeated. After collecting data at 5m depth, the protocol was repeated just below the water surface (0m). When dark-adapted fluorescence had been measured for all three depths, water from the 2L polycarbonate bottles was used to fill four 250mL clear polycarbonate bottles, representing four treatments for each depth sampled: control (C), light 1 (L1), light 2 (L2), and dark (D). The dark bottle was wrapped in tinfoil and electrical tape to prevent any light penetration. Each bottle was filled to the brim, leaving as little headspace as possible (except for RI10-01, when bottles were filled to 250mL), and spiked with 1mL of 28 μM $\text{NaH}^{13}\text{CO}_3$ solution (99 atom % ^{13}C , Sigma-Aldrich), resulting in a total addition of 0.36 mg ^{13}C to each 250mL bottle. Control bottles were immediately filtered onto 25mm pre-combusted (450°C for 4 h) Whatman GFF filters and the filters were frozen and stored at -20°C. The remaining 9 bottles (L1, L2, and D for each of the 3 depths) were suspended from a rope in the water column at the depth from which they were collected (0, 5, and 25m) in order to maintain natural temperatures and light levels throughout

the incubation. With the remaining water in the 2L polycarbonate bottles, a *chl a* sample was collected for each depth (Section 2.2.3). At the end of a 2-hour ^{13}C incubation period, the 9 bottles were removed from the water column and each was filtered through a 25mm pre-combusted GFF filter. These filters were frozen at -20°C for later analysis. In total, 19 field trials were run, comparing FRRF- and ^{13}C -derived measurements of primary productivity, 14 at Dawson's Landing and 5 at the centre of the inlet.

Once in the lab, all filters from the ^{13}C incubation experiments were oven-dried at 50°C for 24 hours. The filters were then fumed with HCl to drive off any inorganic carbon. Once dried and fumed, samples were packed individually into foil sheets and compacted into pellets for analysis on a Europa Scientific 20-20 IRMS linked to an ANCA SL Elemental Analyzer. Results were reported in atom % (atm%), where:

$$\text{atm}\% \text{ } ^{13}\text{C} = 100 \times \frac{^{13}\text{C}}{^{13}\text{C} + ^{12}\text{C}}.$$

In addition to the 19 field experiments, 8 trials were run in the laboratory using cultures of Rivers Inlet isolates, following a similar protocol. Cultures of *Skeletonema costatum* and *Chaetoceros* sp. were grown in HENSW (Harrison et al. 1980) in clear 2L polycarbonate bottles. The cultures were maintained in exponential growth as described above. The culture bottle was placed in front of the FRRF acquisition window and light-adapted fluorescence data were recorded using the protocol described above (Section 2.2.9). The culture was then allowed to dark-adapt for 15-20 minutes and fluorescence was measured a second time in the dark. After collecting the FRRF fluorescence data, the culture was well mixed before being used to fill four 250mL polycarbonate bottles (C, L1, L2, and D), spiked with ^{13}C as described above and

incubated in the growth conditions (12°C, 110 $\mu\text{mol quanta} \cdot \text{m}^{-2} \cdot \text{s}^{-1}$). A *chl a* sample was immediately collected from each treatment, and, after a two-hour incubation, cells were collected on a 25mm pre-combusted GFF filter and processed and the ^{13}C content of particulate organic carbon (POC) analyzed as per the protocol for the field samples.

2.2.11 Calculation of primary productivity from FRRF measurements

Rates of gross carbon fixation were derived from FRRF data following Kolber and Falkowski (1993) using the following equation:

$$\text{FRRF-PP} = P_f^{\text{B}} \times [\text{chl}a]$$

where FRRF-PP is primary productivity derived from FRRF measurements ($\mu\text{g C} \cdot \text{L}^{-1} \cdot \text{hr}^{-1}$); P_f^{B} is photosynthetic electron flow calculated from fluorescence yields ($\text{mol e}^- \cdot \text{mol chl}a^{-1} \cdot \text{hr}^{-1}$); and $[\text{chl}a]$ is the concentration of *chl a* ($\mu\text{g} \cdot \text{L}^{-1}$). P_f^{B} can be calculated using:

$$P_f^{\text{B}} = P_f^{\text{e}^-} \times n_{\text{PSII}} \times (4 \text{ e}^- \cdot \text{C}^{-1})^{-1} \times (12 \text{ mg C} \cdot \text{mol}^{-1}) \times (3600 \text{ sec} \cdot \text{hr}^{-1}) \times (892 \text{ mg chl}a \cdot \text{mol}^{-1})^{-1}$$

where $P_f^{\text{e}^-}$ is the steady-state electron transport rate normalized to PSII reaction centres [$\text{e}^- \cdot (\text{RCII} \cdot \text{s})^{-1}$]; n_{PSII} is the photosynthetic unit size [= 0.002 \times *f* (see below for definition); $\text{mol e}^- \cdot \text{mol chl}a^{-1}$]; 4 $\text{e}^- \cdot \text{C}^{-1}$ assumes 4 electrons are required to fix one atom of carbon (Kolber and Falkowski 1993); and 12 $\text{mg C} \cdot \text{mol}^{-1}$, 3600 $\text{sec} \cdot \text{hr}^{-1}$, and 892 $\text{mg chl}a \cdot \text{mol}^{-1}$ are conversion factors. $P_f^{\text{e}^-}$ is calculated from:

$$P_f^e = E_z \times \sigma_{\text{PSII}} \times \phi_p \times \phi_e \times (10^6 \mu\text{mol} \cdot \text{mol}^{-1}) \times (6.02 \times 10^{23} \text{ atom} \cdot \text{mol}^{-1}) \times (10^{20} \text{ \AA}^2 \cdot \text{m}^{-2})$$

where E_z is photosynthetically active radiation (PAR, $\mu\text{E} \cdot \text{m}^{-2} \cdot \text{s}^{-1}$); σ_{PSII} is the functional absorption cross-section of PSII ($\text{\AA}^2 \cdot \text{quanta}^{-1}$); ϕ_p is the quantum yield of photosynthesis (dimensionless); ϕ_e is the actual quantum yield of electron transfer (dimensionless, 0-1); and $10^6 \mu\text{mol} \cdot \text{mol}^{-1}$, $6.02 \times 10^{23} \text{ atom} \cdot \text{mol}^{-1}$, and $10^{20} \text{ \AA}^2 \cdot \text{m}^{-2}$ are unit conversions. ϕ_p and ϕ_e are calculated as follows:

$$\phi_p = f \times q_p$$

$$\phi_e = 1 \quad \text{when } (E_z \times \sigma \times q_p) > \tau_p^{-1} \text{ (low light)}$$

$$\phi_e = (E_z \times \sigma \times q_p \times \tau_p)^{-1} \quad \text{when } (E_z \times \sigma \times q_p) \leq \tau_p^{-1} \text{ (high light)}$$

where f is the fraction of functional PSII ($f = F_v/F_m \div 0.65$; dimensionless, 0-1); q_p is photochemical quenching (dimensionless, 0-1); and τ_p is the minimum time required to transfer an electron from water to the terminal electron acceptor in steady state at light saturation (4.3 ms). q_p is calculated from the following two equations:

$$q_p = (F_m' - F') \times (F_m' - F_o')^{-1}$$

$$F_o' = F_o \times (F_v/F_m + F_o/F_m')^{-1} \quad \text{(Oxborough and Baker 1997)}$$

where F_o' , F' , and F_m' are *in vivo* fluorescence yields induced by a weak probe flash in the dark, under ambient light, and by a saturating flash, respectively, all are light-adapted fluorescence yields ($F_o' < F' < F_m'$, dimensionless); F_o and F_v/F_m are *in vivo* fluorescence yields measured in dark-adapted samples (dimensionless). F_o is induced by a weak probe flash in the dark. F_v/F_m is variable fluorescence ($F_v = F_m - F_o$) divided by maximum fluorescence (F_m). F_m is measured

using a saturating flash ($F_o < F_m$). A summary of parameters is listed in Table 2 and Table 3 contains sample calculations.

2.2.12 Calculation of primary productivity from ^{13}C bottle incubations

^{13}C data were analyzed using the following equations from Hama et al. (1983):

$$^{13}\text{C-PP} = (\Delta\text{C} \times t^{-1}) \times f_{^{13}\text{C}}$$

$$\Delta\text{C} = \text{C} \times (a_{\text{is}} - a_{\text{ns}}) \times (a_{\text{ic}} - a_{\text{ns}})^{-1}$$

where $^{13}\text{C-PP}$ is the photosynthetic rate corrected with the discrimination factor of ^{13}C [$\mu\text{g C} \cdot (\text{L} \cdot \text{h})^{-1}$]; ΔC is the particulate organic carbon (POC) increase during the incubation ($\mu\text{g C} \cdot \text{L}^{-1}$); t is incubation time (hours); $f_{^{13}\text{C}}$, the ^{13}C discrimination factor, is 1.025 [this is the parameter “f” in Hama et al. (1983), but we have changed it here in order to avoid confusion with f from the FRRF-PP calculation]; C is the particulate organic carbon (POC) concentration of the incubated sample ($\mu\text{g C} \cdot \text{L}^{-1}$); a_{is} is the atm% of ^{13}C in the incubated sample, i.e., the average of the two light bottles (L1 and L2) for a given trial; a_{ns} is the background atm% of ^{13}C in the natural sample, i.e., the control bottle; and a_{ic} is the atm% of total inorganic carbon (TIC; Hama et al. 1983; Table 2). a_{ic} was calculated by estimating DIC values from salinity data collected with a CTD. A DIC/salinity relationship was estimated using Owikeno Lake as a freshwater endpoint (salinity 0.032, DIC 420 μM) and deep Pacific open ocean water (salinity 35, DIC 2200 μM) as a saltwater endpoint (Pawlowicz 2008; R. Pawlowicz, pers. comm.). The following equation was derived from the fresh- and saltwater endpoints and was used to estimate DIC:

$$[\text{DIC}] = (50.86 \times \text{S}) + 419.84$$

where $[\text{DIC}]$ is the concentration of DIC in μM and S is salinity (dimensionless).

Table 3. List of fast repetition rate fluorometer (FRRF) and ^{13}C fixation parameters used to calculate primary productivity.

FRRF Parameters		
F_o', F', F_m'	Dimensionless	<i>In vivo</i> fluorescence yields induced by a weak probe flash in the dark, under ambient light, and by a saturating flash, respectively. All are light-adapted fluorescence yields.
F_o, F_m	Dimensionless	<i>In vivo</i> fluorescence yields induced by a weak probe flash in the dark and by a saturating flash, respectively. Both are dark-adapted fluorescence yields.
F_v', F_v	Dimensionless	Variable fluorescence in light- and dark-adapted samples, respectively. Calculated by $F_v' = F_m' - F_o'$ and $F_v = F_m - F_o$.
$F_v'/F_m', F_v/F_m$	Dimensionless	Photochemical efficiency in light- and dark-adapted samples.
τ_p	ms	Minimum time required to transfer an electron from water to the terminal electron acceptor in steady-state light saturation, 4.3ms.
q_p	Dimensionless	Photochemical quenching, 0-1.
f	Dimensionless	Fraction of potentially open functional photosystem II reaction centres (RCII), 0-1, approaching 1. Calculated as $f = F_v'/F_m' \div 0.65$.
ϕ_e	Dimensionless	Actual quantum yield of electron transport, 0-1, approaching 1.
ϕ_p	Dimensionless	Quantum yield of photosynthesis.
σ_{PSII}	$\text{\AA}^2 \cdot \text{quanta}^{-1}$	Functional absorption cross-section of photosystem II (PSII).
E_z	$\mu\text{E} \cdot \text{m}^{-2} \cdot \text{s}^{-1}$	Photosynthetically active radiance (PAR) at depth z .
n_{PSII}	$\text{mol } e^- \cdot \text{mol chl}a^{-1}$	Photosynthetic unit size. Calculated as $n_{\text{PSII}} = 0.002 \cdot f$. This assumes one electron per 500 chl a .
P_f^e	$e^- \cdot (\text{RCII} \cdot \text{s})^{-1}$	Steady state photosynthesis normalized to PSII reaction centres (RCII).
[chl a]	$\mu\text{g} \cdot \text{L}^{-1}$	Concentration of chlorophyll a .
P_f^B	$\text{mol } e^- \cdot (\text{mol chl}a \cdot \text{h})^{-1}$	Photosynthetic electron flow calculated from fluorescence yields.
FRRF-PP	$\mu\text{g C} \cdot (\text{L} \cdot \text{h})^{-1}$	Primary productivity derived from FRRF measurements.
^{13}C Parameters		
^{13}C -PP	$\mu\text{g C} \cdot (\text{L} \cdot \text{h})^{-1}$	Primary productivity derived from ^{13}C bottle incubations.
ΔC	$\mu\text{g C} \cdot \text{L}^{-1}$	Particulate organic carbon (POC) increase during the incubation.
t	h	Incubation time.
$f_{^{13}\text{C}}$	Dimensionless	^{13}C discrimination factor, 1.025 (Hama et al. 1983).
C	$\mu\text{g C} \cdot \text{L}^{-1}$	POC in the incubated sample.
a_{is}	atm%	Atom % of ^{13}C of the incubated sample.
a_{ns}	atm%	Atom % of ^{13}C of the natural sample.
a_{ic}	atm%	Atom % of ^{13}C of the total organic carbon (TIC) in the sample.

Table 4. Example primary productivity calculation based on fluorescence measurements collected using an FRRF. Sample data from the centre of the inlet April 16, 2009. Where z is depth (m); E_z is photosynthetically active radiation (PAR; $\mu\text{E} \cdot \text{m}^{-2} \cdot \text{s}^{-1}$); σ_{PSII} is the functional absorption cross section of photosystem II (PSII; $\text{\AA}^2 \cdot \text{quanta}^{-1}$); Φ_P is the quantum yield of photosynthesis (dimensionless); Φ_e is the actual quantum yield of electron transport (0-1, dimensionless); F_v/F_m is photochemical efficiency in dark-adapted samples (dimensionless); f is the fraction of potentially open functional PSII reaction centres (RCII; dimensionless); $[\text{chl}a]$ is the concentration of chl a ($\mu\text{g} \cdot \text{L}^{-1}$); $P_f^{e^-}$ is the steady-state photosynthesis normalized to RCII ($e^- \cdot (\text{RCII} \cdot \text{s})^{-1}$); P_f^B is the photosynthetic electron flow calculated from fluorescence yields ($\text{mg C} \cdot (\text{mg chl}a \cdot \text{h})^{-1}$); and FRRF-PP is primary productivity derived from FRRF measurements ($\text{mg C} \cdot \text{m}^{-3} \cdot \text{h}^{-1}$). †When $(E_z \times \sigma_{\text{PSII}} \times q_P) \leq \tau_P^{-1}$, $\Phi_e = 1$ (low light) and when $(E_z \times \sigma_{\text{PSII}} \times q_P) > \tau_P^{-1}$, $\Phi_e = (E_z \times \sigma_{\text{PSII}} \times q_P \times \tau_P)^{-1}$ (high light). Where q_P is photochemical quenching (dimensionless) and τ_P is the minimum time required to transfer an electron from water to the terminal electron acceptor in steady-state light saturation (4.3 ms).

z	E_z	σ_{PSII}	Φ_P	Φ_e^\dagger	F_v/F_m	f	$[\text{chl}a]$	$P_f^{e^-}$	P_f^B	FRRF-PP
m	$\mu\text{E} \cdot \text{m}^{-2} \cdot \text{s}^{-1}$	$\text{\AA}^2 \cdot \text{quanta}^{-1}$	(dimensionless parameters)				$\mu\text{g} \cdot \text{L}^{-1}$	$e^- \cdot (\text{RCII} \cdot \text{s})^{-1}$	$\text{mg C} \cdot (\text{mg chl}a \cdot \text{h})^{-1}$	$\text{mg C} \cdot \text{m}^{-3} \cdot \text{h}^{-1}$
0	864	274	1.19	0.19	0.32	0.49	6.96	362	4.26	29.6
5	127	265	1.16	1	0.29	0.45	1.36	352	3.82	5.19
30	1.4	432	0.89	1	0.13	0.20	0.34	295	1.46	0.50

2.3 Results

2.3.1 Chemical and physical properties

2.3.1.1 Macronutrient seasonal cycle

Rivers Inlet exhibits winter renewal associated with upwelling and mixing, followed by a phytoplankton-mediated spring depletion of nutrients that is typical of temperate estuaries. In 2009, PO_4 concentrations ranged from a maximum of $2.08 \mu\text{M}$ at 30m at the mouth of the inlet in late February to a minimum of $0.00 \mu\text{M}$ at 0m at the head and centre in mid-May (Figures 8 – 10). Maximum values were always observed at 30m, where $[\text{PO}_4]$ remained relatively constant throughout the sampling season at all stations ($\geq 1.11 \mu\text{M PO}_4$). Surface and 5m PO_4 concentrations showed a seasonal trend being high in early spring and depleted by summer. This

temporal trend also had a spatial component, with depletion first occurring at the head and later at either the centre or mouth. For example, at 5m, the lowest PO₄ concentrations were recorded first in mid-June at the head (0.41 μM) and later in mid-July at the centre (0.43 μM) and mouth (0.02 μM) of the inlet (Figures 8 – 10).

Silicic acid, like phosphate, was depleted in the spring and was depleted earlier at the head of the inlet than at the centre or mouth. In 2009, maximum Si concentrations were observed in late February at 5m at the mouth (43.56 μM). Minimum Si values were observed in mid-June at 5m at the head (4.65 μM), mid-August in the centre (17.20 μM), and in mid-July at the mouth of the inlet (1.20 μM; Figures 8 – 10).

Nitrate exhibited the same patterns as PO₄ and Si, with high concentrations in early spring being depleted throughout the inlet by the beginning of summer and with depletion occurring earlier at the head than at either the centre or mouth. Maximum NO₃ concentrations at 5m were recorded in late February at the head (23.02 μM). Minimum 5m NO₃ concentrations occurred in mid-June at the head (1.65 μM), in early July at centre (10.86 μM), and in early May at the mouth (~0.00 μM) of the inlet. Similar to PO₄ and Si, concentrations of NO₃ at 30m were relatively constant (7.72 μM – 23.82 μM) from February to August and across the inlet (Figures 8 – 10).

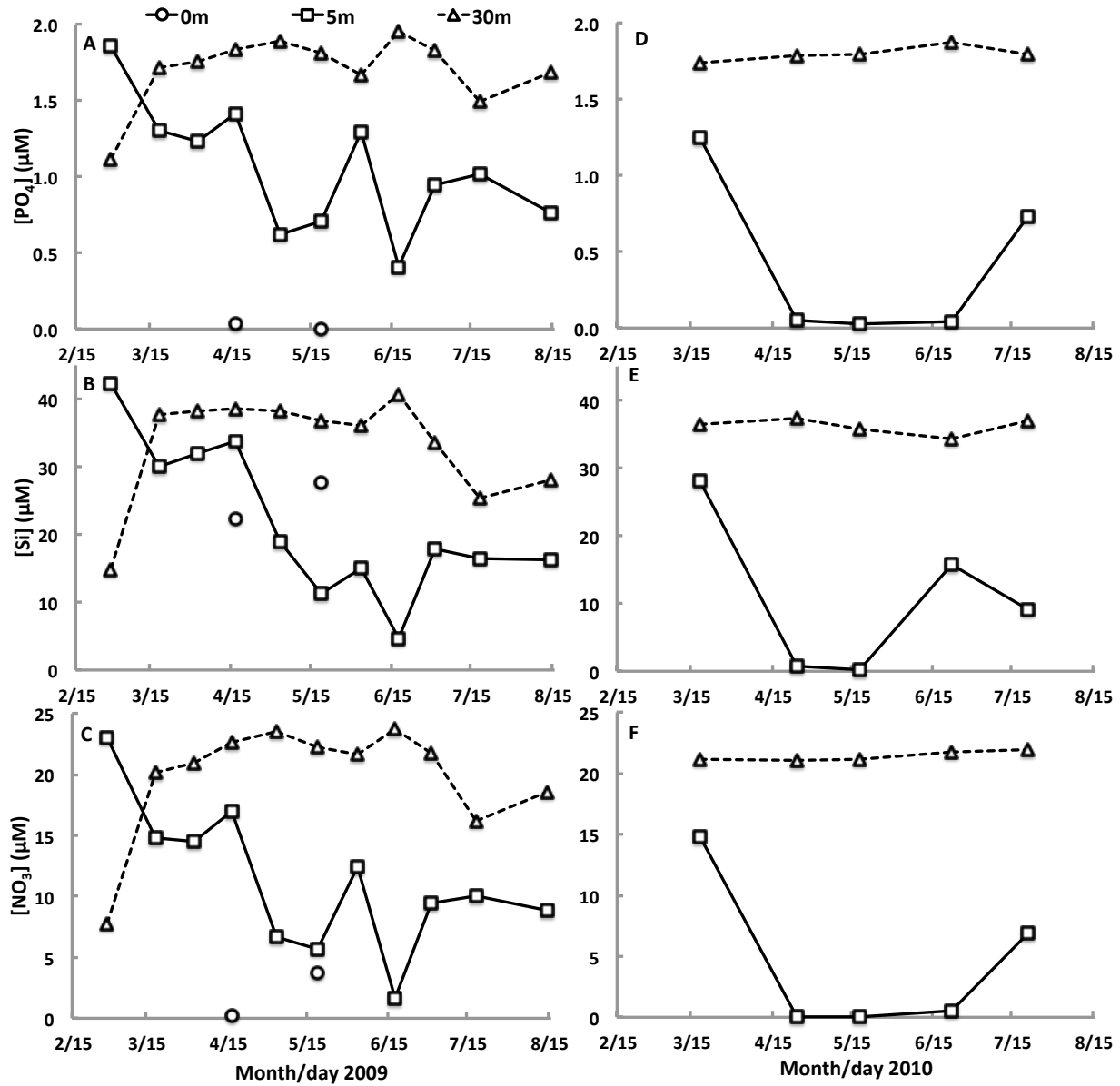


Figure 8. Phosphate, silicic acid, and nitrate concentrations (μM) at 0, 5, and 30m at the head of the inlet (station DFO5) from late February to mid-August 2009 (A-C) and mid-March to mid-July 2010 (D-F).

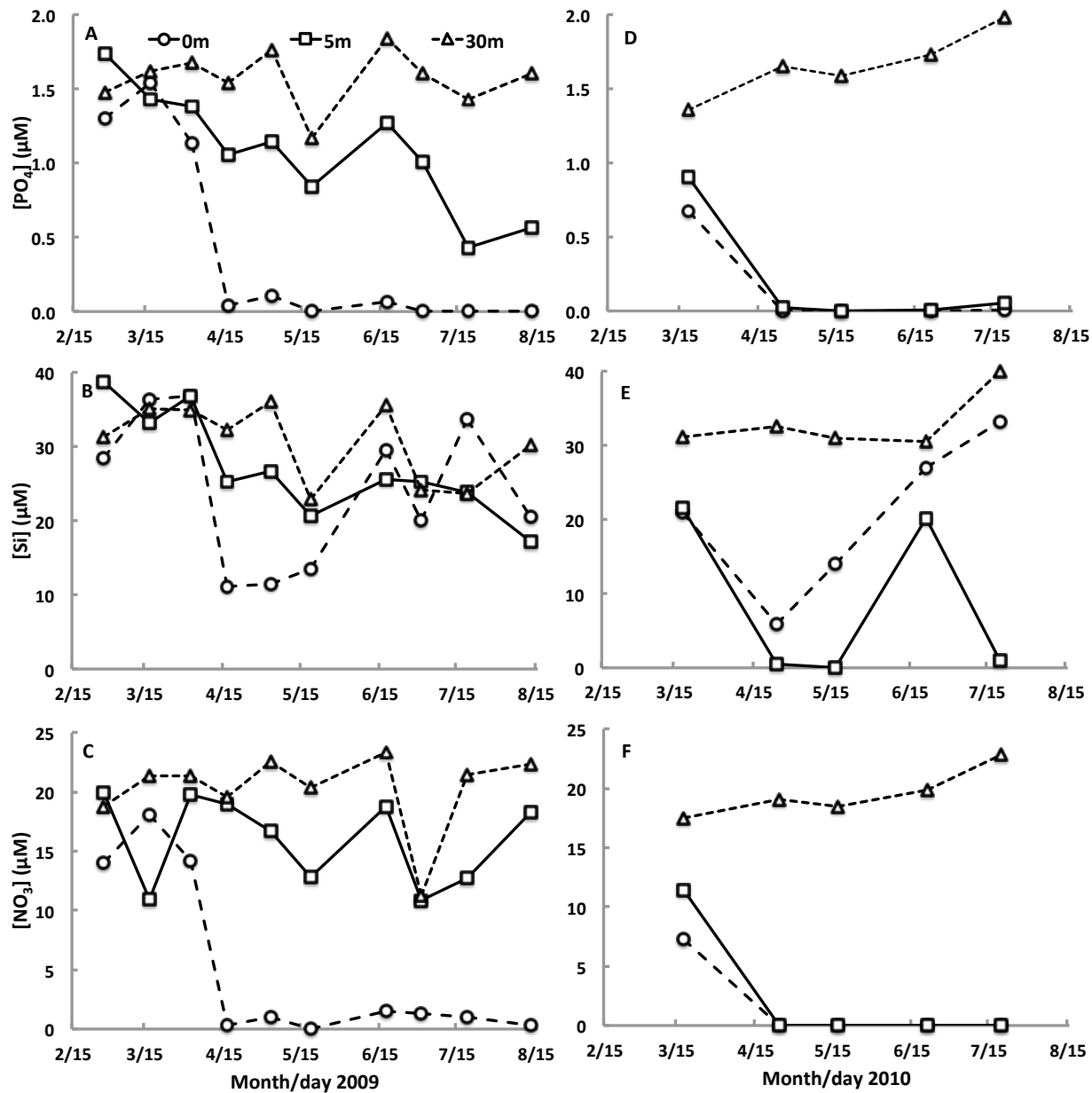


Figure 9. Phosphate, silicic acid, and nitrate concentrations (μM) at 0, 5, and 30m at the centre of the inlet (station DFO2) from late February to mid-August 2009 (A-C) and mid-March to mid-July 2010 (D-F).

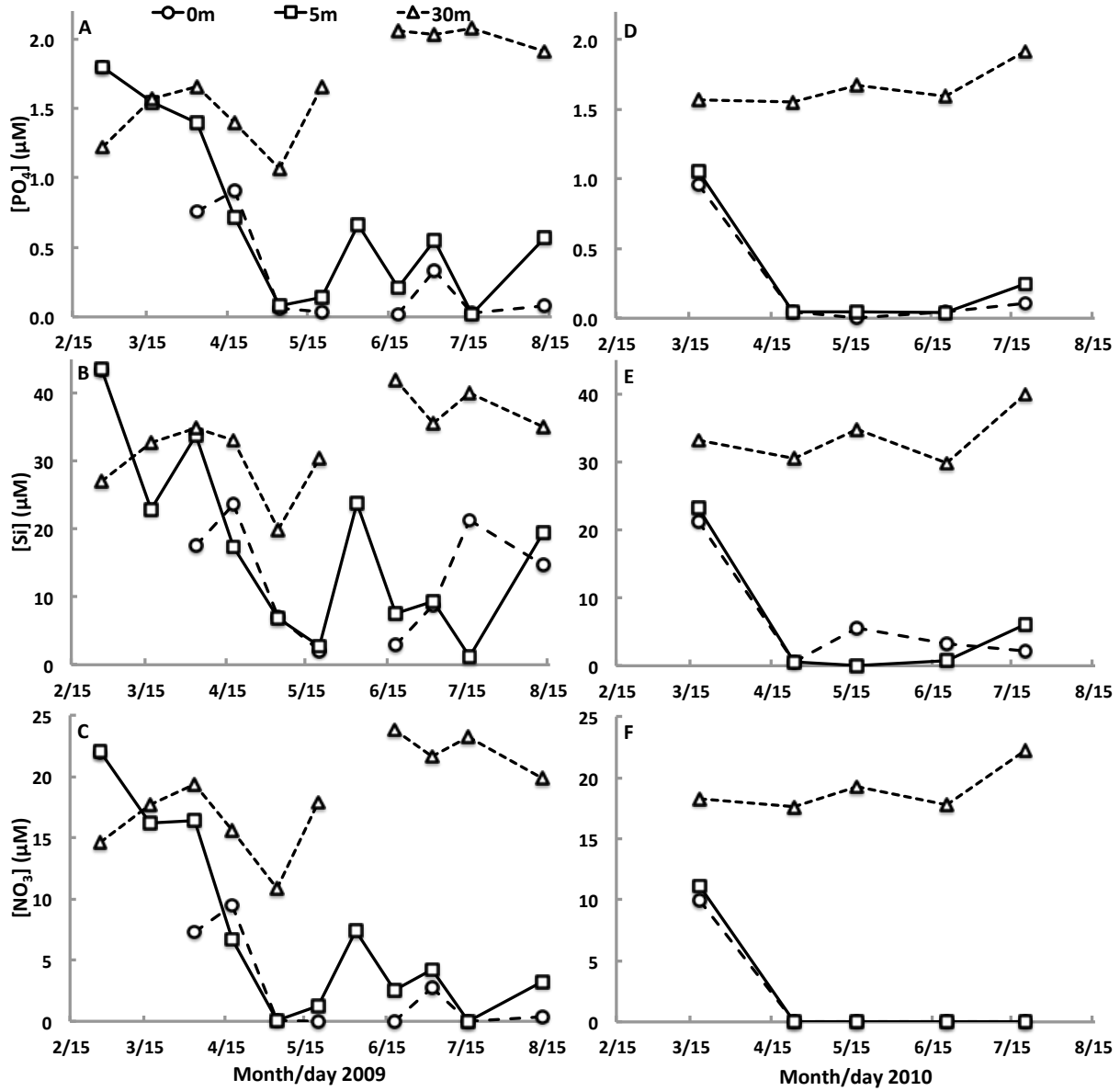


Figure 10. Phosphate, silicic acid, and nitrate concentrations (μM) at 0, 5, and 30m at the mouth of the inlet (station UBC7) from late February to mid-August 2009 (A-C) and mid-March to mid-July 2010 (D-F).

In 2010, macronutrient concentrations and distribution patterns were similar to those observed in 2009, and were strongly depleted ($< 0.05 \mu\text{M PO}_4$, $< 0.58 \mu\text{M Si}$, and $\sim 0.00 \mu\text{M NO}_3$) at 5m by mid-April. In both years, Si concentrations increased in the centre of the inlet after the spring bloom. For example, in 2009, Si increased from 11.14 to 29.48 μM at 0m between mid-April and mid-June.

2.3.1.2 Nutrient drawdown

Overall in 2009, we observed distinct spring drawdown of nutrients at the surface (0m) and at 5m. We observed greater nutrient depletion at 0m than at 5m at the head and centre of the inlet (Figures 8 – 9). At the mouth, 0m and 5m nutrient levels were more similar to each other (Figure 10). In 2009, PO_4 concentrations were depleted during the spring bloom at 0 and 5m throughout the inlet. For example, at the centre of the inlet, PO_4 was drawn down by 1.31 μM (from 1.74 to 0.43 μM) from late February to mid-July at 5m depth (Figure 9a). A distinct decrease in Si was also observed at all stations in 2009 in spring and summer. For example, at the mouth, Si at 5m depth decreased by 40.83 μM (43.56 – 2.74 μM) from late February to mid-May (Figure 10b). NO_3 drawdown was observed throughout the inlet in 2009. This was most evident at 5m at the head (little 0m data available), where NO_3 decreased by 21.37 μM (23.02 – 1.65 μM) from late February to mid-June, and at the mouth at 0m where NO_3 decreased from 21.92 to 0.00 μM between late February and mid-May (Figure 10c). Drawdown of NO_3 and other nutrients was not observed at 30m in 2009. In general, the drawdown of NO_3 at 0 and 5m matched the timing of the drawdown of PO_4 and Si. Similar trends were observed in 2010, though nutrient depletion was more widespread and persistent than in 2009 (Figures 8 – 10).

2.3.1.3 Surface stratified layer depth

The depth of the surface stratified layer (SLD) generally deepened from the head to the mouth and shallowed throughout the inlet as the season progressed. SLD was deepest in late February 2009 at the head (6m) and centre (24m) and in mid-March at the mouth (35m; Table 4). SLD shallowed to 2m and remained at 2 – 3m at the head (mid-March – mid-July), centre (early April – mid-August), and mouth (mid-May – mid-August). In mid-August, SLD was 4m at the head. In 2010, SLD ranged from 2 – 5m. It is likely that we did not observe deeper SLD due to infrequent samples, a shorter sampling season, and an early freshet.

2.3.1.4 Euphotic zone

In 2009, limited PAR data were available and light quality was estimated using secchi depth. Secchi depth was deepest in early spring, with maximum values of 8.8m at the head (mid-March), 9.4m at the centre (early April), and 14.3m at the mouth (early April; Table 4). Secchi depth shallowed to a minimum in summer: 0.6m at the head (mid-August); 1.5m at centre (mid-July); and 2.7m at the mouth (early June). Secchi was generally shallowest at the head and deepest at the mouth. In spring of 2009, euphotic zone depth was deeper than the depth of sampling with the PAR sensor (which ranged from 20m to 115m deep; Table 4). In 2010, the bottom of the euphotic zone ranged from 4.2 – 30m from late April to mid-July (Table 4).

Maximum PAR values were typical of temperate regions. Surface irradiance (I_0) ranged from 139 – 2623 $\mu\text{E} \cdot \text{m}^{-2} \cdot \text{s}^{-1}$ (Table 4). The average irradiance experienced by phytoplankton in the mixed layer ranged from 10 – 746 $\mu\text{E} \cdot \text{m}^{-2} \cdot \text{s}^{-1}$ and tended to be higher in summer when the surface stratified layer shallowed (Section 2.2.5). Because SLD was consistently shallower

Table 4. Surface stratified layer depth (SLD, m), secchi depth (m), and euphotic zone characteristics (surface irradiance, I_0 , $\mu\text{E} \cdot \text{m}^{-2} \cdot \text{s}^{-1}$; euphotic zone depth, m; average PAR in the euphotic zone, $\mu\text{E} \cdot \text{m}^{-2} \cdot \text{s}^{-1}$; and average PAR in the mixed layer, $\mu\text{E} \cdot \text{m}^{-2} \cdot \text{s}^{-1}$) in 2009 and 2010. Where more than one measurement was collected at a station during a single cruise, the values were averaged. Euphotic zone depth was calculated from 1% I_0 . When euphotic zone depth exceeded sampling depth, euphotic zone is reported as > sampling depth and average PAR in the euphotic zone is reported as average PAR from surface to deepest depth sampled. Average PAR in the euphotic zone was calculated from $I_0 \times (k \times D)^{-1} \times (1 - e^{-(k \times D)})$, where k is the extinction coefficient (1.7) and D is the depth of the euphotic zone. Average PAR in the SLD is calculated in the same manner, using SLD instead of euphotic zone depth.

Date	Head				Centre							Mouth						
	I_0	Euphotic zone depth	SLD	Secchi	Avg PAR in euphotic zone	Avg PAR in SLD	I_0	Euphotic zone depth	SLD	Secchi	Avg PAR in euphotic zone	Avg PAR in SLD	I_0	Euphotic zone depth	SLD	Secchi	Avg PAR in euphotic zone	Avg PAR in SLD
2009	$\mu\text{E} \cdot \text{m}^{-2} \cdot \text{s}^{-1}$	m	m	m	$\mu\text{E} \cdot \text{m}^{-2} \cdot \text{s}^{-1}$	$\mu\text{E} \cdot \text{m}^{-2} \cdot \text{s}^{-1}$	$\mu\text{E} \cdot \text{m}^{-2} \cdot \text{s}^{-1}$	m	m	m	$\mu\text{E} \cdot \text{m}^{-2} \cdot \text{s}^{-1}$	$\mu\text{E} \cdot \text{m}^{-2} \cdot \text{s}^{-1}$	$\mu\text{E} \cdot \text{m}^{-2} \cdot \text{s}^{-1}$	m	m	m	$\mu\text{E} \cdot \text{m}^{-2} \cdot \text{s}^{-1}$	$\mu\text{E} \cdot \text{m}^{-2} \cdot \text{s}^{-1}$
Feb 26-28	757.17	> 43	6		10.36	74.23	412.60	>29	24		8.37	10.11	499.43	> 28	15		10.49	19.59
							454.32	> 31	24		8.62	11.14						
Mar 17-19			2	8.8			225.78	> 36	4.5	9.3	3.69	29.50		35	7.5			
							139.16	> 115	4.5		4.55	18.18						
Apr 2-3	350.52	> 31	2	7.7	6.65	99.65	180.15	> 33	2	9.4	3.21	51.22	364.50	> 33	4.5	14.3	6.50	47.62
													298.45	> 32	4.5		5.49	38.99
Apr 16-17	270.29	> 31	2	2.6	5.13	76.84	331.56	> 111	2	5.0	1.76	94.26		6	6.3			
							1,804.92	> 20	2		53.09	513.14						
May 3-4	275.50	> 31	2	3.0	5.23	78.32				2.7			757.54	> 28	8	3.0	15.91	55.70

Date	Head				Centre							Mouth						
	I_0	Euphotic zone depth	SLD	Secchi	Avg PAR in euphotic zone	Avg PAR in SLD	I_0	Euphotic zone depth	SLD	Secchi	Avg PAR in euphotic zone	Avg PAR in SLD	I_0	Euphotic zone depth	SLD	Secchi	Avg PAR in euphotic zone	Avg PAR in SLD
2010	$\mu\text{E} \cdot \text{m}^{-2} \cdot \text{s}^{-1}$	m	m	m	$\mu\text{E} \cdot \text{m}^{-2} \cdot \text{s}^{-1}$	$\mu\text{E} \cdot \text{m}^{-2} \cdot \text{s}^{-1}$	$\mu\text{E} \cdot \text{m}^{-2} \cdot \text{s}^{-1}$	m	m	m	$\mu\text{E} \cdot \text{m}^{-2} \cdot \text{s}^{-1}$	$\mu\text{E} \cdot \text{m}^{-2} \cdot \text{s}^{-1}$	$\mu\text{E} \cdot \text{m}^{-2} \cdot \text{s}^{-1}$	m	m	m	$\mu\text{E} \cdot \text{m}^{-2} \cdot \text{s}^{-1}$	$\mu\text{E} \cdot \text{m}^{-2} \cdot \text{s}^{-1}$
Mar 18-19			2	5.0						3	3.3					4	4.9	
Apr 23-24			2	3.5			1047.73	6.6	2	3.8	93.38	297.87	396.58	10	5	5.8	23.33	46.65
							342.74	11.5	2		17.53	97.44						
							517.74	7.6	2		40.07	147.20						
May 17-18	1239.55	13.3	2	4.8	54.82	352.41	232.24	13.6	2	5.0	10.05	66.03		2	6.9			
Jun 20-22	2041.07	8.6	2	2.6	139.61	580.28	649.14	> 26	2	3.5	14.69	184.55	1502.79	9.5	3	4.9	93.05	292.87
							749.68	14.9	2		29.60	213.13	173.43	17.5	3		5.83	33.80
Jul 20-21	2143.18	5.7	4	1.2	221.16	314.82	912.83	30	3	3.4	17.90	177.90	2622.73	14.5	2	4.1	106.40	745.65
	2477.05	4.2	4		346.65	363.87	344.41	5.4	3		37.51	67.12						

than the bottom of the euphotic zone, average PAR in the euphotic zone ($2 - 347 \mu\text{E} \cdot \text{m}^{-2} \cdot \text{s}^{-1}$) was lower than average PAR in the SLD.

2.3.2 Phytoplankton

2.3.2.1 Seasonal chlorophyll *a* cycle

In 2009, initiation of the phytoplankton bloom appeared to occur first in mid-April near the head of the inlet and latest in early June at the mouth (Figure 11). The biomass (using *chl a* concentration as a proxy) of the spring phytoplankton bloom appeared highest at the head ($15.8 \mu\text{g chl a} \cdot \text{L}^{-1}$), followed by the centre ($12.0 \mu\text{g chl a} \cdot \text{L}^{-1}$), and lowest at the mouth ($9.9 \mu\text{g chl a} \cdot \text{L}^{-1}$; Figure 11). In 2010, no clear spring bloom trend was evident from the monthly samples collected, most likely a result of infrequent sampling and possibly missing the spring bloom due to a late sampling season. Daily 5m *chl a* samples were collected starting March 8, 2010, by which point the bloom was already underway (data not shown).

2.3.2.2 Phytoplankton community composition

In 2009, phytoplankton blooms and high-abundance occurrences (rankings of 4 and 3, respectively; Section 2.2.6) of individual genera and species occurred from mid-April through mid-August (Figure 12). At all stations, high-abundance and bloom-forming taxa were almost exclusively diatoms. Three taxa dominated the phytoplankton community in most samples: *Skeletonema costatum*, *Chaetoceros* spp., and *Thalassiosira* spp. Other high-abundance taxa observed were *Pseudo-nitzschia* spp. and *Leptocylindrus minimus*. Two occurrences of

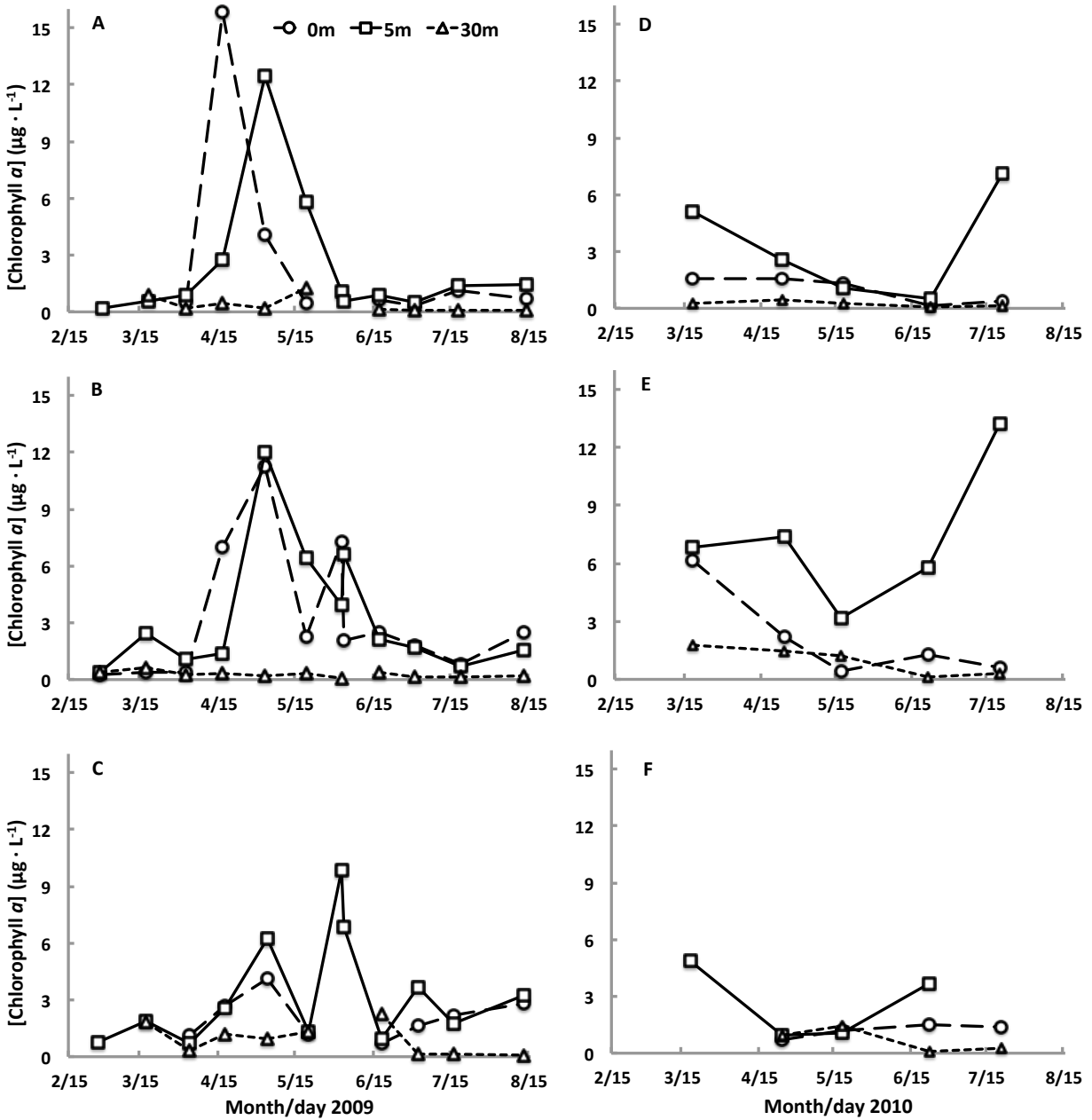


Figure 11. Chlorophyll *a* concentrations ($\mu\text{g} \cdot \text{L}^{-1}$) in 2009 at the (A) head, (B) centre, (C) mouth of the inlet, and in 2010 at the (D) head, (E) centre, and (F) mouth of the inlet.

dinoflagellate-dominated communities were observed. In early July 2009, a surface (0m) bloom of *Heterocapsa triquetra* was observed at the centre of the inlet, while in mid-August a high abundance of *Prorocentrum gracile* was observed at 0m at the mouth (Figure 12). Neither of these species is known to produce toxins.

In 2010, phytoplankton samples were analyzed from mid-May, mid-June, and mid-July. The same three diatom taxa (*Skeletonema costatum*, *Chaetoceros* spp., and *Thalassiosira* spp.) dominated the samples (Figure 12). Other high abundance species observed in 2010 were the diatoms *Thalassionema nitzschioides* and *Rhizosolenia styliformes*. No non-diatoms were observed in high abundance in 2010 samples, which may be due to infrequent sampling. See Appendix C for all data.

2.3.3 Correlations between nutrients and phytoplankton

At 0m and 5m, Rivers Inlet phytoplankton were most likely nutrient-limited (nutrient concentration less than detection limit) from mid-May to mid-August in 2009 and from late April to mid-July in 2010. Nutrient depletion tended to occur earlier at the head and later at the mouth of the inlet. This correlated well with the timing of increases in *chl a* in the spring. In order to better characterize the nutrient concentrations in the water, we normalized the maximum spring nutrient concentrations to the Redfield ratio (1 P : 15 Si : 16 N; Brzezinski 1985). From this, we determined that, in general, phytoplankton throughout the inlet would have run out of NO_3 before either PO_4 or Si (Table 5). Similar seasonal trends were observed in both years. NO_3 -limitation was observed in both years at 5m throughout the inlet and at 0m at the mouth. PO_4 -limitation was only observed at 0m at the head. Some NO_3 - and PO_4 -co-limitation was observed at 0m at the centre and mouth (Figures 8 – 10).

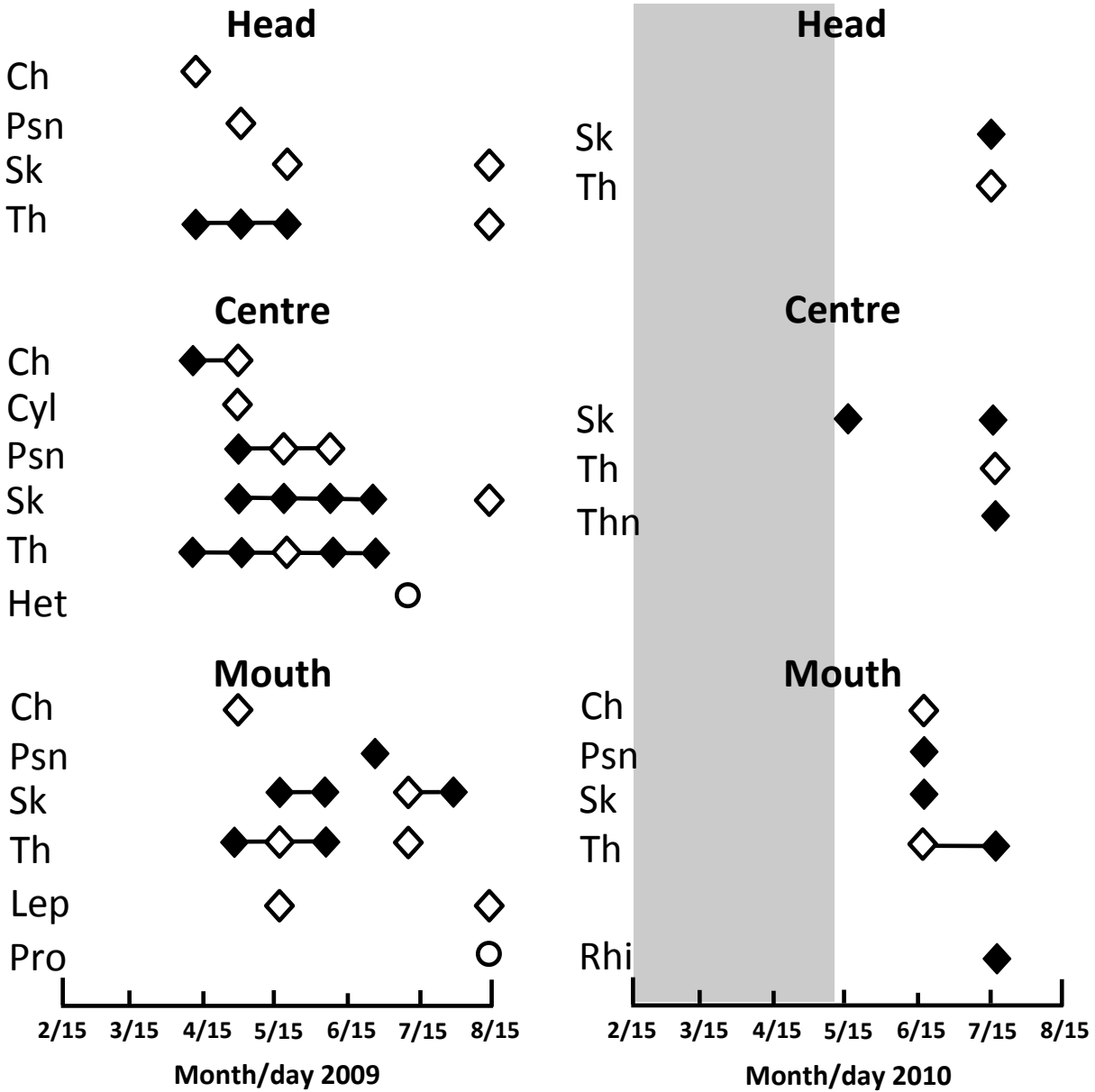


Figure 12 Bloom and high abundance occurrences of phytoplankton taxa in 2009 and 2010 (rankings of 4 and 3, respectively; see text). Solid symbols are blooms, hollow symbols are high-abundance events. Diamonds are diatoms, circles are dinoflagellates. Grey area: no samples analyzed. Ch: *Chaetoceros* spp. Psn: *Pseudo-nitzschia* spp. Sk: *Skeletonema costatum*. Th: *Thalassiosira* spp. Cyl: *Cylindrotheca closterum*. Het: *Heterocapsa triquetra*. Lep: *Leptocylindrus minimus*. Pro: *Prorocentrum minimum*. Thn: *Thalassionema nitzschioides*; Rhi: *Rhizosolenia styliformes*.

Table 5. Maximum spring nutrient concentrations (PO₄, Si, and NO₃; μM) at the head, centre, and mouth of the inlet were divided by the Redfield ratio (1 P : 15 Si : 16 N). Lowest values (*italics*) are the nutrient that will run out first. 30m data excluded because no drawdown was observed at that depth.

		PO ₄	Si	NO ₃
Redfield ratio:		1	15	16
2009	Depth	PO₄	Si	NO₃
Head	0m			
	5m	1.86	2.86	<i>1.44</i>
Centre	0m	1.54	2.46	<i>1.13</i>
	5m	1.74	2.58	<i>1.24</i>
Mouth	0m	1.79	2.90	<i>1.37</i>
	5m	1.80	2.90	<i>1.38</i>
2010				
Head	0m			
	5m	1.25	1.27	<i>0.92</i>
Centre	0m	0.67	1.39	<i>0.45</i>
	5m	0.91	1.44	<i>0.71</i>
Mouth	0m	0.96	1.42	<i>0.62</i>
	5m	1.06	1.55	<i>0.70</i>

2.3.4 FRRF-¹³C primary productivity calibration

In laboratory measurements, FRRF-derived primary productivity measurements (FRRF-PP) correlated well with primary productivity calculated from ¹³C fixation (¹³C-PP; Figure 13). In laboratory trials, rates were higher for FRRF-PP than ¹³C-PP [average 162.3 vs. 152.5 μg C · (L · h)⁻¹], while in the field FRRF-PP rates were lower than ¹³C-PP rates [all depths, average 23.9 vs. 28.0 μg C · (L · h)⁻¹]. At 30m, both FRRF-PP and ¹³C-PP rates were practically negligible (Figure 13d). Unlike laboratory data and 30m field data, the relationship between FRRF-PP and ¹³C-PP data is not significant at 0m or 5m. FRRF-PP and ¹³C-PP at 5m, while not significantly correlated, are on the same order of magnitude (Figure 13b). Surface (0m) ¹³C-PP data were more than 30x greater than 0m FRRF-PP data [average 14.5 vs. 0.31 μg C · (L · h)⁻¹].

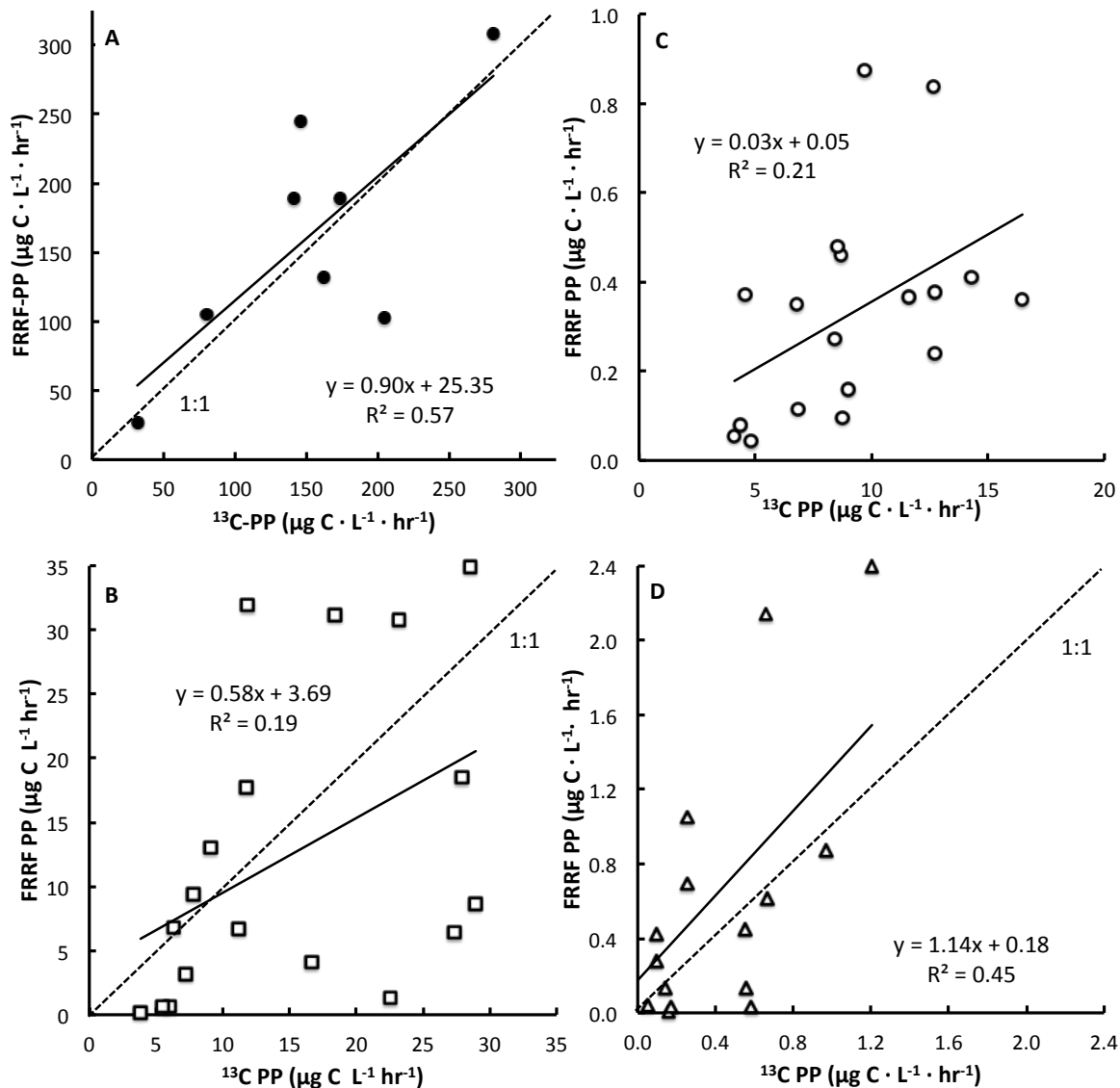


Figure 13. Comparison of primary productivity measurements ($\mu\text{g C} \cdot \text{L}^{-1} \cdot \text{h}^{-1}$) calculated from FRRF measurements and from ^{13}C bottle incubations (A) in the laboratory using cultures of *Skeletonema costatum* and *Chaetoceros* sp. isolated from Rivers Inlet and field data from (B) 5m, (C) 0m, and (D) 30m depth. Vertical and horizontal scales of A, B, and D are equal in each panel. Note that in C, vertical and horizontal scales are not equal.

Laboratory data, obtained with high chl *a* ($9.23 - 64.16 \mu\text{g chl } a \cdot \text{L}^{-1}$) cultures in exponential growth, showed a good correlation between FRRF and ^{13}C estimates of primary productivity and the slope of the regression line is close to 1 (0.90 ± 0.32 , $r^2 = 0.57$, $p = 0.03$; Figure 13a). At 30m, we also observed a significant positive correlation between FRRF and ^{13}C

estimates (slope 1.14 ± 0.30 , $r^2 = 0.45$, $p = 0.0016$; Figure 13d), even though primary productivity values were low [$< 2.4 \mu\text{g C} \cdot (\text{L} \cdot \text{h})^{-1}$]. At 5m depth, even though *chl a* was relatively high (maximum $13.26 \mu\text{g chl a} \cdot \text{L}^{-1}$), did not observe a significant correlation between FRRF-PP and ^{13}C -PP (0.58 ± 0.30 , $r^2 = 0.19$, $p = 0.070$). At 0m, the slope was much lower and the correlation was also not significant (slope 0.03 ± 0.015 , $r^2 = 0.21$, $p = 0.056$; Figure 13c). These field experiments were performed in late May and mid-July, when cells were nutrient limited at 0m and 5m (Section 2.3.3) and *chl a* biomass was low at the surface ($< 1.5 \mu\text{g} \cdot \text{L}^{-1}$).

2.3.5 FRRF-derived primary productivity

In 2009, primary productivity measurements derived from FRRF data (FRRF-PP) ranged from $0.15 - 17.80 \mu\text{g C} \cdot (\text{L} \cdot \text{h})^{-1}$ at 0m. At 5m, FRRF-PP ranged from $0.10 - 32.10 \mu\text{g C} \cdot (\text{L} \cdot \text{h})^{-1}$. We observed an increase in primary productivity throughout the inlet at 0 and 5m that coincided with the timing of the spring phytoplankton bloom, in early to mid-April of 2009. At the head and centre, at 0m and 5m, FRRF-PP continued increasing until mid-May, reaching maximum values of 32.10 and $28.40 \mu\text{g C} \cdot (\text{L} \cdot \text{h})^{-1}$, respectively. No early May data were available at the mouth in 2009. In 2010, we observed an increase in FRRF-derived primary productivity estimates at the centre of the inlet at 5m from mid-June to mid-July (Table 6). This increase was mirrored by *chl a* concentrations, as observed in 2009 (see Section 2.3.6 for a comparison of FRRF-PP, nutrient, and *chl a* at 5m).

After normalizing to *chl a*, FRRF-PP varied over a narrower range [$0.01 - 5.27 \mu\text{g C} \cdot (\mu\text{g chl a} \cdot \text{h})^{-1}$]. FRRF-PP normalized to water volume and *chl a* [$\mu\text{g C} \cdot (\text{L} \cdot \text{h})^{-1}$ and $\mu\text{g C} (\mu\text{g chl a} \cdot \text{h})^{-1}$, respectively] tended to co-vary. From mid-March to early April 2009, however, FRRF-PP normalized to *chl a* decreased at all depths while FRRF-PP increased [e.g., at 5m $0.58 - 0.36 \mu\text{g C} \cdot (\mu\text{g chl a} \cdot \text{h})^{-1}$ versus FRRF-PP $0.38 - 1.54 \mu\text{g C} \cdot (\text{L} \cdot \text{h})^{-1}$].

Table 6. FRRF-derived measurements of primary productivity [FRRF-PP; $\mu\text{g C} \cdot (\text{L} \cdot \text{h})^{-1}$] collected during 2009 and 2010 bio-oceanographic surveys.

2009	Date	FRRF-PP $\mu\text{g C} \cdot (\text{L} \cdot \text{h})^{-1}$		
		0m	5m	30m
Head	2/27			0.045
	3/18		0.79	0.34
	4/3	0.26	1.52	0.001
	4/16	15	4.9	0.080
	5/3	8.0	32	0.026
Centre	2/27	0.15		0.045
	3/17	0.51	1.4	0.34
	4/2	0.19	0.38	0.001
	4/16	9.2	1.5	0.080
	5/3	18	28	0.026
Mouth	4/3	0.47	0.10	0.006
	4/17	0.85	2.5	0.083
2010				
Head	7/21	1.8	16	0.001
Centre	5/19	0.37	6.8	2.4
	6/21	0.020	3.2	0.006
	6/22	0.88	13	0.033
	7/20	0.46	32	0.039
	7/21	0.48	31	0.095
Mouth	6/20	1.0	0.99	0.016
	7/20	0.44		0.050

2.3.6 Correlations between macronutrients, chlorophyll *a* concentrations, and FRRF-derived measurements of primary productivity

In 2009, there was a negative correlation between decrease in macronutrient (NO_3 and PO_4) concentrations and increase in *chl a* and primary productivity. This trend was most evident at the head and mouth. At the head, the decrease in NO_3 and PO_4 and increase in *chl a* and FRRF-PP occurred between mid-April and early May (Figure 14; PO_4 not shown). At the mouth, the same trend was observed, starting in early April. At the centre, FRRF-PP and *chl a*

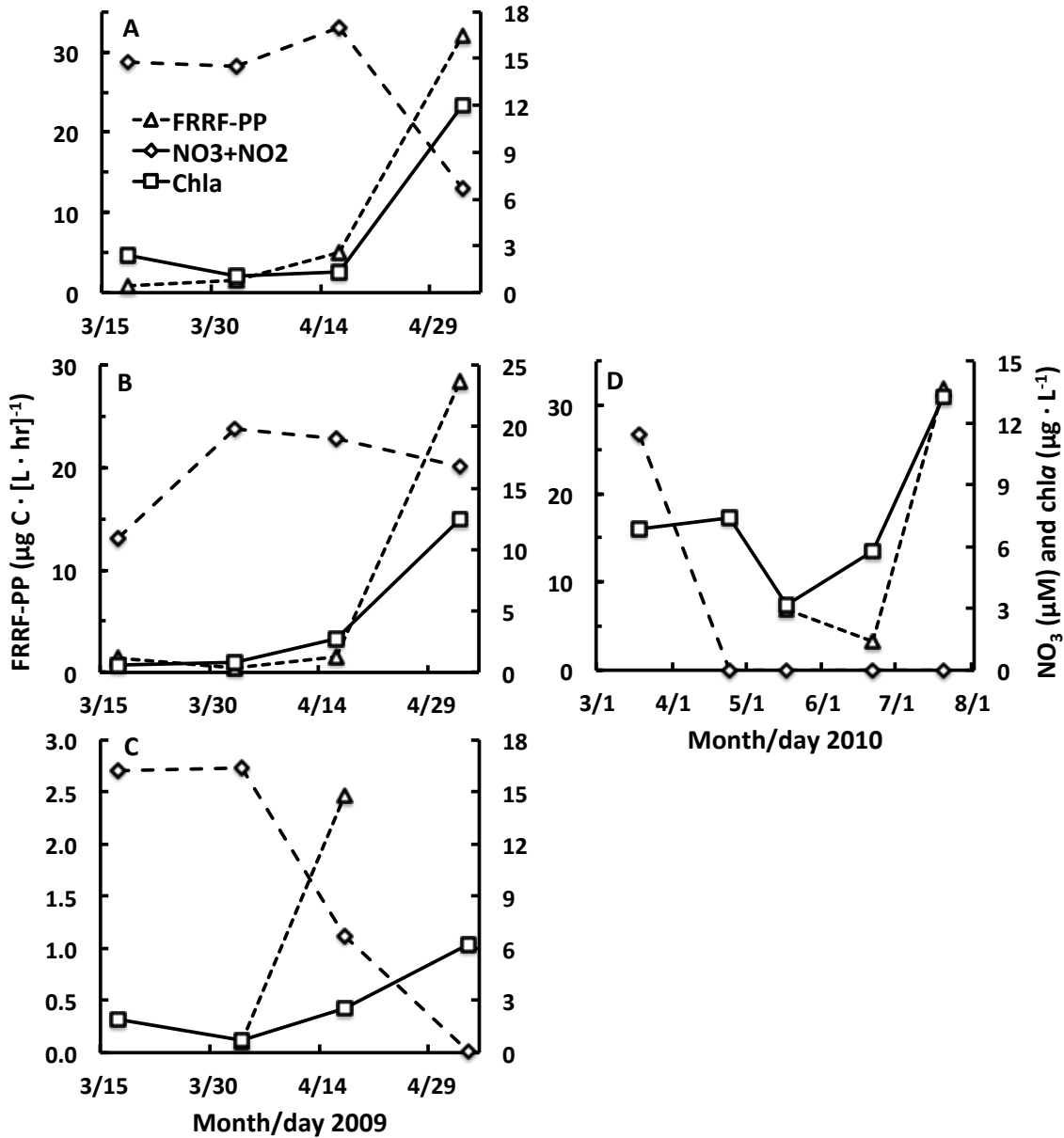


Figure 14. Comparison of NO₃ (µM), chl a (µg · L⁻¹), and FRRF-derived primary productivity measurements [FRRF-PP, µg C · (L · h)⁻¹] from 5m depth in 2009 at the (A) head, (B) centre, (C) mouth, and (D) in 2010 at the centre of the inlet. FRRF-PP is on the primary axis. NO₃ and chl a are on the secondary axis.

increased over the same interval, but nutrient concentrations decreased only slightly. FRRF-PP data were not available beyond early May, though NO₃ and PO₄ concentrations continued to decrease in mid-May.

Assuming a C:chl*a* molar ratio of 45 (average value from Strom et al. 2007), net primary productivity (NPP) estimated from chl*a* measurements at 0 and 5m ranged from 0.18 to 2.05 $\mu\text{g C} \cdot (\text{L} \cdot \text{h})^{-1}$ in 2009 and 0.14 to 0.43 $\mu\text{g C} \cdot (\text{L} \cdot \text{h})^{-1}$ in 2010 (Table 7). Using the Redfield ratio, NPP was also estimated from PO_4 , NO_3 , and Si drawdown. PO_4 and NO_3 estimates of NPP agree well [0.59 – 2.64 $\mu\text{g C} \cdot (\text{L} \cdot \text{h})^{-1}$ and 0.49 – 1.96 $\mu\text{g C} \cdot (\text{L} \cdot \text{h})^{-1}$, respectively] and were similar to chl*a*-derived estimates of NPP. Si drawdown estimates of NPP were generally twice as high as those derived from PO_4 and NO_3 drawdown [0.79 – 6.49 $\mu\text{g C} \cdot (\text{L} \cdot \text{h})^{-1}$]. Estimates of NPP from nutrient drawdown were generally higher than those from chl*a*. It is possible that we did not capture peak chl*a* due to infrequent sampling, resulting in an underestimate of NPP by this method. Comparison between FRRF-PP, which estimates gross primary productivity (GPP), and chl*a*- or nutrient-derived measurements of NPP is more difficult due to the differences in time-scales of the measurements (μs to s versus weeks to months, respectively). Ranges of FRRF-PP observed during nutrient drawdown and chl*a* increase are listed (Table 7).

Table 7. Primary productivity [PP, $\mu\text{g C} \cdot (\text{L} \cdot \text{h})^{-1}$] calculated from *chl a* data using C:*chl a* molar ratios of 65 and 45 (when an increase in *chl a* was observed) and from nutrient concentrations using the Redfield ratio (when nutrient drawdown was observed). PP measured using a fast repetition rate fluorometer [FRRF-PP, $\mu\text{g C} \cdot (\text{L} \cdot \text{h})^{-1}$] are reported here as a range of values that occurred at the same time as *chl a* increase and nutrient drawdown.

2009	Depth	PP from <i>chl a</i> $\mu\text{g C} \cdot (\text{L} \cdot \text{h})^{-1}$		PP from nutrients $\mu\text{g C} \cdot (\text{L} \cdot \text{h})^{-1}$			FRRF-PP $\mu\text{g C} \cdot (\text{L} \cdot \text{h})^{-1}$
		C:Chl a = 65	C:Chl a = 45	from PO ₄	from Si	from NO ₃	range
Head	0m	2.97	2.05				0.26 – 15.13
	5m	1.01	0.70	1.03	2.29	1.14	0.79 – 32.10
Centre	0m	0.95	0.66	2.64	6.49	1.96	0.15 – 17.80
	5m	1.70	1.18	0.59	0.79	0.49	0.38 – 28.39
Mouth	0m	0.26	0.18	2.64	2.30	1.84	0.47 – 0.85
	5m	0.48	0.34	1.36	1.32	1.09	0.10 – 2.46
2010							
Head	0m						1.82
	5m	0.62	0.43	1.71	2.61	1.32	15.69
Centre	0m			0.96	1.43	0.65	0.02 – 0.87
	5m	0.43	0.30	1.26	2.02	1.02	3.19 – 31.98
Mouth	0m			1.35	2.04	0.91	0.44 – 1.02
	5m	0.20	0.14	1.49	2.23	1.03	0.99

2.4 Discussion

2.4.1 Characterizing the spring phytoplankton bloom in Rivers Inlet: nutrients, chlorophyll, and phytoplankton community dynamics

Rivers Inlet exhibits seasonal nutrient patterns typical of temperate estuaries. During winter, upwelling and mixing of the water column brings similarly nutrient-rich deep waters to the surface (e.g., $21.7 \mu\text{M NO}_3$) throughout the inlet. In spring, the upper water column becomes strongly stratified and nutrients are depleted at the surface by large diatom-dominated phytoplankton blooms. During 2009, phytoplankton at 0m were limited by nutrients before those at 5m. Nutrient depletion occurred slightly earlier at the head of the inlet, but was most pronounced at the mouth. However, the pronounced nutrient depletion at the mouth did not

appear to coincide with the highest chl_a concentrations in the inlet. This may have been due to faster rates of biomass turnover and primary productivity at the mouth. Unfortunately, no primary or secondary productivity data are available at the mouth in May 2009. This may also be an artifact of sampling frequency. Daily chl_a data from the centre of the inlet (not shown) indicate 2-3 day cycling of phytoplankton biomass increase and decrease. It is possible that the true chl_a peak was not captured by fortnightly sampling.

In general, NO₃ was the first nutrient to limit primary productivity when salinity was > 28. PO₄-limitation was observed when salinity was < 6, which only occurred at the head at 0m. Because of the freshet and strong summer stratification (Section 2.3.1.3), the surface waters at the head and centre of the inlet resembled the fresh Owikeno Lake water from mid-June to mid-August of 2009. Interestingly, at the surface in the centre of the inlet, we observed NO₃ and PO₄ co-limitation at intermediate salinities (9.7 – 19.3). Because freshwater tends to be PO₄-limited and coastal seawater tends to be NO₃-limited, this shift from PO₄ limitation to PO₄/NO₃ co-limitation followed by NO₃ limitation as salinity increases is a characteristic of temperate estuaries (e.g., Doering et al. 1995, Fisher et al. 1999, Crain 2007, Hartzell and Jordan 2012).

The drawdown of Si was in excess of the 15 Si : 16 N : 1 P ratio predicted by Brzezinski (1985). This has also been observed in previous studies in the Strait of Georgia (Harrison et al. 1990, Riche 2011). Like Riche (2011), we found that the high abundance of robustly silicified diatoms (such as *Skeletonema costatum*, *Chaetoceros* spp., and *Thalassiosira* spp.) most likely explains the excess Si drawdown in Rivers Inlet. Brzezinski (1985) found that Si:N ratios varied widely between species and even between different clones of a single species, ranging from 0.28 for *Thalassiosira pseudonana* to 4.38 for *Thalassionema nitzschioides*. In this context, our Si:N values (1.42 – 2.90) are within the expected range for robustly silicified diatoms.

Fortnightly sampling showed higher *chl a* values and earlier spring blooms at the head of the inlet. More frequent sampling is required to determine whether this is an artifact of our sampling scheme. However, given that pre-bloom nutrient levels were similar throughout the fjord, observed spatial differences in the magnitude and timing of the spring bloom must be controlled by stratification and mixing. Earlier stratification leads to higher average light levels experienced by phytoplankton, an earlier bloom, and higher *chl a*. Enhanced mixing causes dilution of the phytoplankton seed population, reduces light availability, and leads to a delayed spring bloom (Wolfe 2010) and lower *chl a*. Indeed, the surface layer shallowed earlier at the head (from 6m to 2m, late February to mid-March) than at the mouth (15m to 4.5m, late February to early April), supporting our observation that phytoplankton were able to bloom sooner in the former. This difference is presumably due to stronger stratification at the head from the outflow of the Owikeno River and mixing due to wind and currents outside the mouth. Turbidity may also influence the timing of the bloom. Greater turbidity at the head due to the high silt content of Owikeno Lake water would decrease light availability in the water column. This may hasten the termination of the bloom at the head during the freshet.

In spite of these potential differences in the timing and magnitude of the spring bloom, the diatoms *Skeletonema costatum*, *Chaetoceros* spp., and *Thalassiosira* spp. dominated the spring bloom at all three sample locations, and continued to be abundant in the summer when other non-diatom species (dinoflagellates, ciliates, and other flagellates) also bloomed. The composition of the phytoplankton community has important implications for secondary consumers. Copepod grazers that fed on a diverse phytoplankton community, even when diatoms still dominate, have been shown to be a richer food source for their predators (El-Sabaawi et al. 2009). Wolfe (2010) modeled the timing of the spring bloom in Rivers Inlet and

showed that it greatly differed between years (from early to late April in the years 2006 – 2009; Table 8). These modelled results correspond well with our observations and those of Tommasi (2008) and Tommasi et al. (2012a, b). An earlier spring bloom may lead to an earlier transition to the mixed summer phytoplankton community, which may benefit sockeye smolts by producing better prey quality. Changes in the timing of the spring phytoplankton bloom can also negatively impact higher trophic levels via a potential timing mismatch (Cushing 1990). For example, in years of a late phytoplankton bloom (e.g. 2007, 2009; Table 8), the zooplankton bloom was also delayed and reduced (Tommasi 2008 and Tommasi et al. 2012a, b). Furthermore, these later zooplankton blooms contributed to smaller and less robust sockeye smolts (Buchanan 2006, Ajmani 2011). Thus, the timing of the phytoplankton spring bloom (earlier) may be a good proxy for smolt robustness (more robust).

Table 8. Spring phytoplankton bloom dates predicted by Wolfe (2010). Model data is not available for 2010, though the bloom was already underway in early March (data not shown).

Year	Bloom date
2006	April 11
2007	April 28
2008	April 3
2009	April 13
2010	(before March 10)

2.4.2 Comparison of FRRF and ^{13/14}C calculations of primary productivity

Phytoplankton cultured under nutrient-replete conditions, in exponential growth phase exhibited a significant near-1:1 correlation between FRRF-PP and ¹³C-PP (slope = 0.90 ± 0.32 , $R^2 = 0.57$, $p = 0.030$; Table 9). Suggett et al. (2009a) reported an average slope between FRRF-PP and ^{13/14}C-PP of 1.57 (6 different laboratory strains), while Fujiki et al. (2007) measured a slope of 1.52 in *Dunaliella tertiolecta*.

Table 9. FRRF-PP:¹³C-PP slopes for experiments run in the laboratory and in Rivers Inlet. (*) denotes significant correlation.

	Slope ± error	R²	P-value
Laboratory	0.90 ± 0.32	0.57	0.030*
0m field	0.030 ± 0.015	0.21	0.056
5m field	0.58 ± 0.30	0.29	0.070
30m field	1.1 ± .030	0.45	0.002*

Field comparisons of FRRF-PP and ¹³C-PP from 30m in Rivers Inlet showed similar slopes to those from our laboratory data (30m slope = 1.1 ± 0.30, R² = 0.45, p = 0.002). Previous studies of diatom-dominated coastal regions measured higher average slopes of 1.80, 2.98, and 1.43 (Moore et al. 2003, Raateoja et al. 2004, Estevez-Blanco et al. 2006, respectively; Table 10), using 1- to 2-hour bottle incubations. While slopes were similar between our 30m field and lab measurements, our primary productivity measurements at all depths in the field were substantially lower than those in the lab. This can be attributed to differences in phytoplankton biomass (lab chl_a: 9 – 71 μg chl_a · L⁻¹; field chl_a: 0.05 – 13 μg chl_a · L⁻¹) and sub-optimal light and nutrient conditions.

In contrast to the 30m field data, there was no significant relationship between FRRF-PP and ¹³C-PP at 0m or 5m. At 5m (slope 0.58 ± 0.30), the data were scattered, but slopes <1 have been previously reported (e.g., Moore et al. 2003, Smyth et al. 2004). These <1 slopes were reported for communities dominated by smaller phytoplankton such as flagellates. Many of the data points below the 1:1 line (where FRRF-PP < ¹³C-PP; Figure 13b) are from mid-July, when the phytoplankton community had already transitioned to the more diverse summer community. These low “flagellate-influenced” data points contribute to the slightly low slope we observed. In contrast, surface (0m) data had a significantly lower slope for FRRF-PP:¹³C-PP than expected (0.03 vs. 1; Figure 13). At 0m, the ¹³C-PP rates were roughly 30x higher than the FRRF-PP

Table 10. Ratios are reported as ETR:^{13/14}C-PP, calculated in units mol e⁻ · (g chla · h)⁻¹ : mol CO₂ · (g chla · h)⁻¹ or mol e⁻ · (L · h)⁻¹ : mol CO₂ · (L · h)⁻¹. The final ratio is in units of mol e⁻ · (mol CO₂)⁻¹. ETR: electron transfer rate of photosystem II. SIS: simulated *in situ*. PE: photosynthesis light response. Inc: incubation. Modified from Suggett et al. (2009a, 2010). (*) denotes ratios that were reported in the literature as FRRF-PP:^{13/14}C-PP. These were calculated using a conversion factor of 4:1 ETR:FRRF-PP based on the minimum 4 e⁻ (derived from 2 H₂O) required to evolve 1 O₂.

Techniques	Method	Ratio	Dominant group	Location, season	Reference
Pump and probe vs. ¹⁴ C	<i>In situ</i> vs. SIS 4 h PE	5.44	n/a	NW Atlantic, various	Kolber and Falkowski 1993
	<i>In situ</i> vs. 2 h PE	2.45	Coccolithophores	NE Atlantic, summer	Boyd <i>et al.</i> 1997
FRRF vs. ¹⁴ C	<i>In situ</i> vs. 1 h PE	8.66	Cyanobacteria, small flagellates	Northeast Atlantic, spring	Suggett <i>et al.</i> 2001)
	<i>In situ</i> vs. 1-2 h PE	6.03	Diatoms and dinoflagellates	UK Shelf, summer	Moore <i>et al.</i> 2003b
		3.94	Coccolithophores and flagellates		
	<i>In situ</i> vs. 1-2 h PE	11.9	Diatoms and dinoflagellates	Baltic Sea, spring	Raateoja <i>et al.</i> 2004
		8.81	Cyanobacteria and flagellates		
	<i>In situ</i> vs. SIS 24 h PE	2.98	Coccolithophores and flagellates	UK shelf, late spring	Smyth <i>et al.</i> 2004
	<i>In situ</i> vs. SIS (day) PE	8.81	Picoeukaryotes and prochlorophytes	Pacific Ocean, annual	Corno <i>et al.</i> 2005
	<i>In situ</i> vs. 2 h PE	9.09	Diatoms and small flagellates	W Atlantic, late spring	Estévez-Blanco <i>et al.</i> 2006
	<i>In situ</i> vs. SIS 3 h PE	4.60	Diatoms and cyanobacteria	Alpine lake, annual	Kaiblinger and Dokulil 2006
	<i>In situ</i> vs. 1 h PE	4.13	n/a	NE coastal US, annual	Melrose <i>et al.</i> 2006
	<i>In situ</i> vs. SIS 24 h PE	10.1	Coccolithophores and flagellates	UK shelf, late spring	Pemberton <i>et al.</i> 2006
	<i>In situ</i> vs. <i>in situ</i> pH	4.04	Diatoms	UK lake, spring	Suggett <i>et al.</i> 2006a
		6.12	Diatoms and flagellates		
	<i>In situ</i> vs. SIS (day) PE	7.08	Picoeukaryotes and cyanobacteria	Tropical Atlantic, various	Suggett <i>et al.</i> 2006b
		16.9	Prochlorophytes and picoeukaryotes	Atlantic gyres, various	
	<i>In situ</i> vs. 1 h PE	4.36	Cyanobacteria and flagellates	US Great Lakes, late summer	Pemberton <i>et al.</i> 2007
	<i>In situ</i> vs. 2 h PE	9.68	Cyanobacteria and chlorophytes	Netherlands lake, summer	Kromkamp <i>et al.</i> 2008
Step PE (5 min E ⁻¹) vs. 20 min PE	6.08	<i>Dunaliella tertiolecta</i>	Laboratory-based	Fujiki <i>et al.</i> 2007	
FRRF v ¹⁴ C (40-min inc)	9.01	<i>Dunaliella tertiolecta</i>	Laboratory-based	Ross <i>et al.</i> 2008	
FRRF v ¹⁴ C (1-hour inc)	6.26	Various	Laboratory-based	Suggett <i>et al.</i> 2009AME	
FRRF vs. ¹³ C	<i>In situ</i> vs. 1 h PE	5.28 – 7.16*	Diatoms and flagellates	Ariake Bay, southwestern Japan, summer	Tripathy <i>et al.</i> 2010
	<i>In situ</i> vs. 24 h PE	4.36 – 7.28*			
	<i>In situ</i> vs. <i>in situ</i> 2 h PE	3.59*	Diatoms	Laboratory-based	This study
4.44*		Diatoms	Temperate coastal fjord, summer		

rates, but were similar to the 5m ^{13}C -PP rates, suggesting that the error lies with FRRF-PP estimates. High light levels experienced by phytoplankton at the surface (average PAR from 0m data was $740 \mu\text{E} \cdot \text{m}^{-2} \cdot \text{s}^{-1}$) decrease F_v/F_m (Kromkamp et al. 2008) and result in a large error in σ_{PSII} estimates (Oxborough et al. 2012). While σ_{PSII} is directly proportional to FRRF-PP, the relationship between F_v/F_m and FRRF-PP is more complicated. F_v/F_m is used to calculate f (fraction of potentially functional photosystem II; $f = F_v/F_m \times 0.65^{-1}$) and q_p (photochemical quenching), where $q_p = (F_m' - F') \times (F_m' - F_o')^{-1}$ and $F_o' = F_o \times (F_v/F_m + F_o/F_m')^{-1}$. All else being constant, a decrease in F_v/F_m would decrease f and increase q_p by a smaller amount, resulting in a decrease in FRRF-PP. However, other fluorescence parameters (Section 2.2.11) would not remain constant as F_v/F_m changes. Regardless, a change in F_v/F_m causes a smaller change in q_p than in f . Thus, low F_v/F_m decreases FRRF-PP, while ^{13}C -PP is not affected. Low F_v/F_m due to photoinhibition, combined with the high variability of σ_{PSII} observed at high light levels (Oxborough et al. 2012), may partially explain the extremely low FRRF-PP rate estimates for the 0m data.

Nutrient limitation may also affect the calculated FRRF-PP through changes in F_v/F_m and σ_{PSII} . While many studies have investigated this (e.g., Kolber et al. 1988, Geider et al. 1993, Behrenfeld et al. 2006, Moore et al. 2008), there is no consensus in the literature as to how nutrient limitation influences F_v/F_m and σ_{PSII} . Nutrient limitation has been observed to lower F_v/F_m in laboratory cultures (e.g., Kolber et al. 1998, Lippemeier et al. 1999, Parkhill et al. 2001). In contrast, nutrient-limited communities in the mid-Atlantic exhibit high F_v/F_m and low σ_{PSII} (~15% change; Moore et al. 2006a, 2008, reviewed by Suggett et al. 2009b). While the mid-Atlantic and Rivers Inlet are different in many ways, the primary productivity in both regions appears to be limited mainly by NO_3 . This suggests that, like Moore et al. (2006a, 2008), our

F_v/F_m and σ_{PSII} values were high and low, respectively, due to NO_3 limitation. Even though F_v/F_m and σ_{PSII} both change by the same magnitude (increasing and decreasing, respectively, as a result of nutrient limitation), the 15% change in σ_{PSII} has a bigger effect on FRRF-PP estimates than a 15% change in F_v/F_m (due to f and q_p changing in opposite directions). For our data, either (a) low σ_{PSII} or (b) low F_v/F_m and low σ_{PSII} could explain low rates of FRRF-PP determined at 0m. However, low F_v/F_m alone would not sufficiently influence FRRF-PP to explain our results. Recent field studies suggest that these parameters may be controlled more by the dominant phytoplankton taxonomic group than by the nutrient state of the population (diatoms have high F_v/F_m and low σ_{PSII} , while picoeukaryotes have low F_v/F_m and high σ_{PSII} ; Suggett et al. 2009b), further complicating interpretation of the data. A more systematic analysis of the relationship between nutrient levels, community composition, and FRRF parameters is required to disentangle the relationships between these factors.

In our calculation of FRRF-PP, we estimated photosynthetic unit size [n_{PSII}^{-1} , mol chl *a* · (mol e⁻)⁻¹] as a function of F_v/F_m (Section 2.2.11; Kolber and Falkowski 1993). Calculating n_{PSII}^{-1} as a function of F_v/F_m more accurately represents the variation in n_{PSII}^{-1} than assuming a constant value of 500 mol chl *a* · (mol e⁻)⁻¹ (Falkowski et al. 1981, Smyth et al. 2004, Tripathy et al. 2010). However, this method overestimated n_{PSII}^{-1} in our field data [average 2305 ± 197 mol chl *a* · (mol e⁻)⁻¹]. This is approximately 4-fold higher than values reported in the literature (Table 13 in Appendix B), meaning that our FRRF-PP data is lower than we expected. This may explain why our FRRF-PP:¹³C-PP relationship was < 1 in much of the field data. In contrast, most studies measure slopes > 1 (Table 10). In monoalgal laboratory cultures, however, this technique yielded n_{PSII}^{-1} values in the expected range [*Skeletonema costatum* average 623 ± 26 mol chl *a* · (mol e⁻)⁻¹, *Chaetoceros* sp. average 565 ± 25 mol chl *a* · (mol e⁻)⁻¹]. This suggests that estimating

n_{PSII}^{-1} as a function of F_v/F_m is not accurate in natural phytoplankton assemblages. Measuring n_{PSII}^{-1} would yield more accurate results. Various studies have measured n_{PSII}^{-1} on a wide range of phytoplankton taxa under a variety of light and nutrient conditions. Published values of n_{PSII}^{-1} range from 10 – 951 mol chl *a* · (mol e⁻)⁻¹ (Table 13 in Appendix B). In general, phytoplankton grown in higher light or nutrient levels have lower n_{PSII}^{-1} . Unfortunately, it is impractical to measure n_{PSII}^{-1} in the field to improve FRRF-PP estimates. In our study, we attempted to measure n_{PSII}^{-1} in the three dominant diatom taxa in Rivers Inlet (*Skeletonema costatum*, *Chaetoceros* spp., *Thalassiosira* spp.; Appendix B). Our attempts were not successful and we relied on Kolber and Falkowski's (1993) approach for our FRRF-PP calculations.

Overall, the FRRF technique yielded reliable estimates of primary productivity only in unstressed cells. Further work is required to understand how light, nutrients, and community composition affect FRRF-PP calculations. We expect a near-1:1 ratio between FRRF-PP and ^{13/14}C-PP if (a) cells are relatively healthy (e.g., not nutrient-limited); (b) light is not photoinhibiting; and (c) ^{13/14}C-PP bottle incubations are short (< 4 h). Long incubations more closely approximate net productivity (e.g., Marra 2009) whereas the FRRF measures gross primary productivity. Thus, net (long incubation ^{13/14}C-PP estimates) and gross (FRRF-PP estimates) primary productivity are not directly comparable. Caution should be used when interpreting data collected (a) at high light levels, where the FRRF is likely to underestimate primary productivity, (b) at low phytoplankton biomass, where low chl *a* fluorescence can generate scattered, low-quality data, and (c) between different community compositions. Raateoja et al. (2004) suggest ~0.5 μg chl *a* · L⁻¹ as the lower boundary for reliable data. In addition, we gathered poor-quality data when the FRRF was moving through the water during measurements. The best results were obtained when the FRRF was held steady at a single depth

for the duration of the acquisition.

2.4.3 Primary productivity in Rivers Inlet

Using our ^{13}C -PP data, we estimated an annual primary productivity in Rivers Inlet of $1100 \text{ g C} \cdot \text{m}^{-2} \cdot \text{yr}^{-1}$. For this calculation, we averaged all 5m ^{13}C -PP data and assumed that photosynthesis was only occurring in the top 10m (based on Hodal 2011 and on our observations). This is likely an overestimate since our ^{13}C -PP data were collected during the spring and summer, when primary productivity is the highest. Hodal (2011) calculated new production in Rivers Inlet to be $230 \text{ g C} \cdot \text{m}^{-2} \cdot \text{yr}^{-1}$. If we assume that the high primary production that we measured occurs only 6 months per year, our estimate ($550 \text{ g C} \cdot \text{m}^{-2} \cdot \text{yr}^{-1}$) is closer to that of Hodal (2011) and those reported in other temperate estuaries ($0 - 820 \text{ g C} \cdot \text{m}^{-2} \cdot \text{yr}^{-1}$; Table 11).

In an effort to estimate the potential for sockeye production in Rivers Inlet, we calculated fish production based on 5m ^{13}C primary productivity data [$16.7 \mu\text{g C} \cdot (\text{L} \cdot \text{h})^{-1}$]. The chl *a* maximum is generally at 5m depth, so this approach will necessarily overestimate primary productivity in the top 10m. Based on CTD fluorescence profiles (data not shown), average primary productivity per meter in the upper 10m of the water column is 81% of 5m PP [$13.5 \mu\text{g C} \cdot (\text{L} \cdot \text{h})^{-1}$]. Smolts are present in Rivers Inlet for 2 – 3 months each year (Buchanan 2006, Ajmani 2011, Stocks 2012). Thus, we focus on primary production that occurs only during this period. Given that the surface area of the fjord is $1.3580 \times 10^8 \text{ m}^2$ (Hodal 2011), we calculated $2.64 \times 10^{10} - 3.97 \times 10^{10} \text{ g C}$ is produced in Rivers Inlet while smolts are present. We assumed a 30% loss of primary productivity through exudation of dissolved organic carbon (DOC) and a 12% loss of carbon via phytoplankton respiration (value for *Skeletonema costatum* from

Falkowski and Owens 1978). Thus, we calculated $1.53 \times 10^{10} - 2.30 \times 10^{10}$ g of phytoplankton carbon is available to higher trophic levels. Furthermore, we assumed a 10% energy transfer efficiency between each of 3 trophic levels (diatoms, copepods, and small fish). Our calculations estimate $1.53 \times 10^8 - 2.30 \times 10^8$ g C of small fish in Rivers Inlet during smolt season. Using a 9 g fish:1 g C ratio (Ware 2000), Rivers Inlet can support $1.38 \times 10^6 - 2.07 \times 10^6$ kg small fish during this period. When present, sockeye smolts account for 20 – 50% of small fish in Rivers Inlet (B. Hunt unpublished data). Using proportion of fish as a rough proxy for proportion of biomass, we estimate $2.75 \times 10^8 - 1.04 \times 10^9$ g smolts. If the average sockeye smolt weighs 6.4 g (Ajmani 2011), we expect to see $\sim 43,000,000 - \sim 160,000,000$ smolts annually. These estimates are similar to the juvenile sockeye carrying capacity of Owikeno Lake (33 million; Shortreed and Morton 2003). This suggests that the inlet and lake are well-matched in their capacity to support young sockeye and the carrying capacity of the fjord does not limit smolt abundance. No smolt-to-adult return (SAR) rate is known for Rivers Inlet sockeye. Using an average SAR rate of 3% from northwest Pacific salmonid populations (e.g., Foerster 1954, Tipping 1997, Beckman et al. 1999, Levin et al. 2001), we expect 1,300,000 – 4,850,000 adult sockeye returning annually. Although imprecise, these calculations show that current primary production in Rivers Inlet is able to support the current sockeye population ($\sim 100,000 - \sim 400,000$ adults; W. Levesque pers. comm.).

This level of primary productivity could also support historical returns of $> 1,000,000$ sockeye. This suggests that the decline in the sockeye population is not a result of a long-term decrease in primary production. Unfortunately, no historical data on the phytoplankton community is available. Instead of a decrease in primary productivity, we hypothesize that the sockeye decline is a result of a timing mismatch (Cushing 1990) between smolt outmigration

through Rivers Inlet and availability of their food.

2.4.4 Outlook

As global climate continues to shift, we expect these changes to negatively impact the sockeye population of Rivers Inlet. Wolfe (2010) highlighted later spring transitions over the past two decades. The spring transition marks the shift from prevailing outflow winds to inflow winds. This would delay the start of the spring bloom. Hodal (2011) demonstrated a long-term shift to an earlier increase in river-induced advection. As a result, the spring phytoplankton bloom is terminated earlier (Hodal 2011). Together, these two factors will constrain the period during which the spring phytoplankton bloom can occur. Late, truncated phytoplankton blooms will negatively impact higher trophic levels.

Furthermore, we expect increases in both temperature and CO₂ levels in the atmosphere in the coming decades. An increase in air temperature would lead to enhanced glacial melting, increasing freshwater input into Rivers Inlet via Owikeno Lake. Increased freshwater input would increase stratification and surface advection out of the fjord. Wolfe (2010) and Hodal (2011) have shown that advective losses in Rivers Inlet delay spring blooms, which could negatively affect sockeye smolts. This freshwater is low in nutrients, which ultimately limits phytoplankton biomass. Phytoplankton would also experience lower light levels due to high amount of glacial silt present in the freshwater layer. Diatoms flourish under high-nutrient, high-light conditions (Miller 2004, Sarthou et al. 2005) like those that currently occur in Rivers Inlet during spring. A shift toward lower nutrient conditions will likely result in a decrease in the

Table 10. Ranges of annual primary productivity in temperate estuaries. Table modified from Hodal (2011) and Riche (2011).

Reference	Annual euphotic primary productivity (g C · m ⁻² · yr ⁻¹)	Time period	Method (Incubation length, if applicable)	Location
Coastal British Columbia				
This study	219-438	2009-2010	FRRF-PP	Rivers Inlet, BC
Hodal 2011	110-300 (new production)	2008-2009	Model output	Rivers Inlet, BC
Riche 2011	Net 212 (spring/summer 157)	2002-2005	Calculated from PO ₄ uptake	Strait of Georgia, BC
Timothy and Soon 2001	490	1985-1989	¹⁴ C incubations (2 h)	Saanich Inlet, BC
Timothy and Soon 2001	290	1985-1989	¹⁴ C incubations (2 h)	Jervis Inlet, BC
Ware and McQueen 2006	141-278	1992	Calculated from chl _a biomass and [NO ₃]	Hecate Strait, BC
Harrison et al. 1983	Mean 280	Various (review)	¹⁴ C incubations (various lengths)	Strait of Georgia, BC
Other temperate coastal regions				
Testa and Kemp 2008	Net 0-116	1985-2008	Model output	Patuxent River, Chesapeake Bay
Estevez-Blanco et al. 2006	474	Spring 2003	FRRF-PP	NW Spain
Raateoja et al. 2004	183	Apr and Nov 2000	FRRF-PP	Gulf of Finland
Moore et al. 2003	220-548	Aug 1999	FRRF-PP	English Channel
Wilson 2002	0-192	1981-2000	¹⁴ C incubations (various lengths)	5 UK and US estuaries
Harding et al. 2002	282-538 (mean 408)	1982-1995	¹⁴ C incubations (4 – 24 h)	Chesapeake Bay
Tian et al. 2000	100-212	1992-1994	Model output	Gulf of Saint Lawrence model
Savenkoff et al. 2000	range 0-500, maximum in spring	1992-1994	¹⁴ C incubations (24 h)	Gulf of Saint Lawrence
Heip et al. 1995	7-560	1977-1995	¹⁴ C incubations (various lengths)	12 estuaries in Europe and North America
Boyer et al. 1993	395-493 (mean 465)	1985-1988	¹⁴ C incubations (24 h)	Neuse River, North Carolina, US
Pennock and Sharp 1986	190-400 (mean 307)	1981-1985	Calculated from chl _a biomass	Delaware, US
Pennock and Sharp 1986	90-820	1950s-1980s	Calculated from chl _a biomass	10 US estuaries
Therriault and Levasseur 1985	7-470	1974-1984	¹⁴ C incubations (various lengths)	20 estuaries in North America

relative abundance of diatoms in Rivers Inlet. Increased $p\text{CO}_2$ may also result in a decrease in diatom abundance. Hare et al. (2007) found that increased temperature and $p\text{CO}_2$ induced a community shift from diatoms to nanophytoplankton in coastal Bering Sea phytoplankton assemblages. Other studies also predict that, as climate change progresses, temperate phytoplankton will shift from communities dominated by diatoms to smaller, faster-growing taxa such as small flagellates (e.g., Egge et al. 2009, Yoshimura et al. 2009, Lewandowska and Sommer 2010, Marinov et al. 2010), though other outcomes have also been predicted (e.g., Kim et al. 2006, Tortell et al. 2008). A shift away from a diatom-based food web could result in a further reduction of an ecosystem's potential ability to support productive fisheries (Hare et al. 2007) by lengthening the food web. With only 10% of energy transferred to the next trophic level, increasing the number of trophic levels between primary producers and small fish decreases the energy available to the smolts. Instead of 3 trophic levels (diatoms, copepods, smolts) and 1% of energy produced by phytoplankton being transferred to smolts, a shift to 4 trophic levels (flagellates, microzooplankton, copepods, smolts) would transfer only 0.1% of available energy to smolts. Such a shift in Rivers Inlet would negatively impact sockeye smolts.

Chapter 3: Conclusion

3.1 General conclusions

This study is the first to describe seasonal patterns of phytoplankton community structure and primary productivity in the Rivers Inlet ecosystem, to infer how changes in the timing, magnitude, and composition of the spring and summer blooms affect salmon production. We found that diatoms dominated the spring bloom while the summer community, in addition to diatoms, included more dinoflagellates and other flagellates. The spring bloom appears to occur earlier in the more sheltered head of the inlet, where strong stratification is promoted by freshwater input from Owikeno Lake via the Wannock River (Figure 1). Outside the mouth of the inlet, where mixing processes are more pronounced, the phytoplankton seed population is diluted, resulting in a later and smaller bloom. More frequent sampling is needed to support these observations. In addition to spatial variability, the timing of the spring bloom also varies interannually. During five consecutive years of observation, the timing of the spring bloom ranged from early March to late April (Wolfe 2010, Tommasi et al. 2012a, b, this study). Supporting our data, previous modeling studies also predict the timing of the bloom to be determined by freshwater input and outflow wind events (Wolfe 2010). Our study showed that the spring phytoplankton bloom is terminated by NO_3 depletion throughout the majority of the inlet. In the less saline areas of the inlet, the phytoplankton bloom declines due to PO_4 limitation as a result of the influence of oligotrophic, PO_4 -depleted freshwater from Owikeno Lake. Variability in the timing of the spring phytoplankton bloom impacts the quality and quantity of food available to higher trophic levels. Earlier phytoplankton blooms appear to cause larger zooplankton blooms (Tommasi 2008, Tommasi et al. 2012a, b), which lead to more robust sockeye smolts (Buchanan 2006, Ajmani 2011). Furthermore, earlier phytoplankton blooms may transition earlier to the more diverse summer phytoplankton community. This could also

benefit smolts because copepods that fed on a diverse diet are a richer food source for their predators (El-Sabaawi et al. 2009).

In the lab, our primary productivity measurements using a fast repetition rate fluorometer agreed well with measurements using ^{13}C -uptake bottle incubations. The near-1:1 relationship between these parameters was robust when phytoplankton cells were healthy and unstressed, but did not hold when cells were stressed by high light levels or low nutrients. Using robust ^{13}C primary productivity data, we estimated the annual potential for sockeye production in Rivers Inlet. Our calculations suggest that primary productivity in Rivers Inlet is able to support both its current sockeye population (~100,000; W. Levesque pers. comm.) and historical returns (> 1,000,000). Thus, a decrease in primary productivity alone cannot explain the decline of the sockeye stock. A timing mismatch (Cushing 1990) between the spring phytoplankton bloom, zooplankton bloom, and smolt presence in the fjord may contribute to low sockeye returns. We expect global climate change to exacerbate this timing mismatch and reduce phytoplankton (and especially diatom) biomass in the coming decades. Such a shift in biomass will likely negatively impact the sockeye population by decreasing the carrying capacity of the inlet. In addition to reduced phytoplankton biomass, we also expect a shift from a diatom-dominated to a flagellate-dominated phytoplankton community. This will further negatively impact sockeye production by lengthening the food web and reducing the amount of energy available to smolts.

3.2 Future work

The central goal the Rivers Inlet Ecosystem Study, of which this thesis is a part, is to understand the dynamics of spring productivity and how they influence sockeye smolt growth in the fjord. Our work focused on primary productivity and phytoplankton community dynamics. Continued monitoring of the phytoplankton community will yield invaluable data, from which a

predictive whole-ecosystem model can be built to forecast salmon population, and shape management strategies in Rivers Inlet. To our knowledge, no long time-series phytoplankton data are available for coastal regions in the northeast Pacific. A time series of phytoplankton community dynamics would provide invaluable information for predicting how temperate coastal phytoplankton assemblages will respond to environmental shifts due to climate change. Since salmon production has significantly declined throughout the NE Pacific coast, monitoring efforts should be expanded into neighbouring fjords, such as Smith Inlet to the south (Figure 1). This could be accomplished *in situ* or using remote sensing of ocean colour.

Future *in situ* monitoring of the phytoplankton in Rivers Inlet should include a highly temporally resolved sampling scheme. Fluctuations in phytoplankton populations occur more rapidly than monthly or fortnightly sampling can capture (e.g., Harrison et al. 1991). Daily measurements of *chl_a* are available at the centre station in spring (data not shown), but not at other locations in the fjord. Automated sensors placed throughout the inlet would provide a continuous record of phytoplankton dynamics. Otherwise, weekly or twice-weekly monitoring would provide a more accurate picture of the variability in *chl_a* biomass and primary productivity. Sampling efforts should be concentrated towards further resolving phytoplankton dynamics in the upper 10 – 15m of the water column where phytoplankton biomass and productivity occur. Furthermore, an earlier sampling season is required to ensure that the entire spring phytoplankton cycle is captured. Sampling should begin in mid- or late February to capture pre-bloom conditions. This is especially important as we expect the initiation of the spring bloom to occur earlier as climate change progresses.

The already substantial value of the FRRF as a monitoring instrument will be greatly improved as we better our understanding of how nutrient levels, light levels, and community composition influence fluorescence parameter. Furthermore, the development of a methodology

that eliminates the need for dark-acclimated measurements aboard research vessels would also increase the value of the FRRF. This may be possible with the development of a new model for calculating FRRF-PP without the need for parameters collected from dark-adapted cells. In addition, improving the FRRF instrument to collect high-quality data while it is moving through water would allow incorporation into a shipboard underway sampling system. This would greatly increase the spatial resolution of primary productivity data. Phytoplankton distribution is known to be patchy (e.g., Dustan and Pinckney 1989), meaning that measurements collected at fixed sampling stations do not always represent typical conditions. Enlisting the help of local residents and their vessels would increase both the amount of data available and community involvement in the research.

In addition to studying phytoplankton dynamics, it is also important to further investigate trophic linkages between phytoplankton, zooplankton, and sockeye smolts. Similar to the effects of phytoplankton on zooplankton, the timing, magnitude, and composition of the zooplankton bloom affect smolt survival. Late zooplankton blooms, which are associated with late phytoplankton blooms, are lower in biomass (Tommasi et al. 2012a, b). Smolts are smaller and less robust in years of late zooplankton blooms (Buchanan 2006, Ajmani 2011). Zooplankton community composition also changes among years. For example, while copepods were abundant in all years, late blooms contained fewer large calanoids and more acartiids and ectinosomatids. Late zooplankton blooms were also associated with a reduction in the biomass of carnivorous zooplankton, euphausiids, and other taxa (Tommasi et al. 2012a). Food quality, in addition to food type and quantity, may also influence smolt survival. Fatty acid analysis of a key copepod species in the Strait of Georgia showed that a diet of mixed phytoplankton made copepods a richer food source for fish than did a diet of only diatoms (El-Sabaawi et al. 2009). This analysis should be expanded to the whole Rivers Inlet zooplankton community. Seasonal

analyses of the zooplankton community fatty acid composition would point to the timing of the richest food in the inlet, and whether this period overlaps with the smolt outmigration through the inlet. This knowledge would improve our understanding of trophic linkages between zooplankton and wild sockeye populations. Furthermore, this information could help determine when to release hatchery-raised fry to maximize their chances of survival and further refine the management strategies that will facilitate the recovery of the Rivers Inlet sockeye salmon stock.

Bibliography

- Ajmani, A M. 2011. "The Growth and Diet Composition of Sockeye Salmon in Rivers Inlet, British Columbia". University of British Columbia.
- Andersen, R A, and M Kawachi. 2005. "Traditional Microalgae Isolation Techniques." In *Algal Culturing Techniques: a Book for All Phycologists*, ed. R A Andersen, 83–100. London: Elsevier.
- Badger, M R, S von Caemmerer, S Ruuska, and H Nakano. 2000. "Electron Flow to Oxygen in Higher Plants and Algae: Rates and Control of Direct Photoreduction (Mehler Reaction) and Rubisco Oxygenase." *Philosophical Transactions of the Royal Society of London. Series B, Biological Sciences* 355 (1402): 1433–1446.
- Baker, N R, and K Oxborough. 2004. "Chlorophyll Fluorescence as a Probe of Photosynthetic Productivity." In *Chlorophyll a Fluorescence: a Signature of Photosynthesis*, ed. George C Papageorgiou and Govindjee, 65–82. Dordrecht, NLD: Springer.
- Barber, J, S Malkin, A Telfer, and U Schreiber. 1989. "The Origin of Chlorophyll Fluorescence *in Vivo* and Its Quenching by the Photosystem II Reaction Centre." *Philosophical Transactions of the Royal Society of London. Series B, Biological Sciences* 323 (1216): 227–239.
- Barlow, R G, and R S Alberte. 1985. "Photosynthetic Characteristics of Phycoerythrin-containing Marine *Synechococcus* Spp. I. Responses to Growth Photon Flux Density." *Marine Biology* 86 (May 16): 63–75.
- Beamish, R J, D Noakes, G McFarlane, and J King. 1998. *The Regime Concept and Recent Changes in Pacific Salmon Abundance*. Pacific Biological Station. Nanaimo, BC.
- Beardall, J, A Quigg, and J A Raven. 2003. "Oxygen Consumption: Photorespiration and Chlororespiration." In *Photosynthesis in Algae*, ed. A W D Larkum, S E Douglas, and J A Raven, 157–181. 14th ed. Netherlands: Springer.
- Beckman, B R, W W Dickhoff, W S Zaugg, C Sharpe, SHirtzel, R Schrock, D A Larsen, R D Ewing, A Palmisano, C B Schreck, C V W Mahnken. 1999. "Growth, Smoltification, and Smolt-to-adult Return of Spring Chinook Salmon from Hatcheries on the Deschutes River, Oregon." *Transactions of the American Fisheries Society* 128 (6): 1125–1150..
- Behrenfeld, M J, K H Halsey, and A J Milligan. 2008. "Evolved Physiological Responses of Phytoplankton to Their Integrated Growth Environment." *Philosophical Transactions of the Royal Society of London. Series B, Biological Sciences* 363 (1504): 2687–2703.
- Behrenfeld, M J, K Worthington, R M Sherrell, F P Chavez, P Strutton, M McPhaden, and D M Shea. 2006. "Controls on Tropical Pacific Ocean Productivity Revealed Through Nutrient Stress Diagnostics." *Nature* 442 (7106): 1025-1028.

- Bender, M L, K D Grande, K S Johnson, J Marra, P J LeB Williams, J Sieburth, M Pilson, C Langdon, G Hitchcock, J Orchardo, C Hunt, P Donaghay, and K Heinemann. 1987. "A Comparison of Four Methods for Determining Planktonic Community Production." *Limnology and Oceanography* 32 (5): 1085–1098.
- Boyd, P W, J Aiken, and Z Kolber. 1997. "Comparison of radiocarbon and fluorescence base (pump and probe) measurements of phytoplankton photosynthetic characteristics in the Northeast Atlantic Ocean." *Marine Ecology Progress Series* 149: 215–226.
- Boyer, J N, R R Christian, and D W Stanley. 1993. "Patterns of phytoplankton primary productivity in the Neuse River estuary, North Carolina, USA." *Marine Ecology Progress Series* 97: 287–297.
- Brand, L E, R Guillard, and L S Murphy. 1981. "A Method for the Rapid and Precise Determination of Acclimated Phytoplankton Reproduction Rates." *Journal of Plankton Research* 3 (2): 193–201.
- Bryan, J R. 1976. "A Winkler Procedure for Making Precise Measurements of Oxygen Concentration for Productivity and Related Studies." *Journal of Experimental Marine Biology and Ecology* 21: 191–197.
- Brzezinski, M A. 1985. "The Si:C:N Ratio of Marine Diatoms: Interspecific Variability and the Effect of Some Environmental Variables." *Journal of Phycology* 21 (3): 347–357.
- Buchanan, S. 2006. "Factors Influencing the Early Marine Ecology of Juvenile Sockeye Salmon (*O. Nerka*) in Rivers Inlet, British Columbia". Simon Fraser University.
- Büchel, C, and C Wilhelm. 1993. "In vivo analysis of slow chlorophyll fluorescence induction kinetics in algae: progress, problems and perspectives." *Photochemistry and Photobiology* 58 (1): 137–148.
- Corno, G, R M Letelier, and M R Abbott. 2005. "Assessing Primary Production Variability in the North Pacific Subtropical Gyre: a Comparison of Fast Repetition Rate Fluorometry and ¹⁴C Measurements." *Journal of Phycology* 42: 51–60.
- Crain, C M. 2007. "Shifting Nutrient Limitation and Eutrophication Effects in Marsh Vegetation Across Estuarine Salinity Gradients." *Estuaries and Coasts* 30 (1): 26–34.
- Cushing, D H. 1990. "Plankton Production and Year-class Strength in Fish Populations: An Update of the Match/mismatch Hypothesis." *Advances in Marine Biology* 26: 249–293.
- Doering, P H, C A Oviatt, B L Nowicki, and L W Reed. 1995. "Phosphorus and Nitrogen Limitation of Primary Production in a Simulated Estuarine Gradient." *Marine Ecology Progress Series* 124: 271–287.
- Droop, M. 1967. "A Procedure for Routine Purification of Algal Cultures with Antibiotics." *British Phycological Bulletin* 3 (2): 295–297.

- Dubinsky, Z, P G Falkowski, and K Wyman. 1986. "Light Harvesting and Utilization by Phytoplankton." *Plant Cell Physiology* 27 (7): 1335–1349.
- Dustan, P, and J L Pinckney. 1989. "Tidally Induced Estuarine Phytoplankton Patchiness." *Limnology and Oceanography* 34 (2): 410–419.
- Egge, J K, T F Thingstad, A Larsen, A Engel, J Wohlers, R G J Bellerby, and U Riebesell. 2009. "Primary Production During Nutrient-induced Blooms at Elevated CO₂ Concentrations." *Biogeosciences* 6: 877–885.
- El-Sabaawi, R, J F Dower, M Kainz, and A Mazumder. 2009. "Interannual Variability in Fatty Acid Composition of the Copepod *Neocalanus Plumchrus* in the Strait of Georgia, British Columbia." *Marine Ecology Progress Series* 382: 151–161.
- Estevez-Blanco, P, P Cermeño, M Espineira, and E Fernández. 2006. "Phytoplankton Photosynthetic Efficiency and Primary Production Rates Estimated from Fast Repetition Rate Fluorometry at Coastal Embayments Affected by Upwelling (Rias Baixas, NW of Spain)." *Journal of Plankton Research* 28 (12): 1153–1165.
- Falkowski, P G, M Koblížek, M Y Gorbunov, and Z Kolber. 2004. "Development and Application of Variable Chlorophyll Fluorescence Techniques in Marine Ecosystems." In *Chlorophyll a Fluorescence: a Signature of Photosynthesis*, ed. G C Papageorgiou and Govindjee, 757–778. Dordrecht, NLD: Springer.
- Falkowski, P G, and Z Kolber. 1995. "Variations in Chlorophyll Fluorescence Yields in Phytoplankton in the World Oceans." *Australian Journal of Plant Physiology* 22 (2): 341–355.
- Falkowshi, P G and T G Owens. 1978. "Effects of light intensity on photosynthesis and dark respiration in six species of marine phytoplankton." *Marine Biology* 45: 289-295.
- Falkowski, P G, T G Owens, A C Ley, and D C Mauzerall. 1981. "Effects of Growth Irradiance Levels on the Ratio of Reaction Centers in Two Species of Marine Phytoplankton." *Plant Physiology* 68: 969–973.
- Falkowski, P G, and J A Raven. 2007. *Aquatic Photosynthesis*. 2nd edition. Princeton: Princeton University Press.
- Fietz, S, and A Nicklisch. 2002. "Acclimation of the diatom *Stephanodiscus neoastraea* and the cyanobacterium *Planktothrix agardhii* to simulated natural light fluctuations." *Photosynthesis Research*. 72 (1): 95–106.
- Fisher, T R, A B Gustafson, K Sellner, R Lacouture, L W Haas, R L Wetzel, R Magnien, D Everitt, B Michaels, and R Karrh. 1999. "Spatial and Temporal Variation of Resource Limitation in Chesapeake Bay." *Marine Biology* 133 (4): 763–778.

- Fisher, T, J Minnaard and Z Dubinsky. 1996. "Photoacclimation in the marine alga *Nannochloropsis* sp. (Eustigmatophyte): a kinetic study." *Journal of Plankton Research* 18 (10): 1797–1818.
- Foerster, R E. 1954. "On the Relation of Adult Sockeye Salmon (*Oncorhynchus Nerka*) Returns to Known Smolt Seaward Migrations." *Journal of the Fisheries Research Board of Canada* 11 (4): 339–350.
- Foskett, D R. 1958. "The Rivers Inlet Sockeye Salmon." *Journal of the Fisheries Research Board of Canada* 15 (5): 867–889.
- Fujiki, T, T Suzue, H Kimoto and T Saino. 2007. "Photosynthetic electron transport in *Dunaliella tertiolecta* (Chlorophyceae) measured by fast repetition rate fluorometry: relation to carbon assimilation." *Journal of Plankton Research* 29 (2): 199–208.
- Geider, R J, J Roche, R M Greene, and M Olaizola. 1993. "Response of the Photosynthetic Apparatus of *Phaeodactylum Tricornutum* (Bacillariophyceae) to Nitrate, Phosphate, or Iron." *Journal of Phycology* 29 (6): 755–766.
- Genty, B, J-M Briantais, and N R Baker. 1989. "The Relationship Between the Quantum Yield of Photosynthetic Electron Transport and Quenching of Chlorophyll Fluorescence." *Biochimica Et Biophysica Acta* 990 (1): 87–92.
- Gilbert, C H. 1915. "Contributions to the Life History of the Sockeye Salmon." *British Columbia Commissioner of Fisheries for 1914* 3: 27–64.
- Hama, T, T Miyazaki, Y Ogawa, T Iwakuma, M Takahashi, A Otsuki, and S Ichimura. 1983. "Measurement of Photosynthetic Production of a Marine Phytoplankton Population Using a Stable ¹³C Isotope." *Marine Biology* 73: 31–36.
- Hare, C E, K Leblanc, G R DiTullio, R M Kudela, Y Zhang, P A Lee, S Riseman, and D A Hutchins. 2007. "Consequences of Increased Temperature and CO₂ for Phytoplankton Community Structure in the Bering Sea." *Marine Ecology Progress Series* 352: 9–16.
- Harrison, P J, P J Clifford, W P Cochlan, K Yin, M A St John, P A Thompson, M J Sibbald, and L J Albright. 1991. "Nutrient and Phytoplankton Dynamics in the Fraser River Plume, Strait of Georgia, British Columbia." *Marine Ecology Progress Series* 70: 291–304.
- Harrison, P J, J D Fulton, F J R Taylor, and T R Parsons. 1983. "Review of the Biological Oceanography of the Strait of Georgia: Pelagic Environment." *Canadian Journal of Fisheries and Aquatic Sciences* 40 (7): 1064–1094.
- Harrison, P J, M H Hu, Y P Yang, and X Lu. 1990. "Phosphate Limitation in Estuarine and Coastal Waters of China." *Journal of Experimental Marine Biology and Ecology* 140: 79–87.
- Harrison, P J, R E Waters, and F J R Taylor. 1980. "A Broad Spectrum Artificial Seawater Medium for Coastal and Open Ocean Phytoplankton." *Journal of Phycology* 16: 28–35.

- Hartzell, J L, and T E Jordan. 2012. "Shifts in the Relative Availability of Phosphorus and Nitrogen Along Estuarine Salinity Gradients." *Biogeochemistry* 107 (1-3): 489–500.
- Heip, C H R, N K Goosen, M J Peter, H J Kromkamp, J J Middleburg and K Soetaert. 1995. "Production and consumption of biological particles in temperate tidal estuaries." *Oceanography and Marine Biology: an Annual Review* 33: 1–149.
- Helfield, J M, and R J Naiman. 2001. "Effects of Salmon-derived Nitrogen on Riparian Forest Growth and Implications for Stream Productivity." *Ecology* 82 (9): 2403–2409.
- Hennige, S J, D J Suggett, M E Warner, K E McDougall and D J Smith. 2009. "Photobiology of *Symbiodinium* revisited: bio-physical and bio-optical signatures." *Coral Reefs* 28 (1): 179–195.
- Herzig, R, and Z Dubinsky. 1992. "Photoacclimation, photosynthesis, and growth in phytoplankton." *Israel Journal of Botany* 41: 199–211.
- Herzig, R, and P G Falkowski. 1989. "Nitrogen limitation in *Isochrysis galbana* (Haptophyceae). I. Photosynthetic energy conversion and growth efficiencies." *Journal of Phycology* 25 (3): 462–471.
- Hodal, M. 2011. "Net Physical Transports, Residence Times, and New Production for Rivers Inlet, British Columbia". University of British Columbia.
- Iglesias-Prieto, R, and R K Trench. 1994. "Acclimation and adaptation to irradiance in symbiotic dinoflagellates. I. Responses of the photosynthetic unit to changes in photon flux density." *Marine Ecology Progress Series* 113: 163–175.
- Juneau, P, and P J Harrison. 2005. "Comparison by PAM Fluorometry of Photosynthetic Activity of Nine Marine Phytoplankton Grown Under Identical Conditions." *Photochemistry and Photobiology* 81 (3): 649–653.
- Kaiblinger, C and M T Dokulil. 2006. "Application of fast repetition rate fluorometry to phytoplankton photosynthetic parameters in freshwaters." *Photosynthesis Research* 88 (1): 19–30.
- Kim, J-M, Ki Lee, K Shin, J-H Kang, H-W Lee, M Kim, P-G Jang, and M-C Jang. 2006. "The Effect of Seawater CO₂ Concentration on Growth of a Natural Phytoplankton Assemblage in a Controlled Mesocosm Experiment." *Limnology and Oceanography* 51 (4): 1629–1636.
- Koblížek, M, D Kaftan, and L Nedbal. 2001. "On the Relationship Between the Non-photochemical Quenching of the Chlorophyll Fluorescence and the Photosystem II Light Harvesting Efficiency. A Repetitive Flash Fluorescence Induction Study." *Photosynthesis Research* 68 (2): 141–52.
- Kolber, Z, and P G Falkowski. 1993. "Use of Active Fluorescence to Estimate Phytoplankton Photosynthesis *in situ*." *Limnology and Oceanography* 38 (8): 1646–1665.

- Kolber, Z, Ondřej Prášil, and P G Falkowski. 1998. "Measurements of Variable Chlorophyll Fluorescence Using Fast Repetition Rate Techniques: Defining Methodology and Experimental Protocols." *Biochimica Et Biophysica Acta* 1367 (1-3): 88–106.
- Kolber, Z, J Zehr, and P G Falkowski. 1988. "Effects of Growth Irradiance and Nitrogen Limitation on Photosynthetic Energy Conversion in Photosystem II." *Plant Physiology* 88 (3): 923–929.
- Kromkamp, J C, N Dijkman, J Peene, S Simis, and H J Gons. 2008. "Estimating Phytoplankton Primary Production in Lake IJsselmeer (The Netherlands) Using Variable Fluorescence (PAM-FRRF) and C-uptake Techniques." *European Journal of Phycology* 43 (4): 327–344.
- Kromkamp, J C, and R M Forster. 2003. "The Use of Variable Fluorescence Measurements in Aquatic Ecosystems: Differences Between Multiple and Single Turnover Measuring Protocols and Suggested Terminology." *European Journal of Phycology* 38 (2): 103–112.
- Levin, P S, R W Zabel, and J G Williams. 2001. "The Road to Extinction Is Paved with Good Intentions: Negative Association of Fish Hatcheries with Threatened Salmon." *Proceedings of the Royal Society of London B: Biological Sciences* 268 (1472): 1153–1158.
- Levitus, S. 1982. *Climatological Atlas of the World Ocean, NOAA Professional Paper 13*. Rockville, MD: US Government Printing Office. 112.
- Levy, D. 2006. *BC Sockeye Salmon Population Declines: Probable Causes and Recommended Response Strategies*. Victoria.
- Lewandowska, A, and U Sommer. 2010. "Climate Change and the Spring Bloom: a Mesocosm Study on the Influence of Light and Temperature on Phytoplankton and Mesozooplankton." *Marine Ecology Progress Series* 405: 101–111..
- Lewitus, A J, and T M Kana. 1995. "Light Respiration in Six Estuarine Phytoplankton Species: Contrasts Under Photoautotrophic and Mixotrophic Growth Conditions." *Journal of Phycology* 31 (5): 754–761.
- Lippemeier, S, P Hartig, and F Colijn. 1999. "Direct Impact of Silicate on the Photosynthetic Performance of the Diatom *Thalassiosira weissflogii* Assessed by on- and off-line PAM Fluorescence Measurements." *Journal of Plankton Research* 21 (2): 269–283.
- Lucas, L V, J E Cloern, J R Koseff, S G Monismith, and J K Thompson. 1998. "Does the Sverdrup Critical Depth Model Explain Bloom Dynamics in Estuaries?" *Journal of Marine Research* 56 (2): 375–415.
- MacIntyre, H L, T M Kana, and R J Geider. 2000. "The Effect of Water Motion on Short-term Rates of Photosynthesis by Marine Phytoplankton." *Trends in Plant Science* 5 (1): 12–17.
- Malinsky-Rushansky, N, T Berman, T Berner, Y Z Yacobi and Z Dubinsky. 2002. "Physiological characteristics of picophytoplankton, isolated from Lake Kinneret: responses to light and temperature." *Journal of Plankton Research* 24 (11): 1173–1183.

- Marinov, I, S C Doney, and I D Lima. 2010. "Response of Ocean Phytoplankton Community Structure to Climate Change over the 21st Century: Partitioning the Effects of Nutrients, Temperature and Light." *Biogeosciences* 7: 3941–3959..
- Marra, J. 1980. "Vertical Mixing and Primary Production." In *Primary Productivity in the Sea*, ed. Paul G Falkowski, 121–137. New York: Plenum Press.
- . 2009. "Net and Gross Productivity: Weighing in with ^{14}C ." *Aquatic Microbial Ecology* 56 (2-3): 123–131.
- Maxwell, K, and G N Johnson. 2000. "Chlorophyll Fluorescence--a Practical Guide." *Journal of Experimental Botany* 51 (3451): 659–668.
- McKinnell, S M, C C Wood, D T Rutherford, Kim D Hyatt, and David W Welch. 1998. *The Collapse of the Rivers Inlet Sockeye Fishery: The Case Against a Freshwater Cause*. Vancouver, Canada.
- . 2001. "The Demise of Owikeno Lake Sockeye Salmon." *North American Journal of Fisheries Management* 21 (4): 774–491.
- Melrose, D C, C A Oviatt, J E O'Reilly, and M S Berman. 2006. "Comparisons of Fast Repetition Rate Fluorescence Estimated Primary Production and ^{14}C Uptake by Phytoplankton." *Marine Ecology Progress Series* 311: 37–46.
- Miller, C B. 2004. *Biological Oceanography*. Oxford: Blackwell.
- Moore, C M, M I Lucas, R Sanders, and R Davidson. 2005. "Basin-scale Variability of Phytoplankton Bio-optical Characteristics in Relation to Bloom State and Community Structure in the Northeast Atlantic." *Deep Sea Research Part I: Oceanographic Research Papers* 52 (3): 401–419.
- Moore, C M, Matthew M Mills, R Langlois, A Milne, EP Achterberg, J La Roche, and R J Geider. 2008. "Relative Influence of Nitrogen and Phosphorus Availability on Phytoplankton Physiology and Productivity in the Oligotrophic Sub-tropical North Atlantic Ocean." *Limnology and Oceanography* 53 (1): 291–305.
- Moore, C M, M M Mills, A Milne, R Langlois, E P Achterberg, K Lochte, R J Geider, and J La Roche. 2006a. "Iron Limits Primary Productivity During Spring Bloom Development in the Central North Atlantic." *Global Change Biology* 12 (4): 626–634.
- Moore, C M, D J Suggett, A E Hickman, Y-N Kim, J F Tweddle, J Sharples, R J Geider, and P M Holligan. 2006b. "Phytoplankton Photoacclimation and Photoadaptation in Response to Environmental Gradients in a Shelf Sea." *Limnology and Oceanography* 51 (2): 936–949.
- Moore, C M, D J Suggett, P M Holligan, J Sharples, E R Abraham, M I Lucas, T P Rippeth, N R Fisher, J H Simpson, and J Hydes. 2003. "Physical Controls on Phytoplankton Physiology and Production at a Shelf Sea Front: a Fast Repetition-rate Fluorometer Based Field Study." *Marine Ecology Progress Series* 259: 29–45.

- Myers, J., & Graham, J.-R. (1971). "The photosynthetic unit in *Chlorella* measured by repetitive short flashes." *Plant Physiology* 48: 282–286.
- Noh, Yi, and W-S Lee. 2008. "Mixed and Mixing Layer Depths Simulated by an OGCM." *Journal of Oceanography* 64 (2): 217–225.
- Oxborough, K. 2007. *MK II Fasttracka Sensor Handbook*. Surrey, UK.
- Oxborough, K, and N R Baker. 1997. "Resolving Chlorophyll a Fluorescence Images of Photosynthetic Efficiency into Photochemical and Non-photochemical Components – Calculation of qP and F_v'/F_m' Without Measuring F_o' ." *Photosynthesis Research* 54 (2): 135–142.
- Oxborough, K, C M Moore, D J Suggett, T Lawson, H Chan, and R J Geider. 2012. "Direct Estimation of Functional PSII Reaction Center Concentration and PSII Electron Flux on a Volume Basis: a New Approach to the Analysis of Fast Repetition Rate Fluorometry (FRRf) Data." *Limnology and Oceanography: Methods* 10: 142–154.
- Parkhill, J-P, G Maillet, and J J Cullen. 2001. "Fluorescence-based Maximal Quantum Yield for PSII as a Diagnostic of Nutrient Stress." *Journal of Phycology* 37: 517–529.
- Pauley, G B, K Oshima, K L Bowers, and G L Thomas. 1989. *Species Profiles: Life Histories and Environmental Requirements of Coastal Fishes and Invertebrates (Pacific Northwest)-Sea-run Cutthroat Trout*.
- Pawlowicz, R. 2008. "Calculating the Conductivity of Natural Waters." *Limnology and Oceanography: Methods* 6: 489–501.
- Pemberton, K L, K R Clark and I Joint. 2006. "Quantifying uncertainties associated with the measurement of primary production." *Marine Ecology Progress Series* 322: 51–59.
- Pennock, J R, and J H Sharp. 1986. "Phytoplankton production in the Delaware Estuary: temporal and spatial variability." *Marine Ecology Progress Series* 34: 143–155.
- Poole, H H, and W R Atkins. 1929. Photo-electric measurements of submarine illumination throughout the year. *Journal of the Marine Biological Association of the United Kingdom (New Series)* 16 (1): 297-324.
- Prášil, O, Z Kolber, J A Berry, and P G Falkowski. 1996. "Cyclic Electron Flow Around Photosystem II *in Vivo*." *Photosynthesis Research* 48 (3): 395–410..
- Quigg, A, K Kevekordes, J A Raven, and J Beardall. 2006. "Limitations on Microalgal Growth at Very Low Photon Fluence Rates: The Role of Energy Slippage." *Photosynthesis Research* 88 (3): 299–310.

- Raateoja, M P, J Seppälä, and H Kuosa. 2004. "Bio-optical Modelling of Primary Production in the SW Finnish Coastal Zone, Baltic Sea: Fast Repetition Rate Fluorometry in Case 2 Waters." *Marine Ecology Progress Series* 267: 9–26.
- Reynolds, C S. 2006. *The Ecology of Phytoplankton*. Cambridge, UK: Cambridge University Press.
- Riche, O. 2011. "Time-dependent Inverse Box-model For The Estuarine Circulation and Primary Productivity in The Strait of Georgia". University of British Columbia.
- Ross, O N, C M Moore, D J Suggett, H L MacIntyre and R J Geider. 2008. "A model of photosynthesis and photo-protection based on reaction center damage and repair." *Limnology and Oceanography* 53 (5): 1835–1852.
- Sarthou, G, K R Timmermans, S Blain, and P Tréguer. 2005. "Growth Physiology and Fate of Diatoms in the Ocean: a Review." *Journal of Sea Research* 53 (1-2): 25–42.
- Savenkoff, C, A F Vézina, S Roy, B Klein, C Lovejoy, J-C Therriault, L Legendre, R B Rivkin, C Bérubé, J-E Tremblay, and N Silverberg. 2000. "Export of biogenic carbon and structure and dynamics of the pelagic food web in the Gulf of St. Lawrence Part 1. Seasonal variations." *Deep Sea Research Part II: Topical Studies in Oceanography* 47 (3-4): 585–607.
- Shortreed, K S, and K F Morton. 2003. "Current Limnological Status of Owikeno Lake." *Canadian Technical Report of Fisheries and Aquatic Sciences* 2457. 1–42.
- Smyth, T, K L Pemberton, and R J Geider. 2004. "A Methodology to Determine Primary Production and Phytoplankton Photosynthetic Parameters from Fast Repetition Rate Fluorometry." *Journal of Plankton Research* 26 (11): 1337–1350.
- Steemann Nielsen, E. 1952. "The Use of Radio-active Carbon (C14) for Measuring Organic Production in the Sea." *Journal Du Conseil* 118: 117–140.
- Stocks, A. 2012. "Transition Time from Fresh to Saltwater of Juvenile Sockeye Salmon (*Oncorhynchus Nerka*) Determined by Laser Ablation ICP-MS of Otoliths". University of British Columbia.
- Strickland, J D H, and T R Parsons. 1968. *A Practical Handbook of Seawater Analysis. Internationale Revue Der Gesamten Hydrobiologie Und Hydrographie*. First. Vol. 55. Ottawa, Canada: Fisheries Research Board of Canada, Bulletin 167.
- Strom, S L, E L Macri, and M B Olson. 2007. "Microzooplankton Grazing in the Coastal Gulf of Alaska: Variations in Top-down Control of Phytoplankton." *Limnology and Oceanography* 52 (4): 1480–1494.
- Strzepek, R F, and P J Harrison. 2004. "Photosynthetic Architecture Differs in Coastal and Oceanic Diatoms." *Nature* 431 (7009): 689–692.

- Suggett, D J, G Kraay, P M Holligan, M Davey, J Aiken, and R J Geider. 2001. "Assessment of Photosynthesis in a Spring Cyanobacterial Bloom by Use of a Fast Repetition Rate Fluorometer." *Limnology and Oceanography* 46 (4): 802–810.
- Suggett, D J, E Le Floch, G N Harris, N Leonardos, and R J Geider. 2007. "Different strategies of photoacclimation by two strains of *Emiliania huxleyi* (Haptophyta)." *Journal of Phycology* 43: 1209–1222.
- Suggett, D J, Maberly, S C, and R J Geider. 2006. Gross photosynthesis and lake community metabolism during the spring phytoplankton bloom. *Limnology and Oceanography* 51 (5): 2064–2076.
- Suggett, D J, H L MacIntyre, and R J Geider. 2004. "Evaluation of Biophysical and Optical Determinations of Light Absorption by Photosystem II in Phytoplankton." *Limnology and Oceanography: Methods* 2: 316–332.
- Suggett, D J, H L MacIntyre, T M Kana, and R J Geider. 2009b. "Comparing Electron Transport with Gas Exchange: Parameterising Exchange Rates Between Alternative Photosynthetic Currencies for Eukaryotic Phytoplankton." *Aquatic Microbial Ecology* 56 (2-3): 147–162..
- Suggett, D J, C M Moore, and R J Geider. 2010. "Estimating Aquatic Productivity from Active Fluorescence Measurements." In *Chlorophyll a Fluorescence in Aquatic Sciences: Methods and Applications*, ed. D J Suggett, O Prasil, and M A Borowitzka, 103–127. Springer Inc.
- Suggett, D J, C M Moore, A E Hickman, and R J Geider. 2009a. "Interpretation of Fast Repetition Rate (FRR) Fluorescence: Signatures of Phytoplankton Community Structure Versus Physiological State." *Marine Ecology Progress Series* 376 (February 11): 1–19.
- Suggett, D J, C M Moore, E Marañón, C Omachi, R A Varela, J Aiken, and P M Holligan. 2006a. "Photosynthetic Electron Turnover in the Tropical and Subtropical Atlantic Ocean." *Deep-Sea Research II* 53: 1573–1592.
- Suggett, D J, K Oxborough, N R Baker, H L MacIntyre, T M Kana, and R J Geider. 2003. "Fast Repetition Rate and Pulse Amplitude Modulation Chlorophyll A Fluorescence Measurements for Assessment of Photosynthetic Electron Transport in Marine Phytoplankton." *European Journal of Phycology* 38 (4): 371–384.
- Sukenik, A, J Bennett, A Mortain-Bertrand, and P G Falkowski. 1990. "Adaptation of the Photosynthetic Apparatus to Irradiance in *Dunaliella Tertiolecta*: A Kinetic Study." *Plant Physiology* 92 (4): 891–898.
- Testa, J M, and W M Kemp. 2008. "Variability of biogeochemical processes and physical transport in a partially stratified estuary: a box-modeling analysis." *Marine Ecology Progress Series* 356: 63–79.
- Therriault, J-C, and M Levasseur. 1985. "Control of phytoplankton production in the Lower St. Lawrence estuary: light and freshwater runoff." *Le Naturaliste Canadien* 112: 77–96.

- Tian, R C, A F Vézina, L Legendre, R G Ingram, B Klein, T Packard, S Roy, C Savenkoff, N Silverberg, J-C Therriault, J-E Tremblay. 2000. "Effects of pelagic food-web interactions and nutrient remineralization on the biogeochemical cycling of carbon: a modeling approach." *Deep Sea Research Part II: Topical Studies in Oceanography* 47 (3-4): 637–662.
- Timothy, D A, and M Y S Soon. 2001. "Primary production and deep-water oxygen content of two British Columbian fjords." *Marine Chemistry* 73 (1): 37–51.
- Tipping, J M. 1997. "Effect of Smolt Length at Release on Adult Returns of Hatchery-reared Winter Steelhead." *The Progressive Fish-Culturist* 59 (4): 310–311.
- Tommasi, D A G. 2008. "Seasonal and Interannual Variability of Primary and Secondary Productivity in a Coastal Fjord". Simon Fraser University.
- Tommasi, D A G, Brian P V Hunt, Evgeny A Pakhomov, and D Mackas. 2012b. "Mesozooplankton Community Seasonal Succession and Its Drivers: Insights from a British Columbia, Canada, Fjord." *Journal of Marine Systems*: submitted.
- Tommasi, D A G, R Routledge, B P V Hunt, and E A Pakhomov. 2012a. "The Seasonal Development of the Zooplankton Community in a British Columbia (Canada) Fjord During Two Years with Different Spring Bloom Timing." *Marine Biology Research*: in press.
- Tortell, P D, C D Payne, Y Li, S Trimborn, B Rost, W O Smith, C Riesselman, R B Dunbar, P Sedwick, and G R DiTullio. 2008. "CO₂ Sensitivity of Southern Ocean Phytoplankton." *Geophysical Research Letters* 35 (4): L04605.
- Tripathy, S, J Ishizaka, T Fujiki, T Shibata, K Okamura, T Hosaka, and T Saino. 2010. "Assessment of Carbon- and Fluorescence-based Primary Productivity in Ariake Bay, Southwestern Japan." *Estuarine, Coastal and Shelf Science* 87 (1): 163–173.
- Ware, D M. 2000. "Aquatic Ecosystems: Properties and Models." In *Fisheries Oceanography: An Integrative Approach to Fisheries Ecology and Management*, ed. P J Harrison and T R Parsons, 4:161–194. Oxford: Blackwell Science.
- Ware, D M, and D McQueen. 2006. "Hecate Strait climate-forced nutrient, phytoplankton, zooplankton model version 4.3.4." *Canadian Technical Report of Fisheries and Aquatic Sciences* 2653: 1–56.
- Ware, DM, and R E Thomson. 2005. "Bottom-up Ecosystem Trophic Dynamics Determine Fish Production in the Northeast Pacific." *Science* 308 (5726): 1280–1284.
- Williams, P J LeB, and N W Jenkinson. 1982. "A Transportable Microprocessor-controlled Precise Winkler Titration Suitable for Field Station and Shipboard Use." *Limnology and Oceanography* 27 (3): 576–584.
- Wilson, J G. 2002. "Productivity, fisheries and aquaculture in temperate estuaries." *Estuarine, Coastal and Shelf Science* 55 (6): 953–967.

Wolfe, M A. 2010. “Impact of Wind and River Flow on the Timing of the Rivers Inlet Spring Phytoplankton Bloom”. University of British Columbia.

Yoshimura, T, J Nishioka, K Suzuki, H Hattori, H Kiyosawa, and Y W Watanabe. 2009. “Impacts of Elevated CO₂ on Phytoplankton Community Composition and Organic Carbon Dynamics in Nutrient-depleted Okhotsk Sea Surface Waters.” *Biogeosciences Discussions* 6 (2): 4143–4163.

Appendix A: Sampling scheme and dates

Table 11. Summary of cruise dates and samples collected. X denotes sample collected. 0, 5, and 30 refer to depths at which samples were collected (m).

2009 Sampling									
Cruise	Date	Station	CTD profile	PAR profile	Chl <i>a</i>	Phytoplankton sample	Nutrients	FRRF	¹³ C
1	2/28/09	DFO5	X	X	5	5	5, 30		
	2/27/09	DFO2	X	X	0, 5, 30	0, 5, 30	0, 5, 10, 30	0, 5, 30	
	2/26/09	UBC7	X	X	5	5	0, 5, 10, 30		
2	3/18/09	DFO5	X	X	5, 30	5, 30	5, 30	5, 30	
	3/17/09	DFO2	X	X	0, 5, 30	0, 5, 30	0, 5, 10, 30	0, 5, 30	
	3/17/09	UBC7	X	X	5, 30	5, 30	5, 30	0, 5, 30	
3	4/2/09	DFO5	X	X	0, 5, 30	0, 5, 30	5, 30	0, 5, 30	
	4/2/09	DFO2	X	X	0, 5, 30	0, 5, 30	0, 5, 10, 30	0, 5, 30	
	4/3/09	UBC7	X	X	0, 5, 30	0, 5, 30	0, 5, 10, 30	0, 5, 30	
4	4/16/09	DFO5	X	X	0, 5, 30	0, 5, 30	0, 5, 30	0, 5, 30	
	4/16/09	DFO2	X	X	0, 5, 30	0, 5, 30	0, 5, 10, 30	0, 5, 30	
	4/17/09	UBC7	X		0, 5, 30	0, 5, 30	0, 5, 30	0, 5, 30	
5	5/3/09	DFO2	X	X	0, 5, 30	0, 5, 30	0, 5, 10, 30	0, 5, 30	
	5/3/09	DFO5		X	0, 5, 30	0, 5, 30	5, 30	0, 5, 30	
	5/4/09	UBC7	X	X	0, 5, 30	0, 5, 30	0, 5, 10, 30	0, 5, 30	
6	5/19/09	DFO5			0, 5, 30	0, 5, 30	0, 5, 30	0, 5, 30	
	5/19/09	DFO2	X		0, 5, 30	0, 5, 30	0, 5, 10, 30	0, 5, 30	
	5/20/09	UBC7	X		0, 5, 30	0, 5, 30	0, 5, 10, 30	0, 5, 30	
7	6/3/09	DFO5	X		5	5	5, 30	5	
	6/3/09	DFO2	X		0, 5	0, 5	0, 5	0, 5	
	6/3/09	UBC7	X		5	5	5	5	
8	6/17/09	DFO5			0, 5, 30	0, 5, 30	5, 30		
	6/17/09	DFO2	X		0, 5, 30	0, 5, 30	0, 5, 10, 30		
	6/18/09	UBC7	X		0, 5, 30	0, 5, 30	0, 5, 10, 30		
9	7/1/09	DFO5	X		0, 5, 30	0, 5, 30	5, 30		
	7/1/09	DFO2	X		0, 5, 30	0, 5, 30	0, 5, 10, 30		
	7/2/09	UBC7	X		0, 5, 30	0, 5, 30	0, 5, 10, 30		
10	7/18/09	DFO5	X		0, 5, 30	0, 5, 30	5, 30	0, 5, 30	
	7/17/09	DFO2	X		0, 5, 30	0, 5, 30	0, 5, 10, 30	0, 5, 30	
	7/16/09	UBC7	X		0, 5, 30	0, 5, 30	0, 5, 10, 30	0, 5, 30	
11	8/14/09	DFO5	X		0, 5, 30	0, 5, 30	5, 30	0, 5, 30	
	8/13/09	DFO2	X		0, 5, 30	0, 5, 30	0, 5, 10, 30	0, 5, 30	
	8/13/09	UBC7	X		0, 5, 30	0, 5, 30	0, 5, 10, 30	0, 5, 30	

Table 12 (continued). Summary of cruise dates and samples collected. X denotes sample collected. 0, 5, and 30 refer to depths at which samples were collected (m).

2010 Sampling

Cruise	Date	Station	CTD profile	PAR profile	Chl α	Phytoplankton sample	Nutrients	FRRF	^{13}C
1	3/19/10	DFO5	X	X	0, 5, 30	0, 5, 30	5, 30		0, 5, 30
	3/18/10	DFO2	X	X	0, 5, 30	0, 5, 30	0, 5, 10, 30		0, 5, 30
	3/18/10	UBC7	X	X	5	5	0, 5, 10, 30		
2	4/24/10	DFO5	X	X	0, 5, 30	0, 5, 30	5, 30		
	4/24/10	DFO2	X	X	0, 5, 30	0	0, 5, 10, 30		0, 5, 30
	4/23/10	UBC7	X	X	0, 5, 30	0, 5, 30	0, 5, 10, 30		
3	5/18/10	DFO5	X	X	0, 5, 30	0, 5, 30	5, 30		
	5/17/10	DFO2	X	X	0, 5, 30	0	0, 5, 10, 30	0, 5, 30	0, 5, 30
	5/17/10	UBC7	X	X	0, 5, 30	0, 5, 30	0, 5, 10, 30		
4	6/22/10	DFO5	X	X	0, 5, 30		0, 5, 30		
	6/21/10	DFO2	X	X	0, 5, 30	0, 5, 30	0, 5, 10, 30	0, 5, 30	0, 5, 30
	6/22/10	DFO2		X	0, 5, 30			0, 5, 30	0, 5, 30
	6/20/10	UBC7	X	X	0, 5, 30	0, 5, 30	0, 5, 10, 30		
5	7/21/10	DFO5	X	X	0, 5, 30	0, 5, 30	5, 30		
	7/20/10	DFO2	X	X	0, 5, 30	0, 5, 30	0, 5, 10, 30	0, 5, 30	0, 5, 30
	7/21/10	DFO2		X	0, 5, 30			0, 5, 30	0, 5, 30
	7/20/10	UBC7	X	X	0, 5, 30	0, 5, 30	0, 5, 10, 30		

Summary of FRRF/ ^{13}C parallel trials

	Cruise	Date	Station	Time		Date	Phytoplankton culture
Field	1	3/19/10	DFO5	PM*	Laboratory	3/18/10	<i>Skeletonema costatum</i>
		3/19/10	DFO2	PM*		3/18/10	<i>Chaetoceros</i> sp.
	2	4/24/10	DFO2	AM*		3/24/10	<i>Skeletonema costatum</i>
	3	5/19/10	DFO2	AM		3/24/10	<i>Skeletonema costatum</i>
	--	5/26/10	Dawson's	Midday		3/29/10	<i>Skeletonema costatum</i>
	--	5/27/10	Dawson's	AM		3/30/10	<i>Skeletonema costatum</i>
	--	5/27/10	Dawson's	PM		3/30/10	<i>Chaetoceros</i> sp.
	--	5/30/10	Dawson's	Midday		3/31/10	<i>Chaetoceros</i> sp.
	4	6/21/10	DFO2	AM			
		6/22/10	DFO2	AM			
	--	7/15/10	Dawson's	AM			
	--	7/15/10	Dawson's	PM			
	--	7/16/10	Dawson's	AM			
	--	7/16/10	Dawson's	PM			
	--	7/17/10	Dawson's	AM			
	--	7/17/10	Dawson's	PM			
	--	7/18/10	Dawson's	AM			
	--	7/18/10	Dawson's	PM			
	--	7/19/10	Dawson's	AM			
	--	7/19/10	Dawson's	PM			
	5	7/20/10	DFO2	AM			
		7/21/10	DFO2	AM			

*Data not shown

Appendix B: Measuring photosynthetic unit size (n_{PSII}^{-1}) in representative

Rivers Inlet phytoplankton using an oxygen electrode

1.1 Introduction and rationale

Primary productivity measurements are increasingly being made using fluorometric techniques such as the fast repetition rate fluorometry (FRRF) due to the high speed, high resolution, and low cost of data collection. One of the challenges of FRRF measurements of primary productivity (FRRF-PP) has been minimizing the number of assumptions made during data calculation. Photosynthetic unit size is one of the parameters required to calculate FRRF-PP. Photosynthetic unit size is not a physical size, but is the ratio of the concentration of functional photosystem (PS) II reaction centres (RCII) to chlorophyll *a* (chl*a*). There is some confusion in the literature arising from inconsistency in notation. In this study, we define photosynthetic unit size as n_{PSII}^{-1} , with units $\text{mol chl}a \cdot (\text{mol } e^-)^{-1}$. This assumes a 1 electron (e^-) for each functional RCII.

Photosynthetic unit size cannot currently be accurately estimated by fluorometers and is difficult to measure in the field. In the past, some studies have assumed a single “typical” value of n_{PSII}^{-1} , usually $500 \text{ mol chl}a \cdot (\text{mol } e^-)^{-1}$ (e.g., Falkowski et al. 1981, Smyth et al. 2004, Tripathy et al. 2010). Given the range of reported n_{PSII}^{-1} values in the literature [10 – 951 $\text{mol chl}a \cdot (\text{mol } e^-)^{-1}$; Table 13], it is unlikely that a single value can represent the photosynthetic unit size of a phytoplankton community. Kolber and Falkowski (1993) calculated n_{PSII}^{-1} as a function of photochemical efficiency (F_v/F_m), which is an improvement over the previous approach. This relationship has since been shown to change as community composition changes, meaning that it is not always applicable (Koblížek et al. 2001, Suggett et al. 2004, Juneau and Harrison 2005, Suggett et al. 2009a). Others have derived n_{PSII}^{-1} from measurements of chl*a*-specific absorption

Table 12. List of photosynthetic unit size [n_{PSII}^{-1} ; mol chl *a* · (mol e⁻)⁻¹] values reported in the literature. Growth conditions are reported as number of light (E) or nutrient treatments. Values are listed highest to lowest because n_{PSII}^{-1} tends to decrease with increasing light levels or nutrient concentrations. (*) indicates increasing n_{PSII}^{-1} with increasing light, likely due to photoinhibition. Modified from Suggett et al. (2010).

Species	Growth conditions	n_{PSII}^{-1} range	Source
<i>Aureococcus anophagefferens</i>	2 × E	951 – 879	Suggett et al. (2004, 2009b)
<i>Chlorella pyrenoidosa</i>	6 × E	588 – 390	Myers and Graham (1971)
<i>Chaetoceros muelleri</i>	2 × E	591 – 520	Suggett et al. (2004)
<i>Chaetoceros</i> sp.	3 × E	68 – 40	This study
<i>Dunaliella tertiolecta</i>	2 × E	833 – 710	Falkowski et al. (1981)
	2 × E	739 – 528	Sukenik et al. (1990)
	3 × E	742 – 501	Suggett et al. (2004, 2009b)
	3 × E	291 – 112	This study
<i>Emiliania huxleyi</i>	6 × E	720 – 488	Suggett et al. (2004, 2007)
<i>Isochrysis galbana</i>	5 × E	637 – 264	Dubinsky et al. (1986)
	5 × E	756 – 406	Herzig and Dubinsky (1992)
	9 × [NO ₃]	478 – 431	Herzig and Falkowski (1989)
<i>Mychonastes homosphaera</i>	3 × E	243 – 163	Malinsky-Rushansky et al. (2002)
<i>Nannochloropsis</i> sp.	2 × E	830 – 783	Fisher et al. (1996)
<i>Planktothrix agardhii</i>	constant; fluctuating	175; 125	Fietz and Nicklisch (2002)
<i>Prorocentrum micans</i>	4 × E	725 – 514	Dubinsky et al. (1986)
<i>Prorocentrum minimum</i>	3 × E	535 – 488	Suggett et al. (2004, 2009b)
<i>Pycnococcus provasolii</i>	3 × E	938 – 587	Suggett et al. (2004, 2009b)
<i>Rhodomonas salina</i>	2 × E	510 – 471	Suggett et al. (2004)
<i>Scenedesmus quadricauda</i>	5 × E	545 – 406	Herzig and Dubinsky (1992)
<i>Skeletonema costatum</i>	3 × E	605 – 590	Falkowski et al. (1981)
	3 × E	47 – 20	This study
<i>Stephanodiscus neostreaea</i>	constant; fluctuating	553; 282	Fietz and Nicklisch (2002)
<i>Storeatula major</i>	3 × E	518 – 444	Suggett et al. (2004, 2009b)
<i>Symbiodinium</i> spp.	2 × E	632 – 432	Iglesias-Prieto and Trench (1994)
	2 × E	635 – 273	Hennige et al. (2009)
<i>Synechococcus leopoliensis</i>	4 × E	493 – 405	Herzig and Dubinsky (1992)
<i>Synechococcus</i> spp.	5 × E	133 – 311*	Barlow and Alberte (1985)
	2 × E	293 – 236	Suggett et al. (2004)
<i>Tetraedron minimum</i>	2 × E	687 – 702	Fisher et al. (1989)
	3 × E	470 – 10	Malinsky-Rushansky et al. (2002)
<i>Thalassiosira aestivalis</i>	1 × E	49	This study
<i>Thalassiosira oceanica</i>	2 × E	426 – 313	Suggett, Moore, and Lawson (unpubl.)
<i>Thalassiosira pseudonana</i>	2 × E	485 – 499	Suggett and Moore (unpubl.)
<i>Thalassiosira weisflogii</i>	5 × E	723 – 553	Dubinsky et al. (1986)
	2 × E	585 – 420	Suggett et al. (2004, 2009b)
	2 × E	653 – 522	Suggett, Moore, and Lawson (unpubl.)
	2 × E	226 – 163	This study

by PSII ($a_{\text{PSII}}^{\text{chl}}$) and effective absorption by PSII (σ_{PSII} ; Suggett et al. 2004, Moore et al. 2005, 2006b). In spite of these advances, measuring n_{PSII}^{-1} in algal monocultures in the laboratory will yield much more accurate calculations of FRRF-PP than any other approach. Briefly, photosynthetic unit size is measured by inducing a single turnover of electrons with a short, bright, saturating flash of light. This drives O_2 evolution, which can be measured by an oxygen electrode. Changes in O_2 evolution with varying flash frequencies can be used to derive n_{PSII}^{-1} (see Methods for details).

In this study, we first validated our methods of measuring n_{PSII}^{-1} by replicating the experiments of Suggett et al. (2009b). We then measured the photosynthetic unit size of the three dominant phytoplankton taxa of Rivers Inlet, BC (the diatoms *Skeletonema costatum*, *Chaetoceros* spp., *Thalassiosira* spp.) grown under different light intensities in order to more accurately calculate FRRF-PP.

1.2 Methods

1.2.1 Phytoplankton isolation and culturing techniques

1.2.1.1 Comparison to Suggett et al. (2009b)

In order to verify our method, we replicated the experiments of Suggett et al. (2009b). We cultured *Dunaliella tertiolecta* and *Thalassiosira weissflogii* (CCMP 1320 and 1047, respectively; Provasoli-Guillard National Center for Marine Algae and Microbiota, East Boothbay, ME, USA) at 20°C in enriched (f/2) artificial seawater (see Suggett et al. 2009b). Phytoplankton strains were grown in 28 mL polycarbonate tubes under continuous illumination by cool-white fluorescent lights (Sylvania, Mississauga, Canada). *D. tertiolecta* was grown at 18, 80, and 300 $\mu\text{mol quanta} \cdot \text{m}^{-2} \cdot \text{s}^{-1}$ (low light [LL], medium light [ML], and high light [HL],

respectively) and *T. weissflogii* was grown at LL and ML. Cultures were maintained in exponential growth using sterile, semi-continuous batch culturing techniques. Cultures were considered acclimated to these conditions when growth rates varied by less than 10% between consecutive transfers (Brand et al. 1981). As a proxy for biomass, *in vivo* chlorophyll *a* (chl*a*) fluorescence was measured daily using a Water Properties Turner 10 AU fluorometer (Sunnyvale, CA, USA). Absolute growth rates (d^{-1}) were determined using simple linear regressions of the natural log (*ln*) of *in vivo* chl*a* fluorescence versus time (days).

1.2.2 Representative Rivers Inlet phytoplankton

The dominant phytoplankton taxa of Rivers Inlet (*Skeletonema costatum*, *Chaetoceros* spp., and *Thalassiosira* spp.) were identified from preserved samples using light microscopy. *Skeletonema costatum* and a small *Chaetoceros* species were successfully isolated from live seawater samples collected at Dawson's Landing, in Rivers Inlet, BC in July 2009. We were unable to isolate any *Thalassiosira* strains and instead used a laboratory-grown strain (*Thalassiosira aestivalis*, CCMP 975; Provasoli-Guillard National Center for Marine Algae and Microbiota, East Boothbay, ME, USA). *Skeletonema costatum* and *Chaetoceros* sp. cultures were each started from a single cell or chain of cells using the micropipette technique described by Andersen and Kawachi (2005). Cultures were treated with antibiotics to inhibit bacterial growth (Droop 1967) and were monitored to ensure that no contaminants were present. To simulate the natural growth conditions in Rivers Inlet, cells were grown in Harrison's enriched natural seawater (HENS_W; Harrison et al. 1980) at 12°C. Phytoplankton were grown under continuous illumination by cool-white fluorescent lights (Sylvania, Mississauga, Canada). Cultures were grown at 3 light levels representative of natural conditions: 10, 110, and 350 $\mu\text{mol quanta} \cdot \text{m}^{-2} \cdot \text{s}^{-1}$ (LL, ML, and HL respectively).

1.2.3 Experimental design

Prior to beginning the experiment, we bubbled synthetic ocean water (SOW) with air overnight in order to saturate the SOW with O₂. The air-bubbled SOW was placed in a water bath at least one hour before experiments were run, using the temperature to which the phytoplankton were acclimated (12°C or 20°C).

We used an S1 oxygen electrode disc (Hansatech Instruments, Norfolk, England; Figure 15a) and Teflon film as a membrane. A doughnut-shaped spacer of cigarette paper was centred over the electrode's platinum button and wetted with 50% saturated KCl solution before the membrane was placed overtop and secured with a rubber O-ring. Care was taken to avoid trapping air bubbles between the electrode disc and membrane. The electrode disc was fitted into the bottom of a DW1 liquid-phase oxygen electrode chamber (Hansatech) that connected to the water bath (Figure 15b). The cuvet (electrode and chamber) was centred atop a stir plate on medium speed, filled with deionized water (MQ), and a small stir bar was placed inside. To minimize signal noise, the stir plate speed was adjusted until the stir bar was spinning smoothly. Once set, it was not changed during the course of an experiment. The cuvet was visually inspected to ensure that no debris was floating inside and that there were no bubbles on either side of the Teflon membrane. The adjustable lid was placed on top of the cuvet and the plunger was screwed down until no air remained inside the cuvet and some MQ came out of the top of the plunger, effectively sealing the cuvet. The electrode was connected to a CB1D O₂-electrode

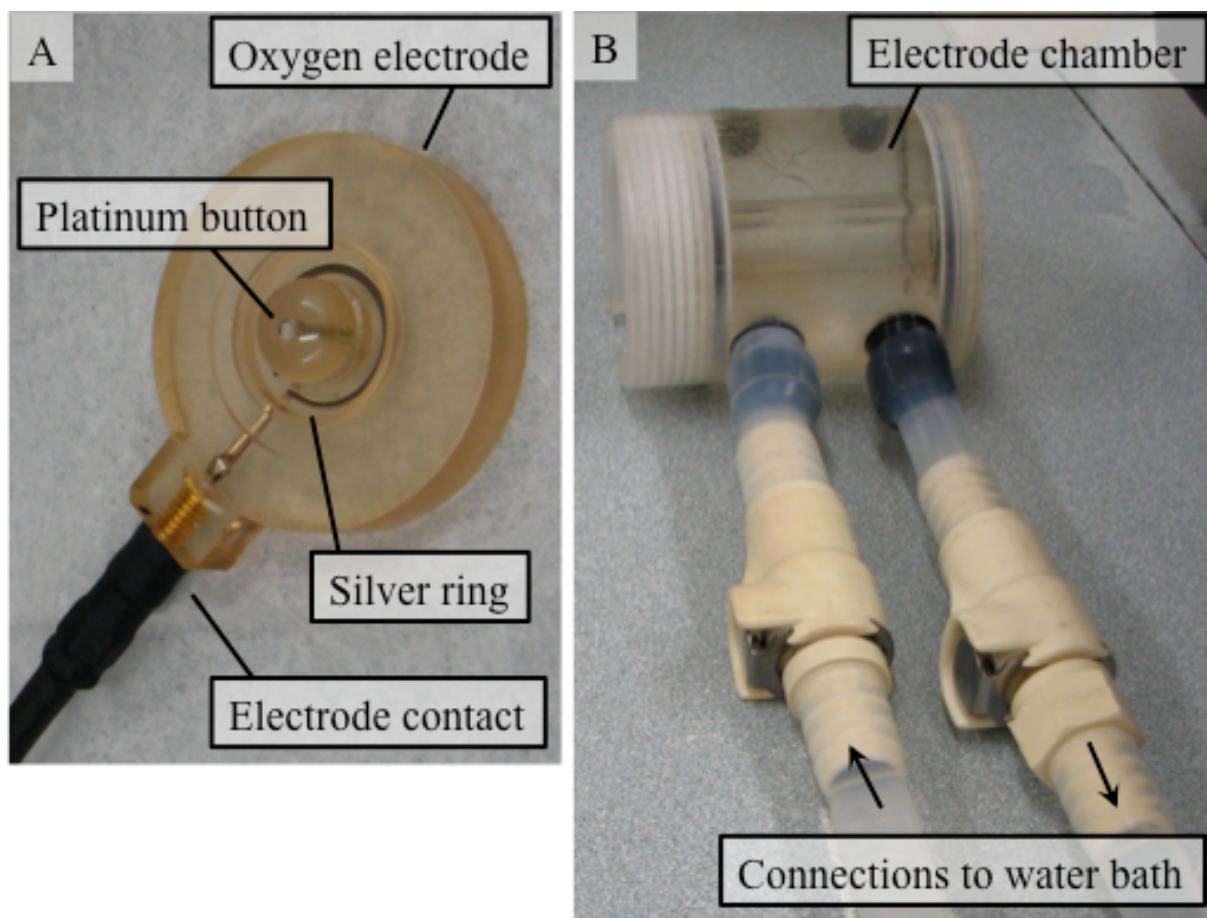


Figure 15. Detail of (a) oxygen electrode and (b) electrode chamber used to measure oxygen flash yields.

control box (Hansatech), which was connected via a U12 voltage-to-USB converter (LabJack, Lakewood, CO, USA) to a laptop where labjackoxy.exe was installed. At this point, the control box was turned on and a steady signal obtained. If the voltage fluctuated, we cleaned the cuvet, electrode, and membrane as needed.

We used a single xenon flash lamp (Oriel Corporation, Stratford, CN, USA) to provide saturating flashes (Strzepak and Harrison 2004). The lamp was situated such that the beam was centred on the cuvet. If necessary, we refocused the lamp's beam according to the manufacturer's instructions. The light level at the cuvet was measured with a light meter and the lamp was not moved throughout all experimental trials. Care was taken to keep the lamp's

power supply far from the electrode contact (Figure 15a) to reduce signal noise. The lamp was set to 1200 mJ, the maximum energy setting for available for the range of frequencies we used (0 – 50 Hz).

1.2.4 Oxygen flash yields

Using approximately 100 mL of phytoplankton culture in exponential growth, we gently centrifuged (7 min, 5000 RCF [relative centrifugal field], at the temperature cultures were grown) the samples to concentrate the phytoplankton. We poured off the supernatant, retaining the loose pellet and 10 – 15 mL of medium. This culture concentrate was used to measure oxygen flash yields.

While samples were in the centrifuge, we calibrated the electrode by filling the cuvet with air-bubbled, O₂-saturated SOW. After collecting several minutes of O₂-saturated data, we gently bubbled the SOW in the cuvet with N₂ and collected several minutes of minimum-O₂ data. After the calibration, the cuvet was emptied, rinsed, and refilled with culture concentrate. In the cuvet, cells were stimulated with a weak light for several minutes to induce oxygen production and encourage recovery after centrifugation. The cuvet, stir plate, and lamp were then covered by a dark chamber to block ambient light and the cells were allowed to dark-adapt for 15 – 20 min. During this period, we measured O₂ consumption. After the period of dark adaptation, we used the xenon lamp to measure O₂ production at flash frequencies of 5, 10, 20 30, 40, and 50 Hz (3 – 5 min at each frequency).

1.2.5 Chlorophyll *a* determination

Two chlorophyll *a* (chl*a*) samples were collected for each experiment. 20 mL of the unconcentrated phytoplankton culture was filtered through a 47mm Whatman GFF filter and 0.5

mL of the concentrated samples was filtered onto a separate GFF. Filters were frozen and stored at -20°C until they could be analyzed according to the protocol described by Strickland and Parsons (1968). For analysis, each filter was soaked in 8 mL 90% acetone and returned to a dark, -20°C freezer for 24 hours. Once the acetone had extracted the *chl a* from the filters, samples were warmed to room temperature and the concentration of *chl a* was determined using a fluorometer (Water Properties Turner 10 AU fluorometer, Sunnyvale, CA, USA) and a blank of 90% acetone. Sample fluorescence was recorded both before and after acidification with 30 μ L of 10% HCl. Fluorescence was converted to *chl a* concentration using the following calibration equation:

$$[\text{chl}a] = 2.68 \times (F_b - F_a) \times (v \times V^{-1})$$

where $[\text{chl}a]$ is the concentration of *chl a* in $\mu\text{g} \cdot \text{L}^{-1}$; 2.68 is a fluorometer-specific correction factor ($\mu\text{g} \cdot \text{L}^{-1}$); F_b is the fluorescence reading before acidification (dimensionless); F_a is the fluorescence reading after acidification (dimensionless); v is the volume of acetone (mL); and V is the volume of phytoplankton culture filtered (mL).

1.2.6 Data processing and calculation

Rates of oxygen evolution for each section of the experiment (O_2 -saturated SOW, N_2 -bubbled SOW, sample in the dark; sample exposed to 5 Hz flashes, 10 Hz flashes, etc.) were extracted using Oxypeak software (Figure 16). These are reported as % change $[\text{O}_2] \cdot \text{min}^{-1}$ and converted to net O_2 evolved ($\mu\text{mol O}_2 \cdot \text{L}^{-1} \cdot \text{s}^{-1}$). These values are plotted against flash frequency (Figure 17). The *chl a* concentration ($\mu\text{g chl}a \cdot \text{L}^{-1}$) was divided by the initial linear slope of the graph (molecules $\text{O}_2 \cdot \text{L}^{-1} \cdot \text{flash}^{-1}$) to give the oxygen flash yield ($\mu\text{mol chl}a \cdot \mu\text{mol}$

O_2^{-1}). Assuming a 4 O_2 :1 electron (e^-) ratio, we converted flash yield to photosynthetic unit size [n_{PSII}^{-1} ; mol chl $a \cdot (mol e^-)^{-1}$]. See Table 14 for sample calculation.

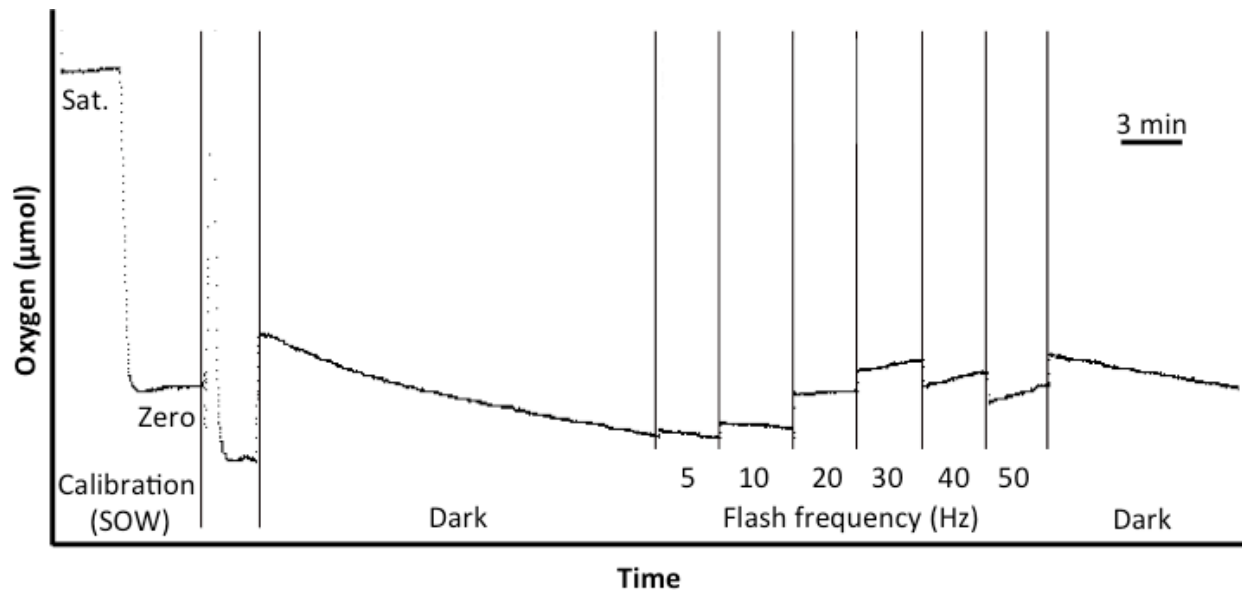


Figure 16. Oxygen evolution trace from *Skeletonema costatum* grown under medium light (ML) conditions. Vertical lines indicate different sections of the experiment. Sat.: O_2 -saturated synthetic ocean water (SOW). Zero: N_2 -bubbled, O_2 -minimum SOW. All other sections measure O_2 evolution on the concentrated phytoplankton culture. Large shifts between sections are an artifact of the experiment. Because slope is measured, these shifts do not affect results.

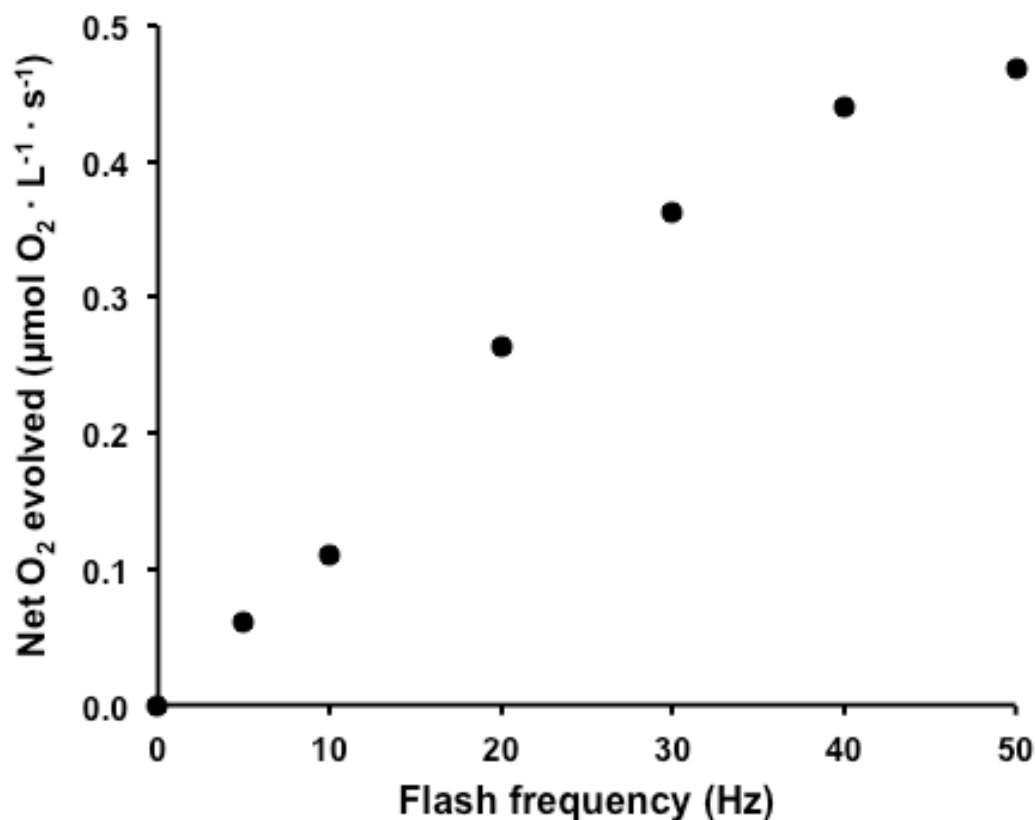


Figure 17. Example plot of oxygen flash yield results from *Skeletonema costatum* grown under medium light (ML) conditions. The initial linear slope of this graph, in this case 0 – 20 Hz, is used to calculate photosynthetic unit size (n_{PSII}^{-1}). See text and Table 13.

Table 13. Example calculation of photosynthetic unit size (n_{PSII}^{-1}) from oxygen flash yields using *Skeletonema costatum* grown under medium light (ML) conditions. Gain: electrical setting on the O₂-electrode control box; in this case, gain was not changed during the experiment. Raw O₂ evolution: data output from linear regression of O₂ measurements by labjackoxy.exe. Gross O₂ evolution: calculated by multiplying raw O₂ evolution and the oxygen saturation constant (in this case, 543.77 µmol · L⁻¹ for salinity 35 and temperature 12°C) then dividing by gain. Slope: the slope of the linear portion of the graph (Figure 17), in this case, 0-20 Hz (*italicized*). Flash yield: chl_a concentration of the concentrated sample divided by slope. n_{PSII}^{-1} : assumes a 4:1 ratio of O₂:e⁻.

Flash frequency	Gain	Raw O ₂ evolution	Gross O ₂ evolution	Gross O ₂ evolution	Net O ₂ evolution	Slope	Chl _a	Flash yield	n_{PSII}^{-1}
Hz		% change O ₂ · min ⁻¹	µmol O ₂ · (L · min) ⁻¹	µmol O ₂ · (L · s) ⁻¹	µmol O ₂ · (L · s) ⁻¹	µM O ₂	µmol · L ⁻¹	mol chl _a · mol O ₂ ⁻¹	mol chl _a · (mol e ⁻) ⁻¹
0	1	-0.020	-10.89	-0.18	0.000	0.013	0.99	75.91	18.98
5	1	-0.013	-7.27	-0.12	0.060				
10	1	-0.0079	-4.27	-0.07	0.110				
20	1	0.009	4.88	0.08	0.263				
30	1	0.020	10.86	0.18	0.362				
40	1	0.029	15.47	0.26	0.439				
50	1	0.032	17.16	0.29	0.468				

1.3 Results

1.3.1 Comparison to n_{PSII}^{-1} from Suggett et al. (2009b)

We measured photosynthetic unit size (n_{PSII}^{-1}) in *Dunaliella tertiolecta* and *Thalassiosira weissflogii* grown under the same conditions as Suggett et al. (2009b). We found that our values were consistently lower than those of Suggett et al. (2009b; Table 15). For example, we measured n_{PSII}^{-1} of 226 mol chl_a · (mol e⁻)⁻¹ for LL *T. weissflogii*, while Suggett et al. (2009b) measured 584 mol chl_a · (mol e⁻)⁻¹. Our measurements also had larger standard errors (SE) than Suggett et al. (2009b). In general, n_{PSII}^{-1} was lower in cultures that were acclimated to higher light levels (both in our data and in Suggett et al. 2009b). The exception to this was LL *D. tertiolecta*, where we measured n_{PSII}^{-1} to be lower than for the ML treatment.

Table 14. Comparison of photosynthetic unit size (n_{PSII}^{-1}) values against those in the literature. PFD: photon flux density. μ : growth rate. SE: standard error. Replicates are measurements of independent cultures. Grey columns contain data from Suggett et al. (2009b).

	Cell size	PFD	μ	μ	n_{PSII}^{-1}	n_{PSII}^{-1}	SE	SE	Replicates
	μm	$\mu\text{E} \cdot \text{m}^{-2} \cdot \text{s}^{-1}$	d^{-1}	d^{-1}	mol chl _a · (mol e ⁻) ⁻¹	mol chl _a · (mol e ⁻) ⁻¹			
<i>Dunaliella tertiolecta</i> (CCMP 1320)	6 – 9	18	0.25	0.28	189	742	58	11	4
		80	1.09	1.72	291	693	47	18	5
		300	0.87	2.42	112	501	20	22	3
<i>Thalassiosira weissflogii</i> (CCMP 1047)	14 – 18	18	0.38	0.24	226	584	26	8	5
		80	1.34	1.37	163	520	45	14	5

1.3.2 n_{PSII}^{-1} of representative Rivers Inlet phytoplankton

In species representing the Rivers Inlet spring phytoplankton community, similar to the comparison with Suggett et al. (2009b), we generally observed n_{PSII}^{-1} to be lower in cultures that were acclimated to higher light levels (Table 16). We measured lower n_{PSII}^{-1} in the Rivers Inlet

trials [20 – 68 mol chla · (mol e⁻)⁻¹] than those described in the previous section [112 – 291 mol chla · (mol e⁻)⁻¹]. SE was also high in these experiments and data from many additional trials were discarded due to low-quality results.

Table 15. Photosynthetic unit size (n_{PSII}^{-1}) of species representative of the spring phytoplankton community in Rivers Inlet, BC. PFD: photon flux density. SE: standard error. Replicates are measurements of independent cultures. n_{PSII}^{-1} from F_v/F_m is calculated as a function of F_v/F_m measured by FRRF (Kolber and Falkowski 1993; Section 2.2.11).

	Cell size	PFD	n_{PSII}^{-1} measured	SE	Replicates	n_{PSII}^{-1} from F_v/F_m	SE	Replicates
	μm	$\mu\text{E} \cdot \text{m}^{-2} \cdot \text{s}^{-1}$	$\text{mol chla} \cdot (\text{mol e}^{-})^{-1}$			$\text{mol chla} \cdot (\text{mol e}^{-})^{-1}$		
<i>Skeletonema costatum</i>	2 – 40	10	47	n/a	1	623	26	5
		110	23	8	8			
		350	20	14	2			
<i>Chaetoceros</i> sp.	6 – 30	10	68	48	2	565	25	3
		110	40	3	6			
		350	43	21	4			
<i>Thalassiosira aestivalis</i> (CCMP 975)	18 – 32	10	-	-	-			
		110	49	n/a	1			
		350	-	-	-			

1.4 Discussion and conclusions

Our n_{PSII}^{-1} measurements ranged from 20 – 291 mol chla · (mol e⁻)⁻¹. These values are low, but are within the range of reported values from the literature [10 – 951 mol chla · (mol e⁻)⁻¹; Table 13]. In Rivers Inlet isolates, we also calculated n_{PSII}^{-1} as a function of photochemical efficiency (F_v/F_m ; Kolber and Falkowski 1993) measured by FRRF (Table 16). Estimated n_{PSII}^{-1} values are significantly higher than our measured n_{PSII}^{-1} , but are similar to the standard assumed value of 500 mol chla · (mol e⁻)⁻¹ and to mean literature values (Table 13).

Our measurements of photosynthetic unit size follow the generally observed trend that n_{PSII}^{-1} decreases as light intensity increases (e.g., Dubinsky et al. 1986, Sukenik et al. 1990, Suggett et al. 2004). Photosynthetic unit size is a ratio of chla to functional photosystem II

reaction centres (RCII). Note that functional RCII and electrons (e^-) are used interchangeably because we assume a 1:1 relationship. Under high-light conditions, cells decrease their light-harvesting ability by first decreasing the number of *chl a* molecules. This explains why n_{PSII}^{-1} decreases in cells adapted to high light intensities. Conversely, under low-light conditions, cells increase *chl a* and n_{PSII}^{-1} decreases. At extremely low light levels, such as our LL treatment, phytoplankton may also increase RCII concentrations. This may explain why n_{PSII}^{-1} was lower in LL *Dunaliella tertiolecta* cultures than in ML cultures. At extremely high light levels, Barlow and Alberte (1985) observed n_{PSII}^{-1} to increase. This is likely due to photoinhibition, which damages cells and decreases the number of functional RCII.

It is not clear why the variability between replicates was so high in our study. We often measured 2 – 3 replicates of the same treatment, with similar *chl a* levels, on the same day. This approach, however, did not improve the precision of our measurements. For example, we measured an n_{PSII}^{-1} of $36.7 \text{ mol chl a} \cdot (\text{mol } e^-)^{-1}$ with a standard error of 21.2 on 3 replicates of HL *Chaetoceros* sp. in a single day. In addition to high error between measurements, we also often altogether failed to measure n_{PSII}^{-1} in the phytoplankton representing the Rivers Inlet community. In some trials, data were low quality (i.e., no clear linear increase in O_2 evolution with increasing flash frequency). In other trials, we observed no changes in O_2 levels at any flash frequency, but observed O_2 consumption in the dark. This was less likely to occur when cells were concentrated by gentle filtration instead of by centrifugation, suggesting that cells were somehow damaged by the centrifuge, but success was still unpredictable. We also inspected the phytoplankton cultures using light microscopy to confirm that cells were growing normally and no other organisms were present. As a result of our isolation techniques, it is likely that bacteria were present in *Skeletonema costatum* and *Chaetoceros* sp. cultures. This would increase O_2 consumption both in the dark and at all flash frequencies. Because we calculate n_{PSII}^{-1} using net O_2 evolution (rather

than gross O₂ evolution), this should not affect our results unless the bacteria were damaging phytoplankton cells either directly (by feeding on them) or indirectly (competition for resources). *Thalassiosira aestivalis* grew poorly, especially at LL, precluding any measurements of n_{PSII}^{-1} on that treatment. Experiments on ML and HL treatments of *T. aestivalis* were largely unsuccessful even though cultures appeared healthy. We also used phytoplankton cultures that were less dense, so as to minimize any self-shading effects. After attempting to identify problems with the phytoplankton cultures, we also cleaned and reset our experimental set-up several times. Ultimately, though, we were unable to identify the sources of error and simply performed many experiments for each treatment, using only the few successful trials in our analyses.

In the future, use of axenic cultures may improve the success rates for measuring n_{PSII}^{-1} , though the reasons for this are not clear. In order to ensure that there is no gas exchange between the sample and the air, the design of the cuvet lid should be improved. Others have successfully measured n_{PSII}^{-1} using this design, meaning that it is unlikely that this is the source of our difficulty. However, it is advisable to minimize all possible sources of errors. Once experimental design has been optimized and data output is more precise, it would be informative to study not only variations in light levels, but also in nutrient concentrations. Having a range of n_{PSII}^{-1} values under different light and nutrient conditions for each of the dominant phytoplankton taxa of Rivers Inlet would allow us to fine-tune our calculations of FRRF-derived primary productivity to the exact physical conditions and community composition observed. This would greatly increase the accuracy of FRRF-PP data and allow us to better understand phytoplankton community dynamics and how they affect higher trophic levels.

Appendix C: All phytoplankton data observed using light microscopy

Table 16. Relative abundances of phytoplankton observed in preserved samples from the head of the inlet in 2009.

Organism	Dates Depth (m)	Head of inlet 2009																											
		2/26 - 28		3/17 - 19			4/2 - 3		4/16 - 17			5/3 - 4			5/19 - 20		6/3	6/17 - 18			7/1 - 2			7/16 - 18			8/13 - 14		
		5	30	0	5	30	0	5	30	0	5	30	0	5	5	0	5	30	0	5	30	0	5	30	0	5	30		
Diatoms																													
<i>Chaetoceros affinis</i>														1															
<i>Chaetoceros convolutus</i>	1			1	1		1	1																					
<i>Chaetoceros curvisetus</i>			1																										
<i>Chaetoceros debilis</i>				1			2	1		1	1																		
<i>Chaetoceros decipiens</i>			1					1			1							1						1					
<i>Chaetoceros laciniatus</i>														1															
<i>Chaetoceros lorenzianus</i>							3																						
<i>Chaetoceros radicans</i>				1						1														1					
<i>Chaetoceros similis</i>	1																												
<i>Chaetoceros teres</i>					1																								
<i>Corethron hystrix</i>	1		1		1			1	1	1	1	1	1					1											
<i>Cosinodiscus</i> spp.						1	1	1		1																			
<i>Cylindrotheca closterium</i>	1		1		1	1	1	1	1	1	1	1	1	1		1		1	1	1				1			1		
<i>Ditylum brightwellii</i>																													
<i>Eucampia zodiacus</i>														1	1														
<i>Grammatophora marina</i>	1																												
<i>Leptocylindrus danicus</i>			1								1																		
<i>Leptocylindrus minimus</i>			1	1	1	1	2	1	1	1	2	1	1	1	1	1	1	1	1	1	1	1	1	1	1	1	1	1	
<i>Melosira granulata</i>				1	1		2						2	1		2		1	1	1	1	1	1	1	1	1	1	1	
<i>Melosira moniliformes</i>				1			1				1					1													
<i>Navicula</i> spp.	1			1						1	1	1	1	1		1													
<i>Odontella aurita</i>										1	1																		
<i>Plagiogrammopsis vanheurckii</i>							1																						
<i>Pleurosigma</i> spp.					1		1	1		1																			
<i>Pseudo-nitzschia pseudo-delicatissima</i>	1		1	1	1	1	1	1	1	1	3	1	1	1	1	1	1	1	1	1	1	1	1	1	1	1	1	1	
<i>Pseudo-nitzschia pungens/multiseriis</i>	1						1			2			1													1			
<i>Rhizosolenia</i> spp.																													
<i>Skeletonema costatum</i>			1	1			2		1	1		2	3				1					1			1	3			
<i>Stephanopyxis nipponica</i>										1																			
<i>Thalassionema nitzschoides</i>	1			1	1	1	1	1	1	1		1	1				1		1			1			1			1	
<i>Thalassiosira anguste-lineata</i>				1			2																						
<i>Thalassiosira pac/nord/aest</i>			1	1	1	1	4	2	1	3	4	1	1	4		1		1	1		1	1		1	1		3		
<i>Thalassiosira rotula</i>							2	1		1	2		2																
Dinoflagellates																													
<i>Akashiwo sanguinea (Gymnodinium splendens)</i>						1										1								1					
<i>Alexandrium ostenfeldii</i>						1			1																				
<i>Alexandrium tamarense</i>																								1					
<i>Amylax tricantha</i>												1		1															
<i>Ceratium fusus</i>								1																					
<i>Corythodinium tessellatum</i>																							1						
<i>Dinophysis acuminata</i>													1																
<i>Gonyaulax digitale</i>																													
<i>Gyrodinium spirale</i>	1		1	1	1	1	2	1	1	1	1	1	1	1	1	1	1	1	1	1	1	1	1	1	1	1	1	1	
<i>Heterocapsa triquetra</i>					1		1	1	1	1	1	1	1	1	1	1	1	1	1	1	1	1	1	1	1	1	1	1	
<i>Miniscula bipes</i>																1													
<i>Oxyphysis oxytoxoides</i>				1									1													1			
<i>Prorocentrum gracile</i>									1		1																		
<i>Prorocentrum micans</i>										1																			
<i>Protoperidinium conicum</i>								1																					
<i>Protoperidinium</i> spp.													1																
<i>Protoperidinium steinii</i>																1									1	1			
<i>Scrippsiella trochoidea</i>																1									1	1	2		
<i>Zygabikodinium lenticulatum</i>																													
Ciliates																													
<i>Myrionecta rubra</i>	1		1	1	1	1	1	1	1	1	1	1	1	1	1	1	1	1	1	1	1	1	1	1	1	1	1	1	
<i>Tintinnid</i> spp.	1		1	1	1	1	1	1	1	1	1	1	1	1	1	1	1	1	1	1	1	1	1	1	1	1	1	1	
Flagellates																													
Flagellate-small	1		1	1	1	1	1	2	1	1	3	1	1	2		1		1	2	1	1	1	1	1	2	1	1	1	
Flagellate-medium	1		1	1	1	1	1	1	1	1	1	1	2	1		1		1	1	1	1	1	1	1	1	1	1	1	
Flagellate-large				1	1	1	1	1	1	3	1	1	1	1		1		1	1	1	1	1	1	1	1	1	1	1	
Silicoflagellates																													
<i>Dityocha speculum</i>	1		1					1								1		1						1					
<i>Ebria tripartita</i>							1																		1				

Table 17. Relative abundances of phytoplankton observed in preserved samples from the centre of the inlet in 2009.

Organism	Centre of inlet 2009																								
	Dates		2/26 - 28		3/17 - 19		4/2 - 3		4/16 - 17		5/3 - 4		5/19 - 20		6/3		6/17 - 18		7/1 - 2		7/16 - 18		8/13 - 14		
	Depth (m)	0	5	30	0	5	30	0	5	30	0	5	30	0	5	30	0	5	30	0	5	30	0	5	30
Diatoms																									
<i>Asterionellopsis glacialis</i>																									1
<i>Chaetoceros anastomosans</i>																									
<i>Chaetoceros convolutus</i>			1	1	1		1	1	1		1	1													1
<i>Chaetoceros danicus</i>											1		1			1									
<i>Chaetoceros debilis</i>					1				3		3	3	1	1	2			1		1	1				1
<i>Chaetoceros decipiens</i>																1									1
<i>Chaetoceros diadema</i>											2		1			1									
<i>Chaetoceros didymus</i>						1				1											1			1	1
<i>Chaetoceros lorenzianus</i>																				1					
<i>Chaetoceros radicans</i>																				1	1				
<i>Chaetoceros similis</i>				1												1									
<i>Chaetoceros vanheukekerii</i>						1																			
<i>Corethron hystrix</i>				1			1			1	1	1		1		1									
<i>Coscinodiscus spp.</i>			1							1															
<i>Cylindrotheca closterium</i>	1	1	1	1	1	1	1	1	1	1	1	1	3	2	1	2	1	1	2	1	1	1	1	1	2
<i>Ditylum brightwellii</i>						1																			
<i>Eucampia zodiacus</i>															2										1
<i>Grammatophora marina</i>										1															1
<i>Guinardia delicatula</i>															1				2						
<i>Lauderia annulata</i>																									
<i>Leptocylindrus danicus</i>												1	2		1								1		
<i>Leptocylindrus minimus</i>	1	1	1	1	1	1	1	1	1	2	1	1	1	2	1	2					1	1	1	1	2
<i>Melosira granulata</i>																1	1								
<i>Navicula spp.</i>						1				1			2	1	1										1
<i>Odontella aurita</i>						1																			1
<i>Paralia sulcata</i>																									
<i>Pleurosigma spp.</i>			1				1			1	1	1	1	1	1										
<i>Pseudo-nitzschia pseudo-delicatissima</i>	1	1	1	1	1	1	1	1	1	1	1	1	4	3	1	2	3	1	1	2	1	2	2	1	1
<i>Pseudo-nitzschia pungens/multiseriis</i>																3		1	1	3		1			1
<i>Skeletonema costatum</i>				2	2	2			1	2	1	1	4	4	1	4	4	1	4	4	1	4	3	1	2
<i>Stephanopyxis nipponica</i>																1									3
<i>Thalassionema nitzschiodes</i>	1	1	1	1	1	1	1	1	2	1	1	1	1	1	1				1	1	1	1	1	1	2
<i>Thalassiosira anguste-lineata</i>																									1
<i>Thalassiosira pac/nord/aest</i>	1	1	1	1	1	1	1	1	1	4	1	1	4	1	3	3	1	4	4	1	4	2	1	1	1
<i>Thalassiosira rotula</i>																									1
Dinoflagellates																									
<i>Akashiwo sanguinea (Gymnodinium splendens)</i>																									1
<i>Alexandrium ostenfeldii</i>						1				1		1		2											1
<i>Amylax triacantha</i>																									
<i>Ceratium fusus</i>			1																						
<i>Corythrodinium tessellatum</i>						1																			1
Dinoflagellate (unidentifiable)			1																						1
<i>Dinophysis acuminata</i>																									1
<i>Dinophysis acuta</i>																									1
<i>Dissodinium pseudolumula</i>																									
<i>Gonyaulax digitale</i>																									
<i>Gymnodinium breve</i>																									
<i>Gyrodinium spirale</i>				1	1	1				1	1	1	1	1	1									1	1
<i>Heterocapsa triquetra</i>																									1
<i>Miniscula bipes</i>																									
<i>Oxyphysis oxytoxoides</i>	1																								1
<i>Prorocentrum gracile</i>	1	1				1																			1
<i>Prorocentrum micans</i>																									1
<i>Protoperidinium conicum</i>																									
<i>Protoperidinium depressum</i>																									
<i>Protoperidinium leonis</i>																									
<i>Protoperidinium spp.</i>																									
<i>Protoperidinium steinii</i>				1	1																				1
<i>Scrippsiella trochoidea</i>																									
Ciliates																									
<i>Myrionecta rubra</i>	1	1	1	1	1	1	1	1	1	2	1	1	1	2	1	1	1	3	2	1	1	1	1	1	2
Tintinnid spp.	1	1	1	1	1	1	1	1	1	1	1	1	1	1	1	1	1	1	1	1	1	1	1	1	1
Flagellates																									
Cryptomonad-small			1										1	1	1										2
Cryptomonad-medium			1										1	1	1										1
Cryptomonad-large																									1
Flagellate-large						1	1	1	1																1
Flagellate-medium	1	1	1	1	1	1	1	1	1	1	1	1	1	1	1									1	
Flagellate-small	1	1	1	2	2	1	1	1	1	1	2	2	1												2
<i>Phaeocystis spp.</i>	1					2																			2
Rotifers																									
<i>Keratella sp.</i>																									1
Silicoflagellates																									
<i>Dicryocha speculum</i>	1	1																							1

Table 18. Relative abundances of phytoplankton observed in preserved samples from the mouth of the inlet in 2009.

		Mouth of inlet 2009																
		0=not present 1=rare 2=moderate 3=abundant 4=bloom																
Organism	Dates Depth (m)	2/26 - 28	3/17 - 19	4/2 - 3	4/16 - 17	5/3 - 4	5/19 - 20	6/3	6/17 - 18	7/1 - 2	7/16 - 18	8/13 - 14						
		5	5	0 5 30	0 5 30	0 5 30	0 5 30	0 5 30	0 5 30	0 5 30	0 5 30	0 5 30	0 5 30	0 5 30	0 5 30	0 5 30	0 5 30	
Diatoms																		
<i>Asterionellopsis glacialis</i>																		1
<i>Athya septentrionalis</i>																		1
<i>Bacillaria paxillifera</i>							1											1
<i>Chaetoceros affinis</i>							2											1
<i>Chaetoceros contortus</i>				1														1
<i>Chaetoceros convolutus</i>			1	1	1													1
<i>Chaetoceros danicus</i>							1		1	1	1							1
<i>Chaetoceros debilis</i>	1	1				1	2	1	2		1	1	1					1
<i>Chaetoceros decipiens</i>				1		1		1	1	1								1
<i>Chaetoceros diadema</i>						2		1	1		1	2	1					1
<i>Chaetoceros didymus</i>					1		1			1	1	1	1					1
<i>Chaetoceros laciniatus</i>	1																	1
<i>Chaetoceros lorentianus</i>	1					3		1		1	1	2						1
<i>Chaetoceros radicans</i>			1					1			1	1	1	1				1
<i>Chaetoceros similis</i>											1	2						1
<i>Chaetoceros subtilis</i>									1									1
<i>Chaetoceros teres</i>										1								1
<i>Corethron hystrix</i>			1			1	1											1
<i>Coscinodiscus spp.</i>			1		1		2	1										1
<i>Cylindrotheca closterium</i>	1	1	1	1	1	2	1	1	1	2	1	1	1	1	1	1	1	1
<i>Ditylum brightwellii</i>	1	1																1
<i>Eucampia zodiacus</i>																		1
<i>Grammatophora marina</i>						1												1
<i>Guinardia delicatula</i>																		1
<i>Lauderia annulata</i>									2									1
<i>Leptocylindrus danicus</i>				1					2		1	1	1					1
<i>Leptocylindrus minimus</i>	1	1	1	1	1	2	1	1	3	3	1	1	1	1	1	1	1	3
<i>Melosira granulata</i>																		1
<i>Melosira moniliformes</i>																		1
<i>Navicula spp.</i>							1		1									1
<i>Odontella aurita</i>													1					1
<i>Odontella longicurvis</i>										1	1							1
<i>Pleurosigma spp.</i>	1			1			1		1									1
<i>Pseudo-nitzschia pseudo/delicatissima</i>	1	1	1	1	1		1	1	1	2	1	4	1	2	1	1	2	1
<i>Pseudo-nitzschia pungens/multiseriis</i>			1	1	3	1		1	1	1	1	2	2	1	1	1	2	2
<i>Rhizosolenia spp.</i>																		1
<i>Skeletonema costatum</i>	1	1	1	1	1		1	1	1	3	4	2	4	2	1	2	3	3
<i>Stephanopyxis nipponica</i>							1	1										1
<i>Thalassionema nitzschioides</i>			1	1	1		1		1	1	1	1	1	2	1	1	1	1
<i>Thalassiosira amuguste-lineata</i>			1															1
<i>Thalassiosira pac/nord/aest</i>	1	1	1	1	1	2	1	2	4	4	2	1	3	2	4	2	1	3
<i>Thalassiosira rotula</i>			1	1	1			3	1	1		2	2	1	1	1	1	1
<i>Tropidoneis antarctica</i>																		1
Dinoflagellates																		
<i>Akashiwo sanguinea (Gymnodinium splendens)</i>							1	1			1	1			2			1
<i>Alexandrium catenella</i>										1					1			1
<i>Alexandrium ostenfeldii</i>											1							1
<i>Alexandrium tamarense</i>																		1
<i>Amylax triantha</i>	1			1						1								1
<i>Ceratium furca/lineatum</i>										1								1
<i>Ceratium fusus</i>								1			1		2					1
<i>Corythodinium tessellatum</i>						1							1		1			1
<i>Dinophysis acuminata</i>									1	1			1		1			1
<i>Dinophysis acuta</i>								1		1	1	1	1	1	1	1		1
<i>Dissodinium pseudolunula</i>											1	1	1					1
<i>Gonyaulax digitale</i>			1		1								1		1			1
<i>Gonyaulax verior</i>										1								1
<i>Gyrodinium spirale</i>	1	1	1	1	1	1	1	1	1	1	1	2	1	1	1	2	1	1
<i>Heterocapsa triquetra</i>	1		1	1	1				1	1	1	1	1		2	1		1
<i>Miniscula bipes</i>	1			1					1						1	1		1
<i>Noctiluca scintillans</i>																		1
<i>Oxyphysis oxytoxoides</i>			1	1	1		1	1	1	1	1		1	1	1			1
<i>Polykrikos schwartzii</i>																		1
<i>Prorocentrum gracile</i>			1			1	1	1			1			1				3
<i>Prorocentrum micans</i>																		1
<i>Protoceratium reticulatum</i>											1							1
<i>Protoperidinium conicum</i>									1									1
<i>Protoperidinium depressum</i>																		1
<i>Protoperidinium leonis</i>											1							1
<i>Protoperidinium spp.</i>																		1
<i>Protoperidinium steinii</i>								1					1					1
<i>Scrippsiella trochoidea</i>													1	1				1
Ciliates																		
<i>Myrionecta rubra</i>	1	1	1	1	1	1	1	1	1	1	1	1	1	1	1	1	1	1
<i>Tintinnid spp.</i>	1	1	1	1	1	1	1	1	1	1	1	1	1	1	2	1	1	1
Flagellates																		
<i>Cryptomonad-small</i>					3			1										2
<i>Cryptomonad-medium</i>					2			1										1
<i>Cryptomonad-large</i>					1													1
<i>Flagellate-small</i>	1	1	1	1	1	2	1	1	1	2	1	2	2	1	2	2	1	3
<i>Flagellate-medium</i>		1	1	1	1	1	1	1	1	2	1	1	1	1	2	1	1	1
<i>Flagellate-large</i>			1	1	1	1			2	1	1	1	1	1	1			1
<i>Phaeocystis spp.</i>				2														1
Silicoflagellates																		
<i>Dicryocha speculum</i>			1						1	1	1	1	1	1				1

Table 19. Relative abundances of phytoplankton observed in preserved samples from the head of the inlet in 2010.

		Head of inlet 2010																
0=not present 1=rare 2=moderate 3=abundant 4=bloom																		
Organism	Dates	3/18 - 19			4/23 - 24			5/17 - 18			6/20 - 22			7/20 - 21				
	Depth (m)	0	5	30	0	5	30	0	5	30	0	5	30	0	5	30		
Diatoms																		
<i>Chaetoceros decipiens</i>								1								1		
<i>Chaetoceros lorenzianus</i>														1	2			
<i>Chaetoceros radicans</i>								1										
<i>Corethron hystrix</i>															1			
<i>Cosinodiscus</i> spp.													1					
<i>Cylindrotheca closterium</i>									1	1		1	1		1	1		
<i>Fragillaria</i> spp.								1										
<i>Leptocylindrus minimus</i>									1				1		1			
<i>Melosira granulata</i>								2	1			1	1	1		1		
<i>Pleurosigma</i> spp.										1								
<i>Pseudo-nitzschia pseudo-/delicatissima</i>									1	1		1	1	1		1	1	
<i>Pseudo-nitzschia pungens/multiseriis</i>															1			
<i>Skeletonema costatum</i>								2	2	1		1	1		1	4	1	
<i>Thalassionema nitzschiodes</i>												1	1		1	1		
<i>Thalassiosira pac/nord/aest</i>										1					3	1		
<i>Thalassiosira rotula</i>																1		
Dinoflagellates																		
<i>Akashiwo sanguinea</i> (<i>Gymnodinium splendens</i>)								1										
<i>Alexandrium tamarense</i>									1	1		1	1			1		
<i>Ceratium fusus</i>									1									
<i>Dinophysis acuta</i>									1									
<i>Gonyaulax digitale</i>								1	1				1					
<i>Gymnodinium</i> spp.								1	1	1		1	1	1			1	
<i>Gyrodinium spirale</i>									1	1		1	1		1	1		
<i>Heterocapsa triquetra</i>								2	1	1			1			1		
<i>Miniscula bipes</i>															1			
<i>Oxyphysis oxytoxoides</i>										1			1		1	1		
<i>Protoperdinium brevipes</i>									1				1					
<i>Protoperdinium leonis</i>										1			1					
<i>Protoperdinium steinii</i>									1									
<i>Scrippsiella trochoidea</i>									1	1		1	1	1		1	1	1
Ciliates																		
<i>Myrionecta rubra</i>								1	1	1		1	2	1		1	1	1
Tintinnid spp.								1	1	1			1	1		1	1	1
Flagellates																		
Flagellate-small								1	1	1		1	2	1		1	1	1
Flagellate-medium								1	1	1		1	1	1		1	1	1
Flagellate-large								1		1		1			1		1	

Table 20. Relative abundances of phytoplankton observed in preserved samples from the centre of the inlet in 2010.

Organism		Centre of inlet 2010														
		3/18 - 19			4/23 - 24			5/17 - 18			6/20 - 22			7/20 - 21		
Dates		0 5 30			0 5 30			0 5 30			0 5 30			0 5 30		
Depth (m)		0 5 30			0 5 30			0 5 30			0 5 30			0 5 30		
Diatoms																
<i>Asterionellopsis socialis</i>																1
<i>Bacteriastrium delicatulum</i>																1
<i>Chaetoceros constrictus</i>											1					
<i>Chaetoceros contortus</i>																1
<i>Chaetoceros convolutus</i>								1	1	1	1					1
<i>Chaetoceros curvisetus</i>																1
<i>Chaetoceros debilis</i>								1		1						1
<i>Chaetoceros decipiens</i>								1	1	1	2			1	1	1
<i>Chaetoceros diadema</i>																1
<i>Chaetoceros didymus</i>											1					
<i>Chaetoceros lorenzianus</i>								1		1				1		1
<i>Chaetoceros radicans</i>								1	1	1	1			1	1	
<i>Chaetoceros similis</i>									1	1	1					1
<i>Chaetoceros vanheukerii</i>											1					
<i>Corethron hystrix</i>								1								
<i>Cosinodiscus</i> spp.																1
<i>Cylindrotheca closterium</i>								1	1	1	1	1		1	1	
<i>Fragillaria</i> spp.								1								
<i>Guinardia striata</i>																1
<i>Leptocylindrus danicus</i>										1	1			1	1	
<i>Leptocylindrus minimus</i>								1		1	1			1	2	1
<i>Melosira granulata</i>								1								
<i>Navicula</i> spp.																1
<i>Pseudo-nitzschia pseudo-/delicatissima</i>								1	1	1	1	1		2	1	
<i>Pseudo-nitzschia pungens/multiseriis</i>								1	1					1	2	
<i>Rhizosolenia styliformes</i>														1	1	
<i>Skeletonema costatum</i>								2	4	3	2	2	1	2	4	1
<i>Thalassionema nitzschioides</i>								1	1	1	1	1	1	1	3	1
<i>Thalassiosira pac/nord/aest</i>								1	2	2	1			1	4	1
<i>Thalassiosira rotula</i>										1				1	2	
Dinoflagellates																
<i>Alexandrium catanella</i>																1
<i>Alexandrium tamarense</i>								1	1		1	1	1	1		1
<i>Amylax tricantha</i>											1					
<i>Corythodinium tessellatum</i>								1								
<i>Dinophysis acuta</i>								1								1
<i>Gonyaulax digitale</i>																1
<i>Gymnodinium</i> spp.								1						1		1
<i>Gyrodinium spirale</i>								1	1	1	1			1	1	
<i>Heterocapsa triquetra</i>								1	1		2	1		1	1	1
<i>Miniscula bipes</i>								1						1	1	
<i>Oxyphysis oxytoxoides</i>											1		1	1	1	1
<i>Protoperdinium brevipes</i>										1						
<i>Protoperdinium leonis</i>										1						
<i>Protoperdinium steinii</i>																1
<i>Scrippsiella trochoidea</i>								1			1	1		1		
Ciliates																
<i>Myrionecta rubra</i>								1	1	1	1	1		1	1	
<i>Tintinnid</i> spp.								1	1	1	1	1	1	1	1	1
Flagellates																
Flagellate-small								1	1	1	1	2	1	1	2	1
Flagellate-medium								1	1		1	2	1	1	1	1
Flagellate-large											1			1		1
Silicoflagellates																
<i>Dictyocha speculum</i>										1		1				1
<i>Ebria tripartita</i>								1								1

Table 21. Relative abundances of phytoplankton observed in preserved samples from the mouth of the inlet in 2010.

Organism	Depth (m)	Mouth of inlet 2010														
		3/18 - 19			4/23 - 24			5/17 - 18			6/20 - 22			7/20 - 21		
		0	5	30	0	5	30	0	5	30	0	5	30	0	5	30
Diatoms																
<i>Asteromphalus heptactis</i>																1
<i>Atheya decora</i>																1 1
<i>Bacteriastrum delicatulum</i>																1
<i>Chaetoceros anastomosans</i>																2
<i>Chaetoceros convolutus</i>									1	1						1 1
<i>Chaetoceros curvisetus</i>									1	1						1 2 1
<i>Chaetoceros debilis</i>									1	1	1					2
<i>Chaetoceros decipiens</i>									1	1	1					1
<i>Chaetoceros didymus</i>																1
<i>Chaetoceros lorenzianus</i>									1	1	1					1 1 1
<i>Chaetoceros radicans</i>									1	2	2					3 2 1
<i>Chaetoceros similis</i>									1	1	1					2 1 1 1
<i>Chaetoceros subtilis</i>																1
<i>Chaetoceros teres</i>																1
<i>Chaetoceros vanheukerri</i>																1
<i>Cosinodiscus</i> spp.																1 1
<i>Cylindrotheca closterium</i>									1	1	1					1 1 1
<i>Ditylum brightwellii</i>																1 1 1
<i>Eucampia zodiacus</i>																1 2
<i>Guinardia delicatula</i>									1	1						1 1 1
<i>Guinardia striata</i>																1
<i>Leptocylindrus danicus</i>									1	1	1					1 1 1
<i>Leptocylindrus minimus</i>									1	1	1					1 1 1
<i>Lycomorpha abbreviata</i>																1
<i>Melosira granulata</i>																1
<i>Odontella longicruris</i>																1
<i>Pleurosigma</i> spp.																1 1
<i>Pseudo-nitzschia pseudo-delicatissima</i>									1	2	1					4 4 1 1 1
<i>Pseudo-nitzschia pungens/multiseriis</i>									1	1	1					2 2 2 1
<i>Rhizosolenia setigera</i>																1 1
<i>Rhizosolenia styliformes</i>																1 1 2 4 1
<i>Skeletonema costatum</i>									2	2	2					2 4 1 1 1 1
<i>Stephanopyxis nipponica</i>																1
<i>Thalassionema nitzschiodes</i>									1	1	1					1 1 1
<i>Thalassiosira anguste-lineata</i>																1
<i>Thalassiosira pac/nord/aest</i>									1	2	2					3 3 1 2 4 1
<i>Thalassiosira rotula</i>									1	1						1 1 1
<i>Tropidoneis antarctica</i>																1
Dinoflagellates																
<i>Alexandrium catanella</i>																1
<i>Alexandrium ostenfeldii</i>																1
<i>Alexandrium tamarense</i>									1	1						1 1 1
<i>Ceratium fusus</i>																1
<i>Ceratium longipes/horridum</i>																1
<i>Ceratium lineatum</i>																1
<i>Corythodinium tessellatum</i>																1
<i>Dinophysis acuminata</i>									1	1						1 1
<i>Dinophysis acuta</i>																1
<i>Gonyaulax digitale</i>									1							1
<i>Gymnodinium</i> spp.																1 1 1
<i>Gyrodinium spirale</i>									1	1	1					1 1 1
<i>Heterocapsa triquetra</i>									1							1 1
<i>Miniscula bipes</i>																1 1
<i>Oxyphysis oxytoxoides</i>									1	1	1	1				1
<i>Polykrikos schwartzii</i>																1
<i>Prorocentrum gracile</i>									1							1
<i>Prorocentrum micans</i>																1
<i>Protoceratium reticulatum</i>																1
<i>Protoperidinium conicum</i>									1							1
<i>Protoperidinium depressum</i>																1
<i>Protoperidinium leonis</i>									1	1						1
<i>Protoperidinium steinii</i>																1
<i>Scrippsiella trochoidea</i>									1	1	1					1 1 1
Ciliates																
<i>Myrionecta rubra</i>									1	1	1					1 2 1
Tintinnid spp.									1	1	1					1 1 1
Flagellates																
Flagellate-small									1	1	1					1 2 1
Flagellate-medium									1	1	1					1 1 1
Flagellate-large																1
<i>Heterostigma akashiwo</i>									1							1
<i>Phaeocystis</i> spp.																1
Silicoflagellates																
<i>Dityocha speculum</i>																1
<i>Ebria tripartita</i>																1